GLASS FIBER REINFORCED GLUED LAMINATED WOOD BEAMS

Alfred B. Dorey and J.J. Roger Cheng
Department of Civil Engineering
University of Alberta
Edmonton, Alberta
T6G 2G7

1996

This is a joint publication of the Canadian Forest Service
and Land and Forest Services pursuant to the
Canada-Alberta Partnership Agreement in Forestry

8005A-4/147

DISCLAIMER

The study on which this report is based was funded in part under the Canada-Alberta Partnership Agreement in Forestry.

The views, conclusions, and recommendations are those of the authors. The exclusion of certain manufactured products does not necessarily imply disapproval nor does the mention of other products necessarily imply endorsement by the Canadian Forest Service or Alberta Land and Forest Services.

Catalogue No.: Fo42-91/147-1996E
ISBN: 0-662-25158-X

Additional copies of this publication are available at no charge from:

Canadian Forest Service
Natural Resources Canada
Northern Forestry Centre
5320 - 122nd Street
Edmonton, Alberta
T6H 3S5
Telephone: (403) 435-7210

or

Land and Forest Services
Alberta Environmental Protection
10th Floor, Bramalea Building
9920 - 108 Street
Edmonton, Alberta
T5K 2M4
Telephone: (403) 427-3551

ABSTRACT

With the ever decreasing availability of prime lumber, research must be conducted to develop more efficient uses for our wood natural resource. This research program was conducted to develop composite glued laminated (glulam) beams using fiber reinforced plastic (FRP) materials. A preliminary study, conducted by Dorey and Cheng (1996), examined the potential of glass (GFRP) and carbon (CFRP) fiber reinforcement for glued laminated (glulam) timber beams and concluded that, despite the superior mechanical properties exhibited by the CFRP, when project economics were considered, GFRP appeared to be superior reinforcing material.

The main test program involved investigating how a number of different parameters, specifically fiber profile, fiber fraction, weathering effects and beam size affect the overall strength and stiffness of a GFRP glulam timber specimen.

Results indicate that all of the fiber reinforced specimens showed a significant increase in strength over the unreinforced samples. Maximum strength and true stiffness enhancements of 127% and 120%, respectively, were achieved for specimens with only tensile reinforcement at a fiber fraction of 7.06%. Maximum strength and true stiffness enhancements of 149% and 202%, respectively, were achieved for doubly reinforced specimens at a fiber fraction of 6.74%. The weathering tests showed that there was no significant effect on the phenolic resorcinol formaldehyde bond between the glass fiber and the adjacent wood fibers. Beam size effects were inconclusive from the test data because of the height to width ratio selected. A strain compatibility model was developed and provided a test to a predicted ratio of 1.062.

ACKNOWLEDGEMENTS

The author would like to acknowledge the many contributions from Dr. J.J.R. Cheng. His guidance and advice were irreplaceable in this Master's project research.

The assistance of Mr. Brian Watson and Mr. Kent Fargey of Western Archrib in Edmonton in terms of their financial aid, their assistance with procuring the glulam specimens, and their technical support was irreplaceable. The assistance of Mr. Andy Chaldezos of Western Archrib in constructing and testing specimens was much appreciated. The donations and technical support of Mr. Gary Steadman of ZCL Composites in Edmonton was also very much appreciated. The suggestions and assistance of the I. F. Morrison Lab Technicians, Larry Burden and Richard Helfrich, from the University of Alberta and Mr. John Alexander of the University of Alberta were also greatly valued.

The research was funded, in part, by the Canada--Alberta Partnership Agreement in Forestry. The guidance of the project manager, Mr. Russel Bohning, was greatly appreciated.

TABLE OF CONTENTS

Page

Disclaimer iii
Abstract iv
Acknowledgments iv
Table of Contents v
List of Figures viii
List of Tables ix
List of Symbols x

1.0 INTRODUCTION 1

1.1 Research Approach 1
1.2 Objectives 2
1.3 Report Outline 3

2.0 EXPERIMENTAL PROGRAM 4

2.1 Test Program Specimens 4
2.1.1 Unreinforced Specimens 5
2.1.2 Reinforced Specimens 5
2.1.2.1 Specimens with only Tensile Reinforcement 6
2.1.2.2 Specimens with Tension and Compression Reinforcement 7
2.1.2.3 Specimens Subjected to Adverse Environmental Conditions 8
2.1.2.4 Size Comparison Specimens 9
2.1.3 Material Tests 9
2.2 Test Set Up and Test Procedure 10
2.3 Reinforcing Procedures 10
2.3.1 Specimens Reinforced with Glass Tow Sheets 10
2.3.2 Specimens Reinforced Using Pultruded Glass Straps 11

TABLE OF CONTENTS (cont.)

Page

3.0 TEST RESULTS AND ANALYSIS 18

3.1 Material Test Results 18
3.1.1 Wood Compression Test (WCT) Results 18
3.1.2 Wood Tension Test (WTT) Results 18
3.1.3 Wood Shear Test (WST) Results 19
3.1.4 Pultruded Glass Fiber Strap Tension Test Results 19
3.1.5 Pultruded Glass Fiber Strap Compression Test Results 20
3.1.6 Specimen Moisture Contents 21
3.2 Unreinforced Beam Specimen Results 23
3.2.1 Unreinforced 240 mm Deep Specimens 23
3.2.2 Unreinforced 300 mm Deep Specimens 26
3.3 Reinforced Specimens 26
3.3.1 Specimens with Only Tensile Reinforcement 27
3.3.2 Specimens with Both Tensile and Compressive Reinforcement 29
3.3.3 Specimens Subjected to Adverse Environmental Conditions 31
3.3.4 Reinforced 300 mm Deep Specimens 32
3.4 Determination of Mechanical Property Enhancement 33
3.4.1 Determination of Strength Enhancement 33
3.4.2 Determination of Stiffness Enhancement 34
3.4.3 Determination of Failure Strains 36
3.4.4 Determination of Failure Stresses 39
3.4.5 Determination of Mean Failure Stresses and Strains 40

4.0 DISCUSSION 61

4.1 Material Test Results 61
4.1.1 Wood Material Test Results 61
4.1.2 Pultruded Glass Strap Material Test Results 63
4.2 Discussion of Specimens With Only Tensile Reinforcing 64
4.3 Discussion of Doubly Reinforced Specimens 67
4.4 Discussion of Weathered Specimens 69
4.5 Discussion of Size Effects 70
4.6 Model Development 71
4.6.1 Design Recommendations 75

TABLE OF CONTENTS (cont.)

Page

5.0 SUMMARY AND RECOMMENDATIONS 83

5.1 Summary 83
5.2 Significance 85
5.3 Recommendations for Future Research 85

6.0 REFERENCES 88

LIST OF FIGURES

Page

Figure 2.1 Photo of Pultruded Glass Fiber Strap 12
Figure 2.2 Schematic of Main Investigation Reinforcing Patterns 13
Figure 2.3 Photo of Main Investigation Reinforcing Schemes 14
Figure 2.4 Pultruded Strap Material Test Specimens 15
Figure 2.5 Schematic of Test Set Up 16
Figure 2.6 Photo of Test Set Up 17

Figure 3.1 Photo of Wood Compression Test 42
Figure 3.2 Typical Load-Deflection Plot for Wood Compression Material Test 43
Figure 3.3 Photo of Wood Tension Test Specimen 44
Figure 3.4 Typical Load-Deflection Plot for Wood Tension Material Test 45
Figure 3.5 Photo of Wood Shear Test Specimen 46
Figure 3.6 Photo of Pultruded Glass Strap Tension Test Specimen 47
Figure 3.7 Typical Load-Deflection Plot for Pultruded Strap Tension Test 48
Figure 3.8 Photo of Pultruded Glass Strap Compression Test Specimen 49
Figure 3.9 Plot of Moisture Content Fluctuation for Weathered Specimens 50
Figure 3.10 Photo of Typical Unreinforced Tensile Fracture 51
Figure 3.11 Typical Regression Analysis for an Unreinforced Specimen 52
Figure 3.12 Photo of Typical Reinforced Tensile Fracture 53
Figure 3.13 Photo of Typical Reinforced Compressive Crushing Failure 54
Figure 3.14 Photo of Typical Reinforced Buckling Failure 55
Figure 3.15 Photo of Typical Reinforced Shear Failure 56
Figure 3.16 Typical Regression Analysis for a Reinforced Specimen 57
Figure 3.17 Typical Demec Data Plot 58
Figure 3.18 Typical Load-Deflection Plot 59
Figure 3.19 Foil Gauge Strain versus Demec Gauge Strain Plot 60

Figure 4.1 Strength Enhancement Plot for Tensile Reinforced Specimens 76
Figure 4.2 Stiffness Enhancement Plot for Tensile Reinforced Specimens 77
Figure 4.3 Strength versus Stiffness Relationship for Tensile Reinforced Specimens 78
Figure 4.4 Strength Enhancement Plot for Doubly Reinforced Specimens 79
Figure 4.5 Stiffness Enhancement Plot for Doubly Reinforced Specimens 80
Figure 4.6 Strength versus Stiffness Relationship for Doubly Reinforced Specimens 81
Figure 4.7 Schematic and Calculations for Strain Compatibility Analysis 82

LIST OF TABLES

		Page
Table 2.1	Properties of the Tow Sheets Used	10
Table 2.2	Quantities of Fiber and Resin Used	11
Table 3.1	Results of Wood Compression Tests	18
Table 3.2	Results of Wood Tension Tests	18
Table 3.3	Results of Wood Shear Tests	19
Table 3.4	Results of Pultruded Strap Tension Tests	19
Table 3.5	Results of Pultruded Strap Compression Tests	20
Table 3.6	Specimen Moisture Content at Time of Testing	22
Table 3.7	Specimen Moisture Content (M.C.) of Weathered Specimens	23
Table 3.8	Strength Test Results for Unreinforced 240 mm Deep Beams	24
Table 3.9	Stiffness Test Results for Unreinforced 240 mm Deep Beams	25
Table 3.10	Strength Test Results for Unreinforced 300 mm Deep Beams	26
Table 3.11	Stiffness Test Results for Unreinforced 300 mm Deep Beams	26
Table 3.12	Strength Test Results for Tensile Reinforced Specimens	27
Table 3.13	Apparent Stiffness Test Results of Tensile Reinforced Specimens	28
Table 3.14	Shear Free Stiffness Test Results of Tensile Reinforced Specimens	29
Table 3.15	Strength Test Results for Doubly Reinforced Specimens	30
Table 3.16	Apparent Stiffness Test Results of Doubly Reinforced Specimens	30
Table 3.17	Shear Free Stiffness Test Results of Doubly Reinforced Specimens	30
Table 3.18	Strength Test Results for Specimens Exposed to Adverse Conditions	31
Table 3.19	Apparent Stiffness of Specimens Exposed to Adverse Conditions	31
Table 3.20	Shear Free Stiffness of Specimens Exposed to Adverse Conditions	32
Table 3.21	Strength Test Results for 300 mm Deep Reinforced Specimens	32
Table 3.22	Apparent Stiffness Results for 300 mm Deep Reinforced Specimens	33
Table 3.23	Shear Free Stiffness Results for 300 mm Deep Reinforced Specimens	33
Table 3.24	Strength Enhancement of Reinforced Specimens	34
Table 3.25	Apparent Stiffness Enhancement of Reinforced Specimens	35
Table 3.26	Shear Free Stiffness Enhancement of Reinforced Specimens	35
Table 3.27	Determination of Ultimate Strains	38
Table 3.28	Failure Mode and Peak Stresses at Failure	40
Table 3.29	Mean Failure Stress and Strain for Each Failure Mode	41
Table 4.1	Mean Wood Material Properties	61
Table 4.2	Normalized Ultimate Stress Comparison	62
Table 4.3	Predicted Failure Loads	73
Table 4.4	Comparison of Test to Predicted Failure Loads and Mechanisms	74
Table 4.5	Design Strains and Stresses for Glass Fiber Reinforced Glulam Beams	75

LIST OF SYMBOLS

a	shear free span length (mm)
~	approximately
A	area (mm^2)
AFRP	Aramid Fiber Reinforced Plastic
ASTM	American Society for Testing Materials
b_{fc}	width of compression zone fiber (mm)
b_{ft}	width of tension zone fiber (mm)
b_w	average width of wood section (mm)
^oC	degrees Celcius
c_c	depth of compression zone (mm)
C_f	force in the compression zone fiber (kN)
CFRP	Carbon Fiber Reinforced Plastic
cm^3	cubic centimeter
comp.	compression
compress.	compression
CSA	Canadian Standards Association
c_t	depth of tension zone (mm)
C_w	force in the wood in the compression zone (kN)
Δ	deflection (mm)
ε	strain (mm/mm)
ε_{cf}	compressive strain in the fiber (mm/mm)
$\varepsilon_{cf(avg)}$	average compressive strain in the fiber (mm/mm)
ε_{cw}	compressive strain in the wood (mm/mm)
ε_{max}	maximum strain (mm/mm)
ε_{tf}	tensile strain in the fiber (mm/mm)
$\varepsilon_{tf(avg)}$	average tensile strain in the fiber (mm/mm)
ε_{tw}	tensile strain in the wood(mm/mm)
E	Modulus of Elasticity (MPa)
E_f	Modulus of Elasticity of the fiber (MPa)
E_w	Modulus of Elasticity of the wood (MPa)
EI	stiffness ($N*mm^2$)
eq.	equation
FiRP	panel construction using KRP by Tingley (1994)
FRP	Fiber Reinforced Plastic
g	gram
GFRP	Glass Fiber Reinforced Plastic
h	height of specimen (mm)
h^2	height squared (mm^2)
h^3	height cubed (mm^3)

List of Symbols (cont.)

I	Moment of Inertia (mm^4)
ID	identification
in	inches
kip	one thousand pounds
kN	kilonewton
kPa	kilopascal (kN/m^2)
KRP	Kevlar® Reinforced Plastic
K_{zcp}	size factor for compression parallel to grain
K_{zt}	size factor for tension parallel to grain
K_{zv}	size factor for shear
L	length (mm)
LVDT	Linear Variable Differential Transducer
LVL	Laminated Veneer Lumber
M	bending moment (kN*m)
m^2	square meter
M.C.	Moisture Content (%)
$\mu\varepsilon$	microstrain (10^6 strain units)
mm	millimeter
mm^2	square millimeter
mm^3	cubic millimeter
mm^4	millimeter to the power of 4
MOE	Modulus of Elasticity (MPa)
MPa	megapascal (N/mm^2)
N	Newton
n/a	not available or not applicable
OSB	Oriented Strand Board
P	Load (kN)
P_{ult}	Ultimate Load (kN)
Q	first moment of area (mm^3)
R	linear regression analysis correlation factor
Reinf.	reinforced
σ_{cf}	compressive stress in the fiber (MPa)
σ_{cmax}	maximum compressive stress (MPa)
σ_{crmax}avg	average maximum reinforced compressive stress (MPa)
σ_{cw}	compressive stress in the wood (MPa)
σ_{tf}	tensile stress in the fiber (MPa)
σ_{tmax}	maximum tensile stress (MPa)
σ_{trmax}avg	average maximum reinforced tensile stress (MPa)
σ_{tw}	tensile stress in the wood (MPa)
S-P-F	Spruce-Pine-Fir

List of Symbols (cont.)

t	thickness (mm)
tens.	tension
t_{fc}	thickness of the compression zone fiber (mm)
t_{ft}	thickness of the tension zone fiber (mm)
τ_{max}	maximum shear stress (MPa)
τ_{rmax}avg	average maximum reinforced shear stress (MPa)
T_f	force in the tension zone fiber (kN)
T_w	force in the wood in the tension zone (kN)
Unreinf.	unreinforced
V	shear load (kN)
vs.	versus
y	distance to neutral axis (mm)

1.0 INTRODUCTION

Primarily for economic and environmental reasons, the concept of an 'engineered wood product' has taken on a renewed interest over the past 15 years. These products have reached the leading edge of timber research and have begun to invade the timber construction market to the extent that the use of sawn timber as main structural elements is becoming obsolete.

One area of interest in the field of engineered wood products has been the use of advanced composite materials (ACM's) to enhance the weaker mechanical properties of wood and wood products. Fiber reinforced plastic (FRP) wood has reached the United States marketplace in the form of aramid fiber reinforced plastic (AFRP) glued-laminated (glulam) beams (Tingely, 1994). However, given that this construction material field is still in a stage of infancy, there is still much research to be conducted into the use of ACM material to reinforce wood.

There are three main types of fiber reinforcement: aramid (AFRP), carbon (CFRP) and glass (GFRP). A state of the art review conducted by Dorey and Cheng (1996), and presented in the Canada-Alberta Partnership Agreement in Forestry Report No. A5030, indicated that there have been extensive studies done by Tingley on the use of AFRP to reinforce glulam beams. However, there appeared to be limited research done on the use of either CFRP or GFRP to reinforce glulam beams. Dorey and Cheng, in conjunction with the Canadian Forest Service and Western Archrib of Edmonton, undertook a preliminary study to investigate the potential of these two fiber types to serve as reinforcement for S-P-F glulam beams (Dorey and Cheng, 1996).

Their preliminary study indicated that significant potential existed for both CFRP and GFRP glulam beams and it was concluded that this area required further investigation.

1.1 Research Approach

From the results of the preliminary investigation presented in Report No. A5030, it was concluded that there was significant technical merit for the use of both CFRP and GFRP to reinforce glulam beams. It was observed that, in this application, the CFRP system only performed marginally better than the GFRP system, but that the CFRP system cost significantly more than the GFRP system. Considering the economic motivations for this research, it was concluded that a GFRP system for reinforcing glulam beams should be investigated in detail. This conclusion forms the basis of this investigation.

The approach of this research was to investigate the improvement of the mechanical properties of the specimens with the application of GFRP reinforcing. Specifically, the

strength and stiffness enhancement of the specimens was measured by comparing the reinforced property with the unreinforced property.

It is recognized that the development of new technologies and products is a vast undertaking and that there are many factors and variables to be considered. The main focus of this research was to assess the potential of GFRP glulam timber. It was felt that the initiation point for this research was to determine the extent of the improvement in the basic mechanical properties of the specimen and to provide a preliminary optimization of the technology.

The improvement of mechanical properties was measured by comparing reinforced properties with unreinforced ones. Specifically, stiffness enhancement was measured by comparing the reinforced stiffness with that of the specimen prior to reinforcing. A non-destructive test was conducted to determine the unreinforced Modulus of Elasticity (MOE) for each individual specimen. Due to the destructive nature of the testing, strength enhancement was measured by comparing the flexural capacity of reinforced specimens with the unreinforced specimens capacity at failure.

In addition to the mechanical property enhancement, a number of other parameters were investigated. These parameters included a comparison between different fiber profiles, the effects of extreme environmental conditions, and if there were any sizing effects.

1.2 Objectives

The purpose of this research was to determine the extent of the potential of GFRP reinforced glulam.

Specifically, the objectives for this project were as follows:

1. To determine the flexural capacity enhancement of GFRP reinforced glulam;
2. To determine the stiffness enhancement of GFRP reinforced glulam;
3. To conduct a series of comparative tests to decide what fiber fraction and profile provide the greatest performance enhancement;
4. To determine the effect of extreme moisture conditions on the reliability of the bond between the fiber reinforcing and the adjacent wood; and,
5. To determine if the technology developed is applicable to different size specimens

1.3 Report Outline

Chapter 2 details the experimental program followed to meet the objectives outlined in section 1.2 and Chapter 3 presents the test results obtained from the experimental program. Chapter 4 provides a discussion and analysis of the results with the summary and subsequent conclusion being presented in Chapter 5.

2.0 EXPERIMENTAL PROGRAM

The purpose of this program was to follow the recommendations of the preliminary test program conducted by Dorey and Cheng (1996) to try to gain a further understanding into the behaviour of fiber reinforced glulam timber. Using the preliminary study recommendations, it was decided that glass fiber would be used in the reinforcing system and that any reinforcement applied to the beams would be placed along an extreme wood fiber, in either tension or compression.

The experimental program was structured as follows:

1. A series of specimens reinforced with glass fiber along the extreme tension wood fiber at varying amounts of fiber or fiber fractions;
2. A parallel series of specimens with similar fiber fractions, except they were reinforced along both the extreme tension wood fiber and the extreme compression wood fiber;
3. A series of specimens with a different base size of the glulam beam to determine if there are any sizing effects;
4. A series of specimens that are exposed to adverse environmental conditions to determine the effectiveness of the reinforcing systems when exposed to such factors; and,
5. The development of a model for predicting the behaviour and failure load for the reinforced specimens.

Testing was conducted at the I.F. Morrison Structural Engineering Laboratory at the University of Alberta and at the manufacturing plant of Western Archrib in Edmonton.

2.1 Test Program Specimens

A total of 34 specimens were tested in this program. All of the specimens were made of S-P-F lumber and taken from the stocks of Western Archrib of Edmonton. The beams were constructed using the standard glulam manufacturing processes at Western Archrib. A nominal size (hereafter referred to as the *standard size*) of 40 mm by 240 mm by 4280 mm was selected for the main testing program. Measured dimensions and other material and sectional properties of the individual specimens are presented in Chapter 3.0 - Test Results.

In general, two specimens of each configuration were tested. This is because of the variability of wood and the lack of confidence associated with a single timber specimen. In cases where the two results were not within the reasonable variations of timber, additional specimens were tested.

2.1.1 Unreinforced Specimens

A total of 4 unreinforced beams of standard size were tested. Because of the variability of the mechanical properties of wood and because all of the achieved enhancement for strength would be based on the mean failure load of these specimens, additional unreinforced specimens were tested to more accurately represent the mean failure strength of the unreinforced specimens.

2.1.2 Reinforced Specimens

The results presented in the Canada-Alberta Partnership Agreement Report No. A5030 indicated that there were insufficient quantities of fiber reinforcing applied to the specimens to determine if there was significant stiffness enhancement achieved through the application of the reinforcement. It was therefore decided to apply substantially greater amounts of fiber to the test specimens.

The construction process for the reinforced specimens built in the preliminary study involved a series of procedural steps recommended by the fiber sheet supplier and a 7 day curing period. While the potential exists for the development of an automated process using this construction technique, this is not within the scope of this research. It was decided that a more efficient method of reinforcing the specimens for the higher fiber fractions was required. With this in mind, alternative procedures for the reinforcement application were investigated. From this study, it was decided that the use of a pultruded glass fiber strap would be investigated.

The pultruded glass fiber straps decided upon were a local product produced for the purposes of anchoring fiberglass storage tanks into the ground. They were made using a standard pultrusion process where strands of glass fiber are saturated in a resin bath, and then pulled together through a dye which casts the finished product into the rectangular cross-sectional shape used in this project. Using this process, the cured product becomes a semi-rigid strap with unidirectional fiber at a predetermined fiber fraction, as shown in Figure 2.1.

The use of these straps as the reinforcing system has many advantages. In the context of this research and in the future potential commercial manufacturing of glass fiber reinforced beams, the most important advantage is the ease of construction. A pultruded strap may be laid up as a regular lam in the glulam manufacturing process, thereby requiring little or no change to current glulam manufacturing processes. Secondly, superior quality control is achieved by using these straps versus the methods used in the preliminary study, and the time of construction may be greatly reduced by pre-manufacturing the straps and having them fully cured prior to application to the glulam beam. In addition to this, for the immediate purposes of this study, large fiber fractions are easily obtained.

However, in the context of this research, the straps do have one major limitation. Currently they are only manufactured with a single cross section, 50 mm by 5 mm and

the glulam specimens do not typically come in a width of 50 mm. Since the cost of a manufacturing dye is significant, it was decided to mill the straps to a width of 40 mm and to work around the current fiber fraction available in the strap. This accounts for the odd fiber fractions selected in the testing program.

Unpublished material tests indicated that, with a minimum of machining, a more than adequate bond could be achieved between these straps and the glulam specimens using the standard phenolic resorcinol formaldehyde glulam glue that Western Archrib uses. This result has a significant advantage in that the product may be produced without any significant changes to the current glulam manufacturing process used.

Machining of the strap was required because during the manufacturing of the strap a compound known as an internal release is added to the resin bath. In essence, this internal release acts as a grease to prevent curing of the strap to the casting dyes during production, resulting in a wax-like finish on the completed strap. This finish on the surface of the strap also prevents adhesion between the strap and the phenolic resorcinol formaldehyde glue, therefore the internal release compound had to be removed from the strap prior to adhesion to the glulam member. It was determined that enough simple sanding to remove the gloss finish from the strap provided a more than adequate bond to be developed between the strap and the phenolic resorcinol formaldehyde glue. It was therefore decided to investigate the use of these straps as the reinforcing system for this project.

All specimens that were to receive any type of glass fiber reinforcing were initially pre-load to approximately half their unreinforced capacity to determine an unreinforced MOE for the individual specimens.

The different reinforcing systems used in this project are discussed below. Figure 2.2 provides a schematic of the cross section of each of these systems and Figure 2.3 provides a photo of these cross sections.

2.1.2.1 Specimens with only Tensile Reinforcing

A total of 16 specimens with only tensile reinforcing were tested and added to the data from the two specimens (PTG-1 and PTG-2), in the preliminary testing program. Some of the specimens with only tensile reinforcement were reinforced with straps and others were reinforced with the multiple layers of glass sheet, in the same manner outlined in the preliminary study. The reason for this are the limitations of the available glass straps. Because there was only one dye on hand, only one cross section for the strap was available. Because of practicality and the mechanics of the pultrusion process, the limits of variation for fiber fraction of the strap would not allow for very low range reinforcement ratios for the beams. Consequently, it was decided to produce the low-end fiber fractions using the tow sheet construction method of tow sheets and epoxy resin used in the preliminary investigation. The high-end fiber fractions were produced using the typical glulam construction techniques and the pultruded glass fiber straps.

Identification labels for the specimens with only tensile reinforcement take on one of the following forms:

1. Specimens with multiple sheets of glass fiber reinforcing applied by hand, constructed according to the tow sheet construction method, are labeled using the coding "PTG" followed by the number of applied reinforcing sheets. For example, a specimen labeled PTG-2a would indicate that the manual construction method was used and that 2 sheets of glass fiber reinforcement were applied. The 'a' is the individual specimen identification;

2. Specimens constructed using the pultruded straps were labeled with the number of straps, a 'TS' to indicate tension strap reinforcing only, and a number to identify individual specimens. For example, a specimen labeled 4TS-2 would indicate that there were four tension straps along the tension side of the specimen and that this was the second specimen with this configuration.

Data gathered in the preliminary study was incorporated into this portion of the research. However, since in the preliminary study only one specimen of each type was manufactured and tested, single specimens with one layer (fiber fraction = 0.042%) and two layers (fiber fraction = 0.083%) of tow sheet were manufactured using the tow sheet construction method. These specimens were tested as a confirmation for the specimens with the corresponding fiber fraction in the preliminary study. Two specimens constructed with 10 layers (fiber fraction = 0.42%) of tow sheets were also constructed and tested.

A total of six specimens were constructed and tested with a single tension strap, which corresponds to 1.04% fiber fraction. A greater number of these specimens were constructed and tested for a number of reasons. Primarily, these specimens were the first ones constructed using the pultruded strap technology and it was felt that additional specimens were required to more accurately understand the typical behaviour. As well, the results from these specimens were to be used as a baseline for additional testing. Further to this, it was observed that two of the specimens initially constructed did not have complete adhesive squeeze out in the bond line from the glulam process. During the construction of glulam beams it is important to ensure that adequate adhesive is placed between the lams prior to subjecting the beams to the curing pressure and temperature. One of the criteria for assessing adequate quantities of bonding adhesive is to look for glue that has squeezed out between the lams in the cured specimen. Along the bond lines between the pultruded strap and the adjacent wood lam for two of the specimens with single straps, there did not appear to be adequate squeeze out, so additional specimens were constructed for data confirmation.

Using the pultruded straps, pairs of specimens were constructed and tested with the following fiber fractions: 1.98%, 3.80%, and 6.90%, which represent two tension straps, four tension straps, and eight tension straps, respectively.

2.1.2.2 Specimens with Tension and Compression Reinforcement

A total of six specimens received both tensile and compressive reinforcing. These specimens were constructed exclusively using the pultruded strap construction method outline in sections 2.1.2 and 2.1.2.1 above.

Specimens in this category were labeled with the letters 'DR', indicating a doubly reinforced specimen. The number in front of the DR indicates the total number of straps on the specimen, with half of them on the compression face and the other half on the tension side. The number following the DR indicates the individual specimen identification. For example, a specimen labeled 4DR-2 would indicate a specimen with 2 reinforcing straps on the compression face and 2 reinforcing straps on the tension face and that this would be the second specimen in this series. Specimens with this 'DR' configuration are depicted schematically in Figure 2.2 and are shown in the photo in Figure 2.3.

Fiber fractions were selected so that they were nominally identical to those selected for the tension reinforced specimens above. The following total fiber fractions were used: 1.98%, 3.80%, and 6.90%, which represent two tension straps, four tension straps, and eight tension straps, respectively.

2.1.2.3 Specimens Subjected to Adverse Environmental Conditions

More so than any other construction material, the mechanical properties and the overall behaviour of wood is highly susceptible to environmental conditions. Specifically, the moisture content of the wood and of the surrounding environment may dramatically affect the behaviour of an individual specimen. With this in mind, it was decided to do a preliminary investigation into the effects of moisture content on the behaviour of the reinforced specimens. This series of tests was conducted on glulam beams that had been reinforced with the pultruded glass straps on only the tensile face, as indicated in Figure 2.2.

A detailed environmental investigation is not within the scope of this research, nevertheless, the author felt that this is an important component to the study and that, at a minimum, an initial investigation should be conducted. In order to evaluate the effects of adverse environmental factors on the test specimens, two different series of tests were conducted. One test series was the complete saturation of a reinforced glulam beam followed by drying. The second test involved a series of reinforced glulam beams that underwent a cyclic moisture fluctuation.

In the first test series, a GFRP reinforced specimen was submerged in water for seven days and then allowed to air dry for 7 weeks until its moisture content stabilized. Only one specimen was available for this test. The specimen was labeled '1SAT-1'. It was reinforced with a single pultruded glass strap in the tension zone and had a fiber fraction of 0.97%.

The second test series was developed where GFRP reinforced specimens were cycled in and out of a water bath. The parameters of the program included a 24-hour submerged phase, followed by a 6-day drying period. This cycle was repeated over a 7-week period, after which the specimens were tested to failure. A total of 3 specimens were tested under this program and were labeled with 'WT' to represent the weathering test. Again, the number preceding the WT indicates the total number of pultruded glass straps used to reinforce the glulam beam and the number succeeding the WT indicates the individual specimen identification number.

During the cycling period, a marker timber specimen was cycled along with the beams. The purpose of this marker was to measure the moisture content. Specimens were taken from the marker before and after each cycle to follow the fluctuation of moisture content. A marker was used because of the need to maintain the overall integrity of the actual specimen for subsequent testing. A moisture content specimen was taken from the actual specimen after failure to ensure agreement with the marker.

2.1.2.4 Size Comparison Specimens

A total of six specimens of a different size were tested to evaluate the effect of sizing on the performance of the GFRP straps. These specimens were also obtained from the stocks of Western Archrib in Edmonton and were constructed using standard glulam manufacturing procedures. These beams had nominal dimensions of 40 mm by 300 mm by 5490 mm. As with the standard specimen used, these dimensions were selected to ensure pure bending behaviour. There were a total of 16 lams in the make up of the larger beams.

Of the six specimens, two were unreinforced, two were reinforced with only tension reinforcement, and two were doubly reinforced. These specimens were labeled 'PT12', '2T12', and '2D12' respectively, with an additional number to represent the individual specimens. For example, a specimen with the label '2T12-2' represents a 300 mm deep specimen (12 in.) with 2 reinforcing straps on only the tension face of the beam.

2.1.3 Material Tests

A series of material tests were conducted to determine the material properties of the components used in this project. Wood material tests were conducted to determine the tensile capacity of the wood, the compressive capacity of the wood, and the shear capacity of the wood. All of the tests are outlined in ASTM Standard D143-94, Standard Methods of Testing Small Clear Specimens of Timber. Details of the wood specimens are given in Section 3.1 - Material Test Results.

Material tests were also conducted on the pultruded glass straps to determine the tensile capacity of the strap and the compressive capacity of the strap. Test specimens were constructed from the sanded and unsanded pultruded strap. The pultruded glass strap tensile capacity specimens were constructed using epoxy to bond grip lengths of the strap to both faces of each end of the test specimen. Test specimen dimensions were

selected based on other material test experience and the testing apparatus configuration. Figure 2.4 presents a schematic of the test specimens.

The pultruded glass strap compressive capacity specimens were constructed from three equal lengths of the pultruded strap bonded together using an epoxy. The test dimensions were based on previous experience, ensuring that the failure was due to crushing of the cross-section, and not due to member buckling. A schematic of the test specimen is given in Figure 2.4.

2.2 Test Set Up and Test Procedure

In order to achieve a shear free span in the specimens, a two point loading scheme was selected to test the specimens. A schematic of the test set-up is given in Figure 2.5 and a photo in Figure 2.6.

In this program, specimens with both tow sheets and pultruded straps were studied, as previously outlined. For the specimens with pultruded glass straps, interlam strain gauges were mounted at the centerline of every fiber-wood interface. Strain gauges were placed on the GFRP straps and a small notch was manufactured in the adjacent wood lam for the lead wires from the strain gauge to ensure a complete bond between the remaining wood and GFRP. It is recognized that this may cause a point of stress concentration when the specimen is loaded, however no specimens showed evidence that this small notch was the initiation point for specimen failure.

2.3 Reinforcing Procedures

2.3.1 Specimens Reinforced with Glass Tow Sheets

The mechanical properties of the tow sheets used to achieve the low level fiber fractions are given in Table 2.1. The tow sheet fiber reinforcement was applied as outlined in the FORCA TOW SHEET TECHNICAL NOTES (1995) received with the fiber and bonding epoxy from the supplier.

Table 2.1 Properties of Tow Sheets Used

Physical Property	Glass Fiber Tow Sheet
Forca Grade	FTS-GE-30
Fiber	E-glass
Fiber Density (g/cm^3)	2.55
Tensile Strength (MPa)	1 520
Tensile Modulus (MPa)	72 590
Ultimate Elongation (%)	2.1

Based on the findings from the preliminary test program, a fiber to resin ratio of 1:3 was used for specimens with a single layer of reinforcing and a ratio of 1:2 for specimens with multiple layers. Table 2.2 presents the amount of fiber and resin in each of the reinforced specimens.

Table 2.2 Quantities of Fiber and Resin Used

Specimen ID Number	Desired Fiber : Resin Ratio	Mass of Fiber Used (g)	Mass of Resin Required (g)	Mass of Resin Used (g)	Actual Fiber to Resin Ratio
PTG-1a	1 : 3	66.9	200.7	212.2	1 : 3.17
PTG-1b	1 : 3	69.4	208.2	207.6	1 : 2.99
PTG-2a	1 : 2	134.0	268.0	293.3	1 : 2.19
PTG-2b	1 : 2	132.9	265.8	272.1	1 : 2.04
PTG-10a	1 : 2	682.1	1364.2	1385.9	1 : 2.03
PTG-10b	1 : 2	673.8	1347.6	1332.6	1 : 1.98

2.3.2 Specimens Reinforced Using Pultruded Glass Straps

The straps used in this reinforcing system were obtained from a local supplier. Due to the manufacturing process for the straps, they required some machining prior to their application to the glulam beams. In this milling process, the width of the strap had to be reduced from 50 mm to 40 mm and any face that was to be bonded to another required a light sanding.

Once the straps had been milled, the specimens were taken to Western Archrib for construction. Glulam bonding adhesive (phenolic resorcinol formaldehyde) was taken from the production line in the plant and applied to the bonding surface of the straps. The straps were then bonded to the specimens and the composite specimens placed in the pressure jigs in the plant. The minimum bonding parameters used in the construction of the original glulam beams include a pressure of at least 690 kPa, at a temperature greater than 20°C for a period of no less than 9 hours. In general, specimens for this study remained under a pressure greater than the required 690 kPa for a minimum of 22 hours at a temperature of approximately 24°C, after which the specimens were released from the jigs.

After adhesion of the strap, specimens were inspected to ensure adequate squeeze out of the bonding adhesive from the joint between the strap and the adjacent wood lam and any deficiencies noted. The specimens were then ready for testing.

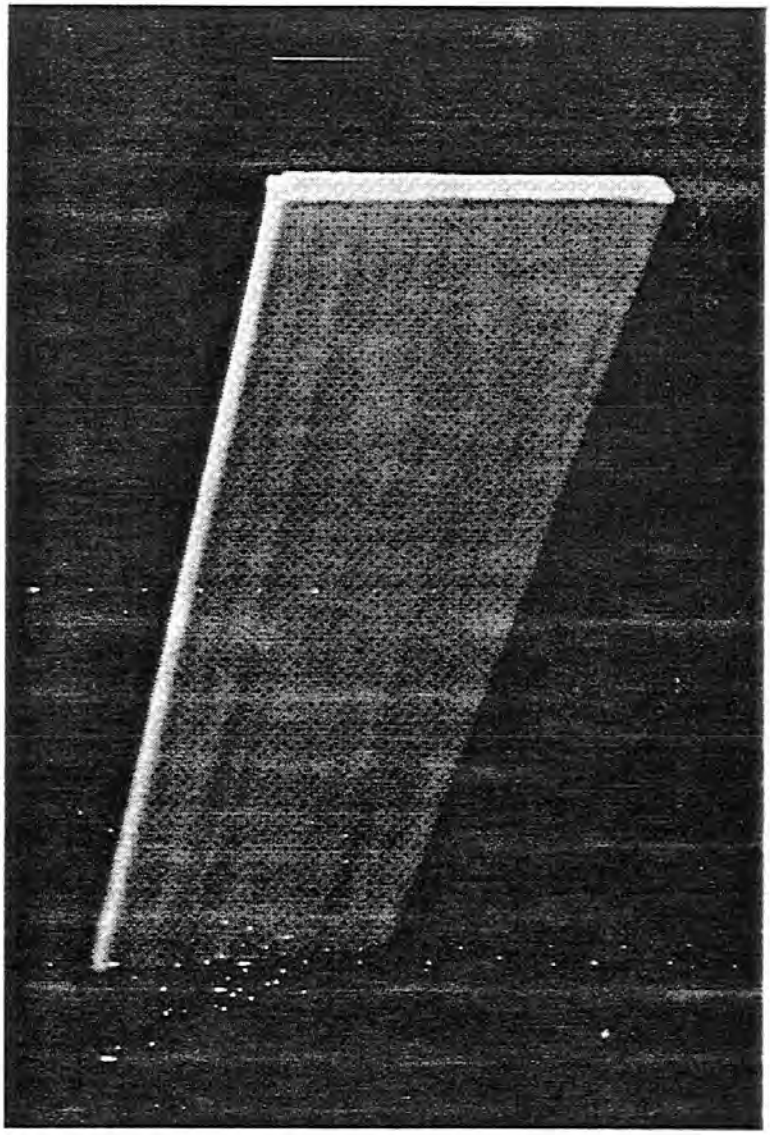

Figure 2.1
Photo of Pultruded Glass Fiber Strap

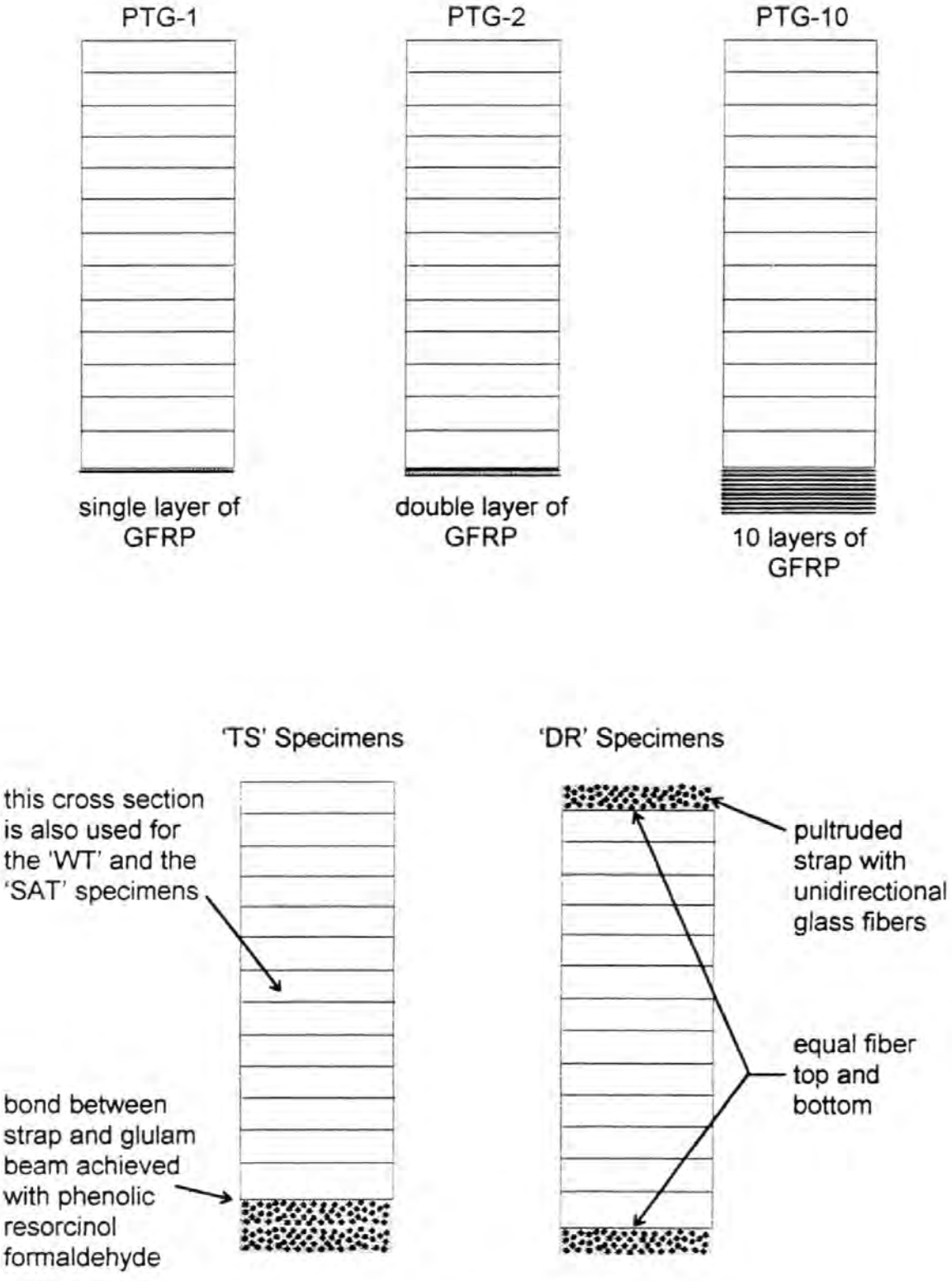

Figure 2.2
Schematic of Main Investigation Reinforcing Patterns

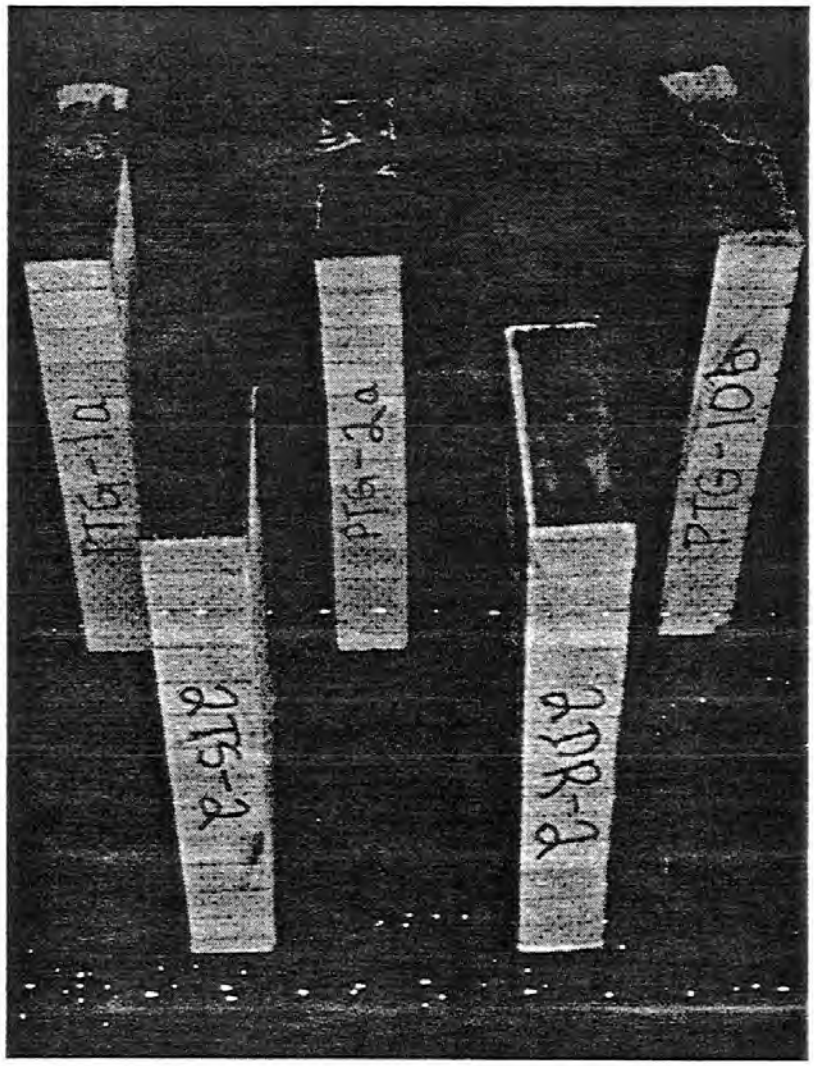

Figure 2.3
Photo of Main Investigation Reinforcing Schemes

Compression Test Specimen:

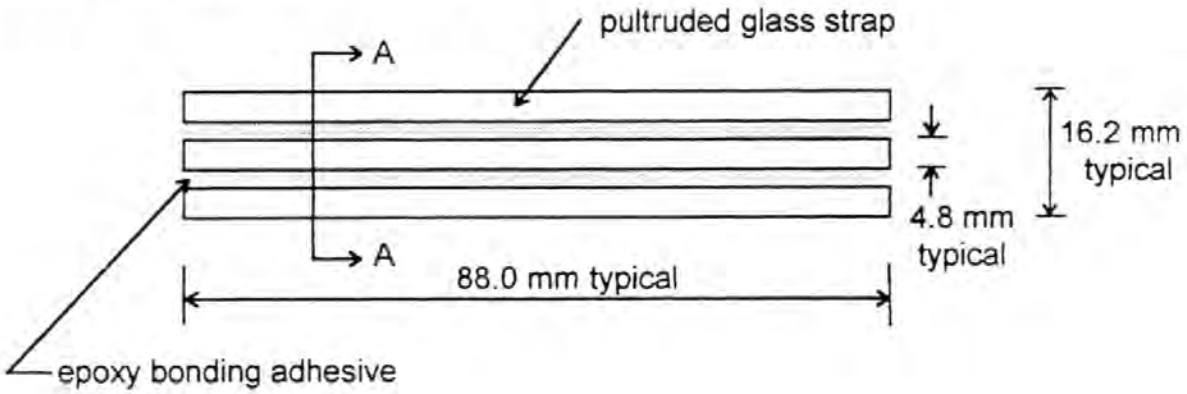

Section A-A:

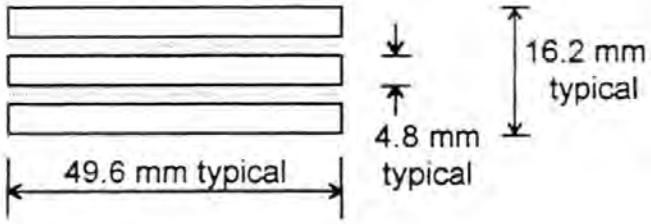

Tension Test Specimen:
(not to scale)

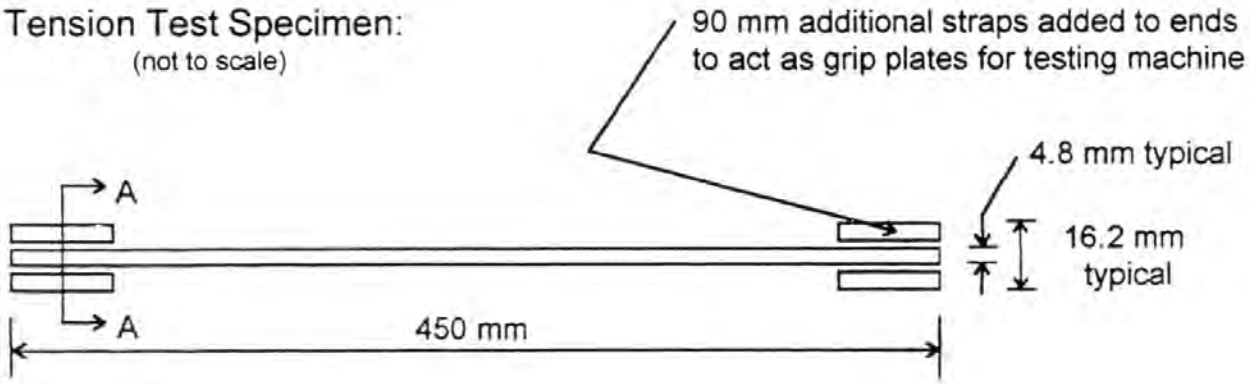

Figure 2.4
Pultruded Strap Material Test Specimens

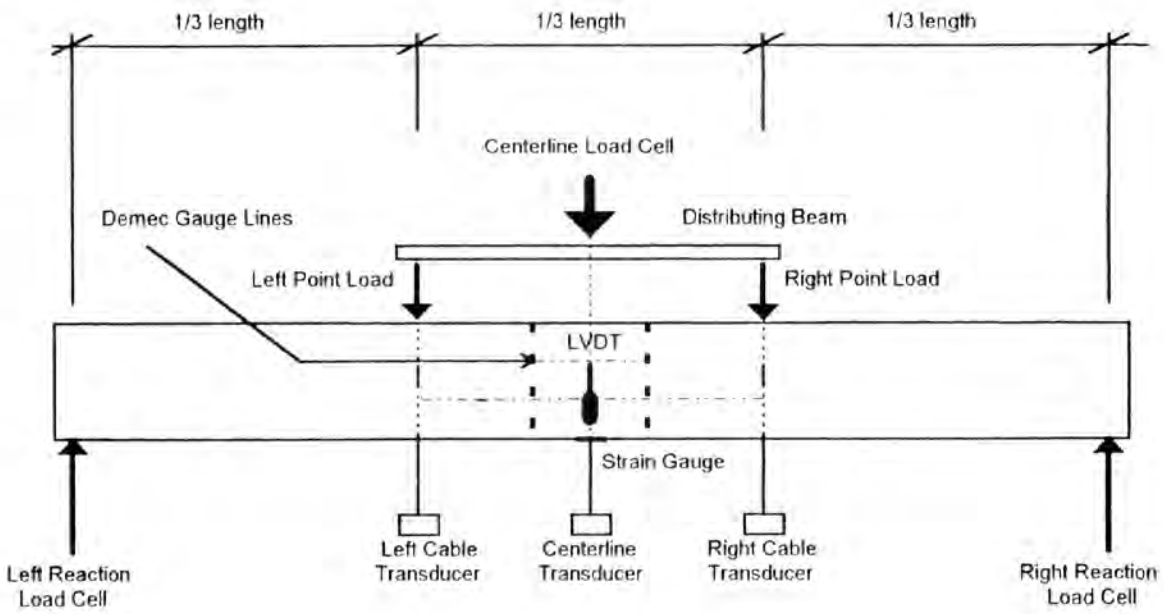

Figure 2.5
Schematic of Test Set Up

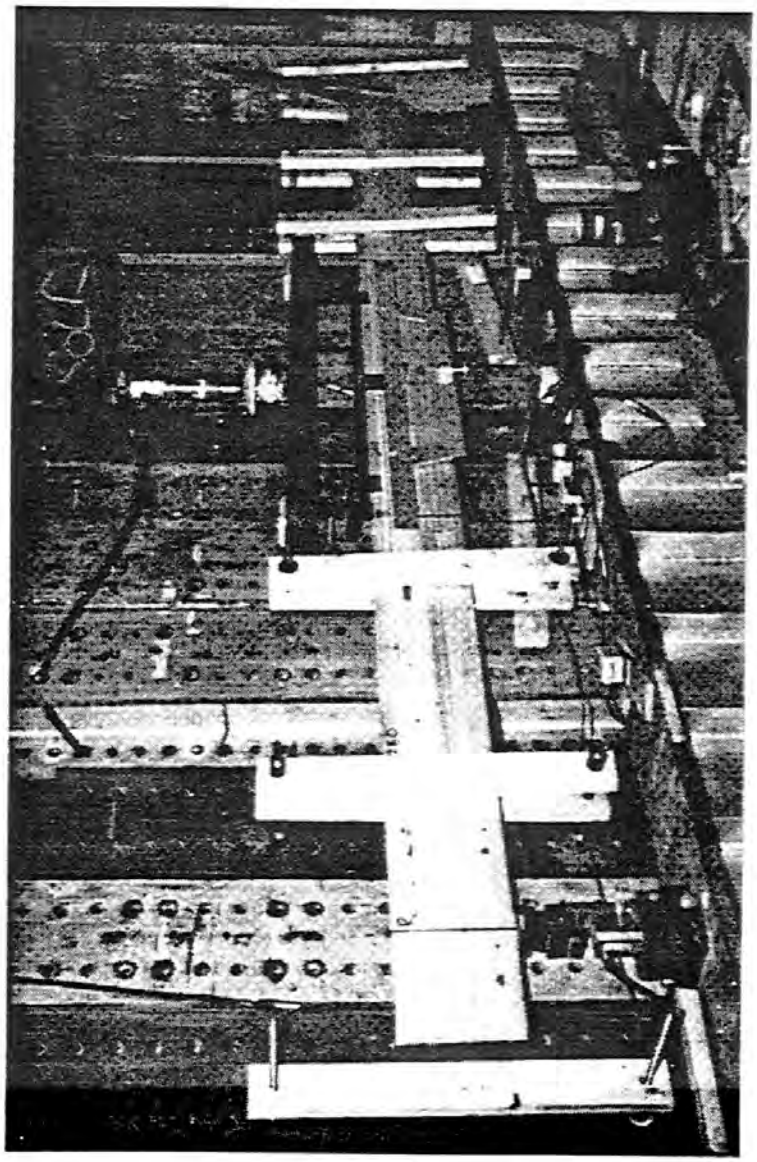

Figure 2.6
Photo of Test Set Up

3.0 TEST RESULTS AND ANALYSIS

3.1 Material Test Results

3.1.1 Wood Compression Test (WCT) Results

A total of five wood compression test specimens were constructed and tested, according to ASTM Standard D143-94 (1994), to determine the ultimate compressive capacity of the glulam timber used in this program. Figure 3.1 shows a typical specimen in the testing apparatus. The specimen dimensions and results are summarized in Table 3.1.

Table 3.1 Results of Wood Compression Tests

Specimen ID	Width (mm)	Depth (mm)	Cross Sectional Area (mm^2)	Length (mm)	Peak Failure Load (kN)	σ_{cmax} at failure (MPa)
WCT1	26.61	26.67	709.7	102.77	39.22	55.3
WCT2	26.23	26.34	690.9	102.95	41.68	60.3
WCT3	26.55	26.48	703.0	102.78	37.02	52.7
WCT4	26.42	26.69	705.2	102.94	40.87	58.0
WCT5	26.61	26.31	700.1	102.87	39.91	57.0
mean						56.7

All specimens failed due to crushing of the cross section. Load deflection plots were generated for each specimen. A typical plot is presented in Figure 3.2.

3.1.2 Wood Tension Test (WTT) Results

A total of four wood tension coupons were tested to determine the ultimate tensile capacity of the timber used in the construction of the glulam beams. Specimens had the typical tension coupon geometry and were constructed in accordance with ASTM Standard D143-94 (1994). Figure 3.3 shows a typical specimen in the test set-up. The specimen dimensions and test results are summarized in Table 3.2.

Table 3.2 Results of Wood Tension Tests

Specimen ID	Width (mm)	Thickness (mm)	Cross Sectional Area (mm^2)	Peak Failure Load (kN)	σ_{tmax} at failure (MPa)
WTT1	13.19	9.66	127.4	7.94	62.3
WTT2	13.21	6.65	87.8	8.58	97.7
WTT3	13.09	9.71	127.1	6.48	51.0
WTT4	13.01	6.74	87.7	8.01	91.3
mean					75.6

All specimens failed due to tensile fracture in the necked region, close to the mid-height of the specimen. Load deflection plots were generated for each specimen. A typical plot is given in Figure 3.4.

3.1.3 Wood Shear Test (WST) Results

A total of four specimens were tested to determine the ultimate shear capacity of the timber used in the construction of the glulam beams. Testing of the shear specimens was conducted at Western Archrib Limited of Edmonton. Test specifications were based on Clause 6 of CSA Standard 0122 (1989). Figure 3.5 shows a typical specimen in the test set-up. Table 3.3 presents the dimensions and test results of the wood shear tests.

Table 3.3 Results of Wood Shear Tests

Specimen ID	Width of Shear Plane (mm)	Height of Shear Plane (mm)	Area of Shear Plane (mm^2)	Ultimate Shear Stress (MPa)
WST1	39.28	50.61	1988	9.63
WST2	39.18	50.45	1977	5.96
WST3	39.86	50.53	2014	10.4
WST4	40.03	50.60	2026	9.99
mean				9.00

All specimens failed due to shear parallel to the grain in the wood. There was no evidence of any glueline failure.

3.1.4 Pultruded Glass Fiber Strap Tension Test Results

A total of six pultruded glass fiber strap tension test specimens were constructed and tested, using ASTM D3379-75 as a guide. In the construction of the main specimens, the pultruded straps had to receive a surface preparation on the faces that were to be bonded to either a wood surface or another pultruded strap. In the material tests, three specimens with single-sided surface preparation (SSTS) and three specimens with double-sided preparation (DSTS) were tested. Figure 3.6 shows a typical specimen during testing. Table 3.4 presents specimen dimensions and the test results.

Table 3.4 Results of Pultruded Strap Tension Tests

Specimen ID	Width (mm)	Depth (mm)	Gross Area (mm^2)	Peak Failure Load (kN)	MOE (MPa)	% Fiber Fraction (%)	σ_{tmax} (MPa)
SSTS1	49.61	4.82	239.1	109.34	34417	46.7	457.3
SSTS2	49.65	4.80	238.3	121.01	33977	46.1	507.8
SSTS3	50.02	4.77	238.6	101.61	36153	49.1	425.9
DSTS1	49.53	4.94	244.7	139.97	36052	48.9	572.0
DSTS2	49.75	4.81	239.3	135.51	38180	51.8	566.3
DSTS3	49.68	4.74	235.5	108.19	40520	55.0	459.4
average					36551	49.6	498.1

Specimens were loaded to tensile fracture. A typical load-deflection plot is presented in Figure 3.7. From the slope of the linear portion of the respective plots and equation 3-1, the MOE for each specimen was determined.

$$E = \frac{P}{A\,\varepsilon} \qquad \text{[eq. 3-1]}$$

where:

E = MOE of strap (MPa)
P = applied tensile load (N)
A = area of fiber (mm^2)
ε = extensometer strain (mm/mm)

It should be noted that, although Figure 3.7 shows a load vs. overall deflection plot, the 50 mm extensometer strain data were used in the regression analysis to determine the slope of the linear portion of the plot to exclude the end effects from the grips. Figure 3.7 is plotted with the stroke data to show the non-linear behaviour as the load increased beyond the elastic limit because the extensometer had to be removed to protect it at specimen fracture.

One of the primary unknowns for the pultruded glass strap was the fiber to resin ratio. The manufacturer of the strap uses a variety of fiber fractions in the construction of these straps, so it was necessary to determine the fiber content of the strap for further analysis in this project. The fiber content was determined by dividing the strap MOE by the MOE for the unbonded glass fiber (73700 MPa). The respective fiber fractions are given in Table 3.4.

3.1.5 Pultruded Glass Fiber Strap Compression Test Results

A total of four pultruded glass fiber strap compression test specimens were constructed and tested. ASTM D3410/D3410M outlines the procedure for testing pultruded fiber reinforced plastics. However, due to the limitations imposed by the size of the specimen produced by the manufacturer and the limitations of the available equipment for testing the pultruded strap in compression, it was not possible to adhere to the recommended specimen size specified in ASTM D3410/D3410M. Using the cross section of the manufactured pultruded straps, three 90 mm lengths of the strap were bonded together using a high bond epoxy in order to create a specimen with sufficient dimensions that a compression failure would occur before buckling during loading. Figure 3.8 shows a typical specimen in the test set-up.

The specimen dimensions and test results are summarized in Table 3.5.

Table 3.5 Results of Pultruded Strap Compression Tests

Specimen ID	Width (mm)	Depth (mm)	Gross Area (mm^2)	Peak Failure Load (kN)	MOE (MPa)	σ_{cmax} (MPa)
SCT1	49.58	14.43	715.4	142.3	12812	198.9
SCT2	49.65	14.52	720.1	150.8	14878	209.4
SCT3	49.60	14.38	713.2	138.0	15791	193.5
average					14494	200.6

According to the manufacturer, the MOE of the strap should be equal in both tension and compression. Clearly, the compression test results do not agree with the results obtained in the pultruded glass strap tension tests. Examination of the compression test specimens showed that all specimens failed in the polyvinyl ester bonding adhesive used in the manufacturing of the pultruded strap, with no evidence of fiber crushing. Considering these factors, it was concluded that the results were indicative of an adhesive failure and therefore should not agree with the tension test results. Consequently, due to compression test limitations, it was assumed that the material properties determined in the tension test results would be used as the material properties for the strap in both tension and compression, as recommended by the manufacturer.

3.1.6 Specimen Moisture Contents

The moisture content of each specimen was determined immediately after testing. Method B - Oven-Drying (Secondary) outlined in Clause 6 of ASTM D4442-92 (1992) was used in this project. Moisture content samples were cut from the center portion of the specimen. Each specimen measured a nominal 50 mm by 50 mm by 25 mm, with the 25 mm dimension being parallel to the grain of the sample. Two moisture content samples, labeled 'a' and 'b' respectively, were cut from each test specimen to serve as a confirmation of the result.

The moisture content samples were dried at an average temperature of 102.1°C until there was no appreciable change in the final mass readings. The drying period ranged from a minimum of 49.5 hours to a maximum of 62.5 hours.

The results from the two determinations for each sample are given in Table 3.6, along with the mean of each of these test pairs.

In addition to recording the moisture content at the time of testing, the specimens that were subjected to adverse environmental conditions, specifically the '1WT' and the '1SAT' series, had their moisture contents monitored on a regular basis after the initial exposure to the water environment. Table 3.7 presents these moisture contents and the time at which they were recorded. The column labeled 'Event' describes what happened to the specimens on that particular day. 'Submerged' indicates that the specimens were placed into the water tank and 'removed' indicates that the specimens were taken out.

Table 3.6 Specimen Moisture Content at Time of Testing

Specimen ID	Trial 'a' Moisture Content (%)	Trial 'b' Moisture Content (%)	Mean Moisture Content (%)
PTN-1	6.71	n/a	6.7
PTN-2	7.73	n/a	7.7
PTN-3	6.54	6.59	6.6
PTN-4	7.06	7.07	7.1
PTG-1a	6.17	n/a	6.2
PTG-1b	7.61	7.24	7.4
PTG-2a	8.04	n/a	8.0
PTG-2b	8.22	8.31	8.3
PTG-10a	7.79	8.01	7.9
PTG-10b	6.43	6.71	6.6
1TS-1	7.32	6.89	7.1
1TS-2	7.21	7.06	7.1
1TS-3	7.25	6.62	6.9
1TS-4	6.67	6.37	6.5
1TS-5	6.51	6.69	6.6
1TS-6	7.95	7.03	7.5
2TS-1	7.49	7.23	7.4
2TS-2	7.05	6.65	6.9
4TS-1	8.94	7.96	8.5
4TS-2	10.20	8.79	9.5
8TS-1	8.60	9.31	9.0
8TS-2	8.36	7.65	8.0
2DR-1	9.09	8.10	8.6
2DR-2	9.06	8.87	9.0
4DR-1	9.19	9.07	9.1
4DR-2	8.90	8.11	8.5
8DR-1	8.57	9.02	8.8
8DR-2	7.86	7.44	7.6
1WT-1	7.33	7.56	7.4
1WT-2	7.49	729	7.4
1WT-3	7.58	7.46	7.5
1SAT-1	7.31	7.04	7.2
PT12-1	8.72	8.69	8.7
PT12-2	7.42	6.96	7.2
2T12-1	6.67	6.82	6.7
2T12-2	9.01	9.24	9.1
2D12-1	7.43	7.67	7.6
2D12-2	8.23	8.91	8.6

Table 3.7 Specimen Moisture Content (M.C.) of Weathered Specimens

Day	'1WT' Event	M.C. of 1WT-1 (%)	M.C. of 1WT-2 (%)	M.C. of 1WT-3 (%)	'1SAT' Event	M.C. of 1SAT-1 (%)
0	submerged	9.8	8.8	8.4	submerged	9.2
1	removed	22.4	20.9	21.2		
7	submerged	13.2	14.1	14.0	removed	34.2
8	removed	26.8	25.5	23.9		
14	submerged	15.4	16.7	13.8		24.4
15	removed	29.2	28.2	25.5		
21	submerged	16.1	17.0	14.0		16.3
22	removed	30.1	31.5	26.6		
28	submerged	16.4	16.8	14.7		
29	removed	30.4	33.3	27.0		10.6
35	submerged	16.2	17.4	15.0		
36	removed	60.2	33.0	26.9		8.2
42	submerged	17.7	16.7	15.3		
43	removed	30.4	33.7	26.7		
49	submerged	14.8	17.5	15.3		
50	removed	30.8	33.6	26.9		7.3
56		16.7	16.6	14.2		
66		8.2	7.9	8.1		
74		7.4	7.4	7.5		7.2

Figure 3.9 provides a graphical representation of the moisture content fluctuation of the specimens subjected to adverse conditions.

3.2 Unreinforced Beam Specimen Results

A total of six unreinforced beam specimens were tested. Of these six beams, four were the standard 240 mm deep beams used for the majority of the testing program. The remaining two were used as the reference for the 300 mm deep beams tested in the size comparison analysis.

The results of this set of specimens were used to determine the strength enhancement ratios for the reinforced specimens. All specimens tested failed due to tensile fracture in the extreme tension lams of the specimen.

3.2.1 Unreinforced 240 mm Deep Specimens

Specimens in this series were labeled as 'PTN'. Table 3.8 presents the strength test results for the 240 mm deep unreinforced beams and well as the stresses developed in the beams.

σ_{cmax} is the maximum compressive stress developed in each beam and was calculated using the bending stress formula given in equation 3-2.

$$\sigma_{max} = \frac{My}{I} \qquad \text{[eq. 3-2]}$$

where:

M = applied moment (kN*m)
y = distance from neutral axis to stress location (mm)
I = transformed wood moment of inertia (mm^4)

σ_{tmax} is the maximum tensile stress developed in each beam and was also calculated using the bending stress formula given in equation 3-2. τ_{max} is the maximum shear stress developed in each beam. This maximum occurs at the neutral axis and was calculated using the shear stress formula in equation 3-3.

$$\tau_{max} = \frac{VQ}{It} \qquad \text{[eq. 3-3]}$$

where:

V = applied shear (N)
Q = first moment of area (mm^3)
I = transformed wood moment of inertia (mm^4)
t = thickness of specimen at τ_{max} (mm)

Table 3.8 Strength Test Results for Unreinforced 240 mm Deep Beams

Specimen ID	Width (mm)	Depth (mm)	Observed Mode(s) of Failure	Failure Load (kN)	σ_{cmax} (MPa)	σ_{tmax} (MPa)	τ_{max} (MPa)
PTN-1	39.8	241.2	tension fracture at 12 mm knot	20.9	34.7	34.7	1.71
PTN-2	40.4	240.4	finger joint fracture in bottom tension lam	22.1	36.4	36.4	1.75
PTN-3	40.3	238.7	tension fracture at 15 mm knot	21.2	35.5	35.5	1.87
PTN-4	40.4	239.9	tension fracture at 8 mm & 16 mm knots	22.3	36.9	36.9	1.91
mean				21.6	35.9	35.9	1.81

All specimens failed due to tensile fracture in the lower lams of the specimen. A typical tensile fracture is shown in Figure 3.10.

In addition to the load characteristics, the apparent and shear free stiffness were calculated for each of the specimens as a reference point for the reinforced specimens. Three load-deflection plots were generated for each specimen. A typical set of these three graphs and their respective regression analysis is given in Figure 3.11. The first

plot shows the relationship between the centerline load and the centerline deflection. From this graph, the apparent stiffness was calculated using the slope of the linear portion of the graph and equation 3.4.

$$\Delta = \frac{23PL^3}{1296E_aI} \qquad \text{[eq. 3-4]}$$

where:

P = total applied load (N)
L = total member length (mm)
E_aI = apparent stiffness ($N*mm^2$)

The second and third Load-Deflection plots presented in Figure 3.11 show the relationship between the centerline load and the deflection over the zero shear span. The second graph is based on the data collected using the cable transducer and the third one is based on the data collected using the LVDT set up. Because of the small deflection recorded over the zero shear span and the increased possibility of error, two methods were used to collect the data for confirmation. Given the increased sensitivity and the lower potential for error, the shear free results used for the data presentation and analysis sections of this project come from the LVDT data. However, in cases of clear error the cable transducer data were used. Table 3.9 gives the stiffness results for the unreinforced beams.

Table 3.9 Stiffness Test Results for Unreinforced 240 mm Deep Beams

Specimen ID	Moment of Inertia (mm^4)	Apparent Stiffness ($N*mm^2$)	Apparent MOE (MPa)	Shear Free Stiffness ($N*mm^2$)	Shear Free MOE (MPa)
PTN-1	46.48×10^6	5.537×10^{11}	11913	5.594×10^{11}	12036
PTN-2	46.72×10^6	5.051×10^{11}	10811	4.837×10^{11}	10353
PTN-3	45.56×10^6	4.995×10^{11}	10964	5.503×10^{11}	12079
PTN-4	46.43×10^6	4.842×10^{11}	10429	5.276×10^{11}	11363
mean	46.3×10^6	5.106×10^{11}	11029	5.303×10^{11}	11458

The shear free, or true, stiffness was calculated from the slope of the linear portion of the appropriate graph and equation 3-5.

$$\Delta = \frac{Pa^3}{16E_tI} \qquad \text{[eq. 3-5]}$$

where:

P = total applied load (N)
a = shear free span length (mm)
E_tI = true stiffness ($N*mm^2$)

3.2.2 Unreinforced 300 mm Deep Beams

The unreinforced 300 mm deep beams were labeled with 'PT12' (12 inches deep). Table 3.10 gives the dimensions and strength results for the unreinforced 300 mm deep beams as well as the stresses developed in the beams.

Table 3.10 Strength Test Results for Unreinforced 300 mm Deep Beams

Specimen ID	Width (mm)	Depth (mm)	Observed Mode(s) of Failure	Failure Load (kN)	σ_{cmax} (MPa)	σ_{tmax} (MPa)	τ_{max} (MPa)
PT12-1	40.0	301.0	tension fracture at 8 mm knot	37.6	39.9	39.9	2.28
PT12-2	40.3	301.7	tension fracture at 7 mm knot	36.0	37.7	37.7	2.23
mean				36.8	38.8	38.8	2.26

In addition to the load characteristics, the apparent and shear free stiffness were calculated for each of these specimens as a reference point for the other 300 mm deep specimens. As shown in Figure 3.11 for the 240 mm deep beams, three load-deflection plots were generated for each PT12 specimen, from which the respective apparent or shear free MOE's were calculated. Table 3.11 gives the stiffness results for the unreinforced 300 mm deep beams.

Table 3.11 Stiffness Test Results for Unreinforced 300 mm Deep Beams

Specimen ID	Moment of Inertia (mm^4)	Apparent Stiffness ($N*mm^2$)	Apparent MOE (MPa)	Shear Free Stiffness ($N*mm^2$)	Shear Free MOE (MPa)
PT12-1	90.84×10^6	9.700×10^{11}	10678	10.90×10^{11}	12002
PT12-2	92.07×10^6	10.23×10^{11}	11110	11.35×10^{11}	12328
mean	91.46×10^6	9.965×10^{11}	10894	11.13×10^{11}	12165

3.3 Reinforced Specimens

A total of 30 reinforced beams were tested in the main program. Since the results from the preliminary study specimens PTG-1 (hereafter PTG-1b) and PTG-2 (hereafter PTG-2a) fit directly into the main program investigation, their results were included with the main study specimens, making 32 the total number of reinforced beams used in this study. Each of these beams fell into one of four categories: specimens with tensile reinforcement only, specimens with equal compressive and tensile reinforcement, specimens subjected to adverse environmental conditions, and specimens designed to provide a size comparison. Each of these specimens were non-destructively preloaded with no reinforcing to approximately 50% of their unreinforced capacity. This was done so that unreinforced stiffness data could be collected to later determine the exact

stiffness enhancement achieved with the reinforcement. In the following sections, both the unreinforced and reinforced stiffness data are presented.

The reinforced stiffness was calculated using the same procedure that was used to determine the unreinforced stiffness, except the moment of inertia was calculated using a transformed section. Load-deflection data was plotted and the slopes of the respective graphs were used in equation 3-4 and equation 3-5 to determine the reinforced specimen's apparent and shear free stiffness and the corresponding MOE.

All of the reinforced specimens failed in one of the following four different modes: tensile fracture, compressive crushing, compressive buckling of the top lams, or shear failure. Figures 3.12, 3.13, 3.14, and 3.15 show an example of each of these respective failure modes.

3.3.1 Specimens with Only Tensile Reinforcement

A total of 18 specimens were reinforced with glass fiber only along the tension face of the beam, including PTG-1b and PTG-2a. Six of these specimens received multiple layers of glass fiber tow sheets and the remainder were reinforced with the pultruded glass straps. Table 3.12 presents the dimensions and strength results for the specimens with glass fiber reinforcement only in the tension zone of the beam.

Table 3.12 Strength Test Results for Tensile Reinforced Specimens

Specimen ID	Width (mm)	Depth (mm)	Observed Mode(s) of Failure	Peak Load (kN)	σ_{cmax} (MPa)	σ_{tmax} (MPa)	τ_{max} (MPa)
PTG-1a	40.5	241.1	tension lam-9mm knot	24.2	39.3	39.1	1.57
PTG-1b	40.2	239.3	tension fingerjoint	28.3	46.9	46.6	1.85
PTG-2a	39.9	241.3	tension lam-13mm knot	26.3	43.0	42.6	2.03
PTG-2b	40.2	239.8	tension lam fracture	31.0	51.0	50.5	2.48
PTG-10a	40.0	240.8	buckling of top 2 lams	26.8	42.3	40.2	2.10
PTG-10b	40.1	239.5	crushing & tension-8mm knot	34.4	54.5	51.6	2.62
1TS-1	39.4	238.3	shear & tension lam fingerjoint	38.0	58.6	52.1	2.85
1TS-2	40.2	239.2	shear & tension lam fracture	27.9	41.9	37.3	2.27
1TS-3	40.4	239.0	tension lam-9mm knot	28.5	42.6	37.9	2.17
1TS-4	39.5	238.3	shear & tension lam fingerjoint	31.4	48.0	42.5	2.46
1TS-5	40.0	238.8	shear & tension lam	32.1	49.3	44.7	2.51
1TS-6	39.2	238.9	delamination due to poor bond	24.4	37.7	33.7	1.93
2TS-1	40.2	239.3	buckling of top lam	34.6	47.8	38.4	2.41
2TS-2	39.3	239.5	buckling & crushing-top 3 lams	37.2	51.9	41.1	2.84
4TS-1	39.8	241.0	crushing in top 2 lams & shear	41.7	48.4	29.9	2.78
4TS-2	40.6	241.3	top lam crushing & shear	42.7	50.5	33.8	2.80
8TS-1	39.4	241.4	shear	48.3	46.7	19.9	2.84
8TS-2	40.3	241.0	shear	49.8	47.6	20.7	2.43

Both the unreinforced and reinforced apparent and shear free MOE's were determined for each of these specimens. These were again determined from the slope of the load-deflection plot and equation 3-4 and equation 3-5 respectively. Figure 3.16 shows a series of these plots with their respective regression analysis for a typical reinforced specimen. Table 3.13 presents the apparent stiffness results for the specimens with tensile reinforcing only.

Table 3.13 Apparent Stiffness Test Results of Tensile Reinforced Specimens

Beam ID	Unreinf. Moment of Inertia 10^6 (mm^4)	Unreinf. Apparent Stiffness 10^{11} ($N*mm^2$)	Unreinf. Apparent MOE (MPa)	Reinf. Moment of Inertia 10^6 (mm^4)	Reinf. Apparent Stiffness 10^{11} ($N*mm^2$)	Reinf. Apparent MOE (MPa)
PTG-1a	47.30	5.183	10957	47.68	5.123	10745
PTG-1b	45.96	5.086	11066	46.34	5.382	11614
PTG-2a	46.72	5.186	11101	47.43	5.539	11678
PTG-2b	46.15	4.936	10696	46.83	5.259	11230
PTG-10a	46.59	5.000	10732	50.10	5.644	11265
PTG-10b	45.95	5.012	10909	49.74	5.652	11363
1TS-1	44.43	5.053*	11374*	52.36	6.162	11769
1TS-2	45.85	5.215*	11374*	53.99	6.376	11810
1TS-3	45.94	5.225*	11374*	54.15	5.910	10914
1TS-4	44.54	5.066*	11374*	52.93	6.076	11480
1TS-5	45.39	5.860	12910	52.13	6.327	12136
1TS-6	44.54	5.501	12352	52.28	5.964	11408
2TS-1	45.91	5.932	12921	61.46	7.083	11525
2TS-2	44.99	5.436	12082	61.28	6.716	10959
4TS-1	46.43	5.162	11117	82.21	7.860	9561
4TS-2	47.54	5.419	11398	78.24	7.567	9672
8TS-1	46.19	4.915	10640	111.95	10.47	9349
8TS-2	47.01	5.179	11016	112.51	10.15	9020

* - for the specimens labeled with an asterisk the mean unreinforced MOE was used in the calculations because this data was unavailable.

Table 3.14 presents the shear free stiffness results. As with the unreinforced specimens, the shear free MOE was calculated from the data collected using the LVDT. In cases where this data was unavailable the data collected using the three cable transducers was substituted.

Table 3.14 Shear Free Stiffness Test Results of Tensile Reinforced Specimens

Beam ID	Unreinf. Moment of Inertia 10^6 (mm^4)	Unreinf. Shear Free Stiffness 10^{11} ($N*mm^2$)	Unreinf. Shear Free MOE (MPa)	Reinf. Moment of Inertia 10^6 (mm^4)	Reinf. Shear Free Stiffness 10^{11} ($N*mm^2$)	Reinf. Shear Free MOE (MPa)
PTG-1a	47.30	5.472	11568	47.67	6.410	13444
PTG-1b	45.96	5.202	11318	46.34	5.701	12302
PTG-2a	46.72	5.569	11921	47.43	7.104	14978
PTG-2b	46.15	5.764	12489	46.83	5.452	11642
PTG-10a	46.59	5.580	11976	50.10	6.102	12180
PTG-10b	45.95	5.033	10953	49.74	6.206	12477
1TS-1	44.43	5.029*	11318*	52.36	7.743	14787
1TS-2	45.85	5.189*	11318*	53.99	6.608	12240
1TS-3	45.94	5.199*	11318*	54.15	6.740	12446
1TS-4	44.54	5.041*	11318*	52.93	6.922	13077
1TS-5	45.39	6.630	14607	52.13	6.551	12567
1TS-6	44.54	5.715	12832	52.28	7.242	13853
2TS-1	45.91	5.826	12689	61.46	8.332	13556
2TS-2	44.99	5.743	12765	61.28	8.225	13422
4TS-1	46.43	5.270	11351	82.21	9.619	11700
4TS-2	47.54	6.274	13198	78.24	10.34	13219
8TS-1	46.19	5.444	11787	111.95	12.64	11295
8TS-2	47.01	5.484	11665	112.51	11.39	10126

* - for the specimens labeled with an asterisk the mean unreinforced MOE was used in the calculations because this data was unavailable.

3.3.2 Specimens with Both Tensile and Compressive Reinforcement

A total of six specimens were reinforced with glass fiber along both the tension face and the compression face of the beam. All of these specimens were reinforced using the pultruded glass straps.

The total number of straps bonded to the individual specimens is indicated in the first digit in the Specimen ID column. Of this total number of straps, half were bonded to the compression face of the specimens and the other half to the tension face.

Table 3.15 presents the dimensions and strength results for the specimens with glass fiber reinforcement in both the tension zone and the compression zone of the beam.

Table 3.15 Strength Test Results for Doubly Reinforced Specimens

Specimen ID	Width (mm)	Depth (mm)	Observed Mode(s) of Failure	Peak Failure Load (kN)	σ_{cmax} (MPa)	σ_{tmax} (MPa)	τ_{max} (MPa)
2DR-1	39.4	241.0	shear & tension fingerjoint	38.7	47.2	47.2	2.79
2DR-2	38.5	239.9	delamination due to poor bond	25.4	30.2	30.4	1.71
4DR-1	39.6	240.2	shear failure	42.5	38.7	38.6	2.79
4DR-2	38.5	240.0	shear & tension failure	47.9	44.6	44.4	3.47
8DR-1	41.1	239.3	shear failure	51.8	31.5	31.1	2.63
8DR-2	41.2	239.1	shear failure	55.6	33.1	33.5	3.22

Table 3.16 presents the unreinforced and reinforced apparent stiffness results for the doubly reinforced specimens.

Table 3.16 Apparent Stiffness Test Results of Doubly Reinforced Specimens

Beam ID	Unreinf. Moment of Inertia 10^6 (mm^4)	Unreinf. Apparent Stiffness 10^{11} ($N*mm^2$)	Unreinf. Apparent MOE (MPa)	Reinf. Moment of Inertia 10^6 (mm^4)	Reinf. Apparent Stiffness 10^{11} ($N*mm^2$)	Reinf. Apparent MOE (MPa)
2DR-1	45.96	5.289	11508	63.22	6.643	10507
2DR-2	44.30	4.734	10687	64.38	5.950	9243
4DR-1	45.73	4.843	10591	84.52	7.786	9212
4DR-2	44.35	4.953	11167	82.52	8.350	10118
8DR-1	46.93	5.420	11549	126.73	12.14	9582
8DR-2	46.93	5.251	11188	127.93	11.96	9350

Table 3.17 presents the unreinforced and reinforced shear free stiffness results for the doubly reinforced specimens.

Table 3.17 Shear Free Stiffness Test Results of Doubly Reinforced Specimens

Beam ID	Unreinf. Moment of Inertia 10^6 (mm^4)	Unreinf. Shear Free Stiffness 10^{11} ($N*mm^2$)	Unreinf. Shear Free MOE (MPa)	Reinf. Moment of Inertia 10^6 (mm^4)	Reinf. Shear Free Stiffness 10^{11} ($N*mm^2$)	Reinf. Shear Free MOE (MPa)
2DR-1	45.96	5.714	12432	63.22	7.538	11923
2DR-2	44.30	4.685	10575	64.38	7.075	10990
4DR-1	45.73	5.241	11462	84.52	10.17	12029
4DR-2	44.35	5.090	11476	82.52	10.19	12344
8DR-1	46.93	5.646	12030	126.73	15.23	12016
8DR-2	46.93	5.440	11591	127.93	18.26	14276

3.3.3 Specimens Subjected to Adverse Environmental Conditions

A total of four specimens were reinforced with glass fiber along the tension face and then subjected to adverse environments. All of these specimens were reinforced using the pultruded glass straps.

Specimens with the '1WT' prefix were cycled on a 7-day period. The specimen with the '1SAT' prefix was fully immersed for a 7-day period and then allowed to dry for 7-weeks prior to being tested.

Table 3.18 presents the dimensions and strength results for the specimens subjected to these adverse conditions.

Table 3.18 Strength Test Results for Specimens Exposed to Adverse Conditions

Specimen ID	Width (mm)	Depth (mm)	Observed Mode(s) of Failure	Peak Failure Load (kN)	σ_{tmax} (MPa)	σ_{tmax} (MPa)	τ_{max} (MPa)
1WT-1	40.6	239.1	shear and tension fingerjoint	37.5	55.8	49.6	2.96
1WT-2	39.7	238.9	tension fracture	27.4	41.5	36.8	2.17
1WT-3	39.9	238.7	shear and tension fingerjoint	36.9	56.0	49.9	3.10
1SAT-1	39.4	238.3	tension fracture	28.4	43.5	38.5	2.27

Table 3.19 presents the unreinforced and reinforced apparent stiffness results for the specimens exposed to adverse environmental conditions.

Table 3.19 Apparent Stiffness of Specimens Exposed to Adverse Conditions

Beam ID	Unreinf. Moment of Inertia 10^6 (mm^4)	Unreinf. Apparent Stiffness 10^{11} ($N*mm^2$)	Unreinf. Apparent MOE (MPa)	Reinf. Moment of Inertia 10^6 (mm^4)	Reinf. Apparent Stiffness 10^{11} ($N*mm^2$)	Reinf. Apparent MOE (MPa)
1WT-1	46.22	5.257*	11374*	54.46	5.327	9782
1WT-2	45.15	5.135*	11374*	53.47	5.980	11184
1WT-3	45.22	5.143*	11374*	53.18	5.402	10159
1SAT-1	44.46	5.057*	11374*	52.85	5.630	10653

* - for the specimens labeled with an asterisk the mean unreinforced MOE was used in the calculations because this data was unavailable.

Table 3.20 presents the unreinforced and reinforced shear free stiffness results for the specimens exposed to adverse environmental conditions.

Table 3.20 Shear Free Stiffness of Specimens Exposed to Adverse Conditions

Beam ID	Unreinf. Moment of Inertia 10^6 (mm^4)	Unreinf. Apparent Stiffness 10^{11} ($N*mm^2$)	Unreinf. Apparent MOE (MPa)	Reinf. Moment of Inertia 10^6 (mm^4)	Reinf. Apparent Stiffness 10^{11} ($N*mm^2$)	Reinf. Apparent MOE (MPa)
1WT-1	46.22	5.231*	11318*	54.46	5.970	10962
1WT-2	45.15	5.110*	11318*	53.47	7.231	13523
1WT-3	45.22	5.118*	11318*	53.18	6.210	11677
1SAT-1	44.46	5.032*	11318*	52.85	5.969	11295

* - for the specimens labeled with an asterisk the mean unreinforced MOE was used in the calculations because this data was unavailable.

3.3.4 Reinforced 300 mm Deep Specimens

A total of four specimens 300 mm deep were tested. Two of the specimens were reinforced with glass fiber straps in only the tension zone and two were reinforced with glass fiber straps along both the tension face and the compression face of the beam. The specimens with only the tensile reinforcement have the specimen identification code '2T12' and the specimens with the double reinforcing are identified with '2D12'. All of these specimens were reinforced using the pultruded glass straps. It was noted that all of the reinforced deep beams failed in shear. Table 3.21 presents the dimensions and strength results for the reinforced specimens with a beam depth of 300 mm.

Table 3.21 Strength Test Results for 300 mm Deep Reinforced Specimens

Specimen ID	Width (mm)	Depth (mm)	Observed Mode(s) of Failure	Peak Failure Load (kN)	σ_{cmax} (MPa)	σ_{tmax} (MPa)	τ_{max} (MPa)
2T12-1	41.1	301.2	shear failure	39.3	34.4	28.5	2.50
2T12-2	38.8	301.6	shear failure	39.5	36.3	29.9	2.25
2D12-1	40.1	300.3	buckling in top lam then shear failure	42.1	35.3	35.2	2.36
2D12-2	39.4	300.0	shear failure	36.8	32.3	32.3	2.18

Table 3.22 presents the unreinforced and reinforced apparent stiffness results for the 300 mm deep reinforced specimens.

Table 3.22 Apparent Stiffness Results of 300 mm Deep Reinforced Specimens

Beam ID	Unreinf. Moment of Inertia 10^6 (mm^4)	Unreinf. Apparent Stiffness 10^{11} ($N*mm^2$)	Unreinf. Apparent MOE (MPa)	Reinf. Moment of Inertia 10^6 (mm^4)	Reinf. Apparent Stiffness 10^{11} ($N*mm^2$)	Reinf. Apparent MOE (MPa)
2T12-1	93.59	11.00	11750	120.54	13.59	11272
2T12-2	88.66	8.745	9864	115.16	11.81	10259
2D12-1	90.45	9.795	10829	114.72	14.46	12605
2D12-2	88.52	8.901	10056	109.35	11.63	10635

Table 3.23 presents the unreinforced and reinforced shear free stiffness results for the 300 mm deep reinforced specimens.

Table 3.23 Shear Free Stiffness Results of 300 mm Deep Reinforced Specimens

Beam ID	Unreinf. Moment of Inertia 10^6 (mm^4)	Unreinf. Apparent Stiffness 10^{11} ($N*mm^2$)	Unreinf. Apparent MOE (MPa)	Reinf. Moment of Inertia 10^6 (mm^4)	Reinf. Apparent Stiffness 10^{11} ($N*mm^2$)	Reinf. Apparent MOE (MPa)
2T12-1	93.59	10.73	11460	120.54	13.29	11028
2T12-2	88.66	8.866	10001	115.16	11.09	9626
2D12-1	90.45	11.50	12718	114.72	14.37	12527
2D12-2	88.52	9.919	11205	109.35	10.97	10037

3.4 Determination of Mechanical Property Enhancement

3.4.1 Determination of Strength Enhancement

The strength enhancement of each specimen was determined as the percent increase in strength of the reinforced specimens when compared with the mean of the unreinforced specimens of corresponding depth. For the specimens with a nominal depth of 240 mm, the results of the 'PTN' specimens in Table 3.8 were used to determine the strength enhancement. For the specimens with a nominal depth of 300 mm, the results of the 'PT12' specimens in Table 3.10 were used.

The fiber fraction for each specimen with pultruded glass fiber straps was calculated based on the 49.6% glass fiber fraction of the pultruded straps determined from the material property tests in section 3.1.4. Since the glass tow sheets were applied as raw glass fiber and could be measured directly, a 100% fiber fraction was used for the tow sheets.

Table 3.24 presents the mean values for the fiber fraction of glass fiber, the failure load and the percent increase in strength of the reinforced specimen as compared to the unreinforced ones for each respective reinforcing scheme.

Table 3.24 Strength Enhancement of Reinforced Specimens

Specimen ID	Number of Specimens	Fiber Fraction (%)	Actual Failure Load (kN)	% Strength Enhancement (%)
PTN	4	0.00	21.6	0.00
PT12	2	0.00	36.8	0.00
PTG-1	2	0.042	26.3	21.5
PTG-2	2	0.083	28.7	32.6
PTG-10	2	0.414	30.6	41.7
1TS	6	0.965	31.6	46.2
2TS	2	2.00	35.9	66.2
4TS	2	3.82	42.2	95.4
8TS	2	7.06	49.1	127.1
2DR	2	1.97	38.7	79.2
4DR	2	3.78	45.2	109.3
8DR	2	6.74	53.7	148.6
1WT	3	0.962	33.9	57.1
1SAT	1	0.974	28.4	31.5
2T12	2	1.59	39.4	7.1
2D12	2	1.53	39.5	7.2

Note: In the cases where there was premature delamination of the reinforcement due to poor bond between the wood and the adjacent reinforcing, those specimens (1TS-6 and 2DR-2) were neglected from the averages determined in Table 3.24.

3.4.2 Determination of Stiffness Enhancement

Unlike the determination of the strength enhancement, the stiffness (EI) enhancement for the individual specimens was determined exactly. Since the specimens were also 50% pre-loaded prior to reinforcing, an unreinforced stiffness for the individual specimens was available, and the exact stiffness increase was determined.

The enhancement of both the apparent and the shear free stiffness were calculated. Table 3.25 presents the mean apparent stiffness enhancement for the reinforced specimens and Table 3.26 presents the mean shear free stiffness enhancement for the reinforced specimens.

Table 3.25 Apparent Stiffness Enhancement of Reinforced Specimens

Specimen ID	Fiber Fraction (%)	Unreinforced Apparent Stiffness (x 10^{11} N*mm^2)	Reinforced Apparent Stiffness (x 10^{11} N*mm^2)	% Apparent Stiffness Enhancement (%)
PTN	0.00	5.106	n/a	0.00
PT12	0.00	9.965	n/a	0.00
PTG-1	0.042	5.135	5.253	2.30
PTG-2	0.083	5.061	5.399	6.68
PTG-10	0.414	5.006	5.648	12.8
1TS	0.965	5.284	6.170	16.8
2TS	2.00	5.684	6.900	21.4
4TS	3.82	5.291	7.714	45.8
8TS	7.06	5.047	10.31	104.3
2DR	1.97	5.012	6.297	25.6
4DR	3.78	4.898	8.068	64.7
8DR	6.74	5.336	12.05	125.9
1WT	0.962	5.178	5.570	7.56
1SAT	0.974	5.057	5.630	11.3
2T12	1.59	9.873	12.70	28.6
2D12	1.53	9.348	13.05	39.6

Table 3.26 Shear Free Stiffness Enhancement of Reinforced Specimens

Specimen ID	Fiber Fraction (%)	Unreinforced Shear Free Stiffness (x 10^{11} N*mm^2)	Reinforced Shear Free Stiffness (x 10^{11} N*mm^2)	% Shear Free Stiffness Enhancement (%)
PTN	0.00	5.303	n/a	0.00
PT12	0.00	11.13	n/a	0.00
PTG-1	0.042	5.337	6.056	13.5
PTG-2	0.083	5.667	6.278	10.8
PTG-10	0.414	5.307	6.154	16.0
1TS	0.965	5.235	7.051	34.7
2TS	2.00	5.785	8.279	43.1
4TS	3.82	5.772	9.980	72.9
8TS	7.06	5.464	12.02	120.0
2DR	1.97	5.200	7.307	40.5
4DR	3.78	5.166	10.18	97.1
8DR	6.74	5.543	16.75	202.1
1WT	0.962	5.153	6.470	25.6
1SAT	0.974	5.032	5.969	18.6
2T12	1.59	9.798	12.19	24.4
2D12	1.53	11.50	14.37	25.0

3.4.3 Determination of Failure Strains

Failure strains at the interface between the wood fiber and the adjacent glass fiber reinforcing were calculated using three different methods. The first method of determining the strain at failure (ε_{max}) was using the bending strain formula given in equation 3-6.

$$\varepsilon_{max} = \frac{My}{EI} \qquad \text{[eq. 3-6]}$$

where:

M = applied moment (kN*m)
y = distance from neutral axis to stress location (mm)
I = transformed wood moment of inertia (mm^4)
E = shear free MOE (MPa)

The second method used to determine ε_{max} involved the data from the demec point readings. In this analysis it was assumed that the material behaved linearly. To test this linearity, plots of the demec data were constructed for each specimen. Figure 3.17 shows a typical demec plot.

From Figure 3.17, it can be observed that the specimens exhibited linear behaviour during loading up to the last recording. However, due to the practical limitations of the demec gauges, failure strains were not recorded directly. In order to determine failure strains from the demec data, it was assumed that the specimens maintained linear behaviour throughout the loading and a regression analysis was done on the available demec data to establish a relationship between the applied load and the demec strains at various depths of the test specimens. Once this relationship was established, a strain was extrapolated for the corresponding failure load. The recognized limitation here is that there may be some non-linear behaviour of the composite construction as it approaches ultimate loading and that the procedure used here may over estimate the actual strain at failure.

To test whether the specimens exhibited any significant inelastic behaviour as the load approached ultimate, the strains recorded using the demec data was compared to the strain values calculated using the bending strain formula in equation 3-6.

The third method used to determine ε_{max} involved the data from the strain gauges which were mounted directly on the glass fiber pultruded straps. Despite the accuracy associated with this particular type of direct measurement, this method had certain limitations. Because of the mechanics of the data acquisition system used, quite often the data for the ultimate load were not recorded. Therefore an extrapolation was required to determine the strain at the ultimate load.

The second limitation of this strain was the strain gauge used. Since composite material specific strain gauges were not available, steel strain gauges were used. At the time of testing, it was unclear how well these gauges would perform in this testing environment. Finally, peak strains were not only recorded in the straps, but also in the wood. Since this type of strain gauge does not lends itself to applications directly onto timber, the use of the gauge was limited. Consequently, it was decided that the main purpose of the strain gauge data was to confirm their accuracy with other methods used so that they might be used in subsequent research of this nature.

Peak strains were recorded or determined for both the compressive and tension faces of the beam specimens. A comparison of the strain determined from the demec data and the strain from the bending strain calculation is provided to determine if the demec data remained linear right up to the failure of the specimen. The percent difference is determined by dividing the difference between the two strain values by the bending strain.

Table 3.27 presents the strain data for each of the 38 specimens, as determined from the three different analysis methods.

From the results in Table 3.27, the average difference for the compressive strain data was found to be 2.54% with a coefficient of variance of 13.67%, and the average difference for the tensile strain data was found to be 6.16% with a coefficient of variance of 12.59%. Since these averages are positive, this means that the demec data strains are slightly greater than the bending strains calculated from equation 3-6. This suggests that there may be some slight inelastic behaviour occurring in the specimens. However, given the magnitude of these average differences, the inelastic effect is very small and the differences observed may be considered well within experimental variation and neglected. Therefore, it may be concluded that the section remains linear throughout loading and that using the strain bending formula in equation 3-6 is an acceptable method for determining the failure strain for the specimens.

A comparison was made between the strains determined from the demec data, the strains calculated using bending theory, and the strains recorded with the strain gauges. This comparison showed that the strains measured form the demec data and the strains calculated using the bending theory were nearly identical, but that the strain gauge data was an average 8.4% greater than the other two methods. There are two possible explanations for this observed difference.

The first is that the difference may indicate that there is some inelastic behaviour occurring at the extreme wood fibers of the specimens. One of the main functions of the fiber reinforcing was to reduce the effect of discontinuities on the loading of the extreme wood fibers. The fiber reinforcement acts as a bridge to help the load bypass these discontinuities. Essentially, it redistributes the load. It is therefore logical that the stress developed in the extreme wood fibers exceeds the linear elastic limit of the wood and that there may be some inelastic behaviour occurring in the specimen.

It should also be noted that the ultimate strain calculated from the demec data is an extrapolation of the 'plane-sections-remain-plane' data and that any inelastic behaviour that may occur at higher loads would not be recorded and compensated for in the analysis done. Consequently, this leads one to believe that some inelastic behaviour may be being observed in these results.

Table 3.27 Determination of Ultimate Strains

ID Code	Peak Compressive Strain				Peak Tensile Strain			
	demec data	ε =My/EI	% difference	strain gauge	demec data	ε =My/EI	% difference	strain gauge
PTN-1	2736	2884	-5.13	n/a	2989	2884	3.64	n/a
PTN-2	3145	3515	-10.52	n/a	3293	3515	-6.31	n/a
PTN-3	2375	2943	-19.29	n/a	3074	2943	4.46	n/a
PTN-4	2468	3245	-23.95	n/a	3077	3245	-5.16	n/a
PTG-1a	4499	3772	19.25	n/a	3388	3753	-9.73	n/a
PTG-1b	4471	3812	17.31	n/a	3849	3791	1.51	n/a
PTG-2a	3393	2873	18.09	n/a	3603	2844	26.69	n/a
PTG-2b	4154	4385	-5.26	n/a	4371	4342	0.67	n/a
PTG-10a	3189	3469	-8.06	n/a	3216	3300	-2.54	n/a
PTG-10b	4094	4364	-6.20	n/a	3887	4132	-5.93	n/a
1TS-1	4658	3961	17.60	n/a	3990	3525	13.21	4241
1TS-2	2991	3419	-12.52	n/a	3125	3044	2.65	3219
1TS-3	3238	3423	-5.39	n/a	2993	3045	-1.73	3186
1TS-4	4239	3672	15.44	n/a	3925	3246	20.90	4015
1TS-5	3545	3922	-9.60	n/a	3464	3559	-2.69	2918
1TS-6	2637	2722	-3.12	n/a	2513	2430	3.44	2566
2TS-1	3816	3525	8.27	n/a	2931	2835	3.36	4336
2TS-2	4036	3867	4.36	n/a	3463	3066	12.97	lost
4TS-1	4815	4133	16.48	n/a	2925	2557	14.40	3459
4TS-2	4262	3817	11.66	n/a	2764	2553	8.24	lost
8TS-1	3910	4138	-5.50	n/a	2164	1766	22.53	2037
8TS-2	4073	4697	-13.30	n/a	1786	2041	-12.48	lost
2DR-1	3800	3957	-3.98	lost	3855	3961	-2.70	lost
2DR-2	2954	2749	7.45	3040	2616	2763	-5.30	2609
4DR-1	3409	3213	6.08	lost	3387	3211	5.50	4016
4DR-2	3495	3615	-3.31	4279	3938	3598	9.45	lost
8DR-1	3104	2620	18.47	3034	2635	2586	1.92	lost
8DR-2	3103	2319	33.80	2901	3116	2344	32.95	3234
1WT-1	4956	5086	-2.55	n/a	4950	4526	9.36	5265
1WT-2	3134	3071	2.05	n/a	3014	2722	10.71	2889
1WT-3	4362	4800	-9.12	n/a	4760	4278	11.28	lost
1SAT-1	3411	3852	-11.46	n/a	3351	3404	-1.56	3942
PT12-1	4437	3322	33.55	n/a	3948	3322	18.84	n/a
PT12-2	3222	3062	5.23	n/a	4464	3062	45.80	n/a
2T12-1	3006	3115	-3.49	n/a	3018	2585	16.74	2885
2T12-2	4148	4287	-3.25	n/a	2982	3533	-15.58	lost
2D12-1	4004	3373	18.70	lost	3600	3370	6.80	2423
2D12-2	3864	3593	7.55	lost	3525	3601	-2.09	2836

'n/a' - indicates no strain gauge was applied to record this strain.
'lost' - indicates that the strain gauge was damaged during specimen construction

However, the load-deflection plots refute this. If there was any significant inelastic behaviour occurring in the test specimens, the load-deflection plots would show a 'tailing' of the curve as the specimen approached their failure loads. A typical plot is given in Figure 3.18. In these plots, the load-deflection relationship appears to be essentially linear over the entire loading history and there is very little indication of any plastic behaviour occurring in the specimens.

The second possible explanation for this behaviour is that there may be some compression effects being exhibited by the strain gauges. In this project, the strain gauges were mounted in the glueline between the glass fiber reinforcing and the wood section. Therefore, because there is tension in the strap, and the overall specimen develops curvature, stresses normal to the fibers in the strap are developed between the strap and the adjacent wood. Further to this, because the curvature developed under the prescribed loads was positive, the normal stresses that developed under the applied loading in this research were compressive. Such a compressive stress on the through thickness of the strain gauge would have the effect of increasing the strain recorded by the gauge in the longitudinal direction due to the Poisson's ratio effect of the gauge itself. This could account for the increase in strain recorded by these "internally" placed gauges.

A typical Load versus Strain curve using the demec data and the strain gauge data is shown in Figure 3.19. It was observed that even in the elastic region of the loading, the strain gauges recorded a consistently higher strain than the demec gauges did. It is probable that this is due to the compressive stresses placed on the gauges as a result of their "internal" placement. Consequently, all subsequent analysis will be conducted using the ultimate strain calculated using the strain bending formulation. This is done for two main reasons. First is the potentially unreliable strain gauge readings. Secondly, due to the delicate handling required by the strain gauges and the rough treatment they received during construction, only a few of the strain gauges applied to the specimens were actually intact at the time of testing. Therefore, there is little strain gauge data available to support or refute the postulate that the inter fiber-wood compressive stresses on the strain gauge are over-estimating the actual strain.

3.4.4 Determination of Failure Stresses

In order to determine a suitable model for predicting the behaviour of glass fiber reinforced glulam timber beams, it is necessary to determine the stresses developed in the specimens at failure. Once these stresses have been determined, a correlation between the different failure modes and the failure stresses may be made. This correlation will allow for the determination of the failure limit state stresses.

Three different failure modes were observed during testing: tensile, compressive and shear. Both the tensile and compressive stresses at failure were determined by assuming that the sections remain linear up to failure and then multiplying the failure strain from Table 3.27 by the shear free MOE determined for the specimen. The shear

free MOE was used because the point of maximum stress occurs in the zero shear span of the test specimen.

Table 3.28 shows the failure mode and the corresponding limit state stress for each of the specimens tested. The stresses that correspond to the failure mode have been shaded.

Table 3.28 Failure Mode and Peak Stresses at Failure

Specimen ID	Mode of Failure	Shear Free MOE (MPa)	Peak Compressive Stress, σ_{cmax} (MPa)	Peak Tensile Stress, σ_{tmax} (MPa)	Peak Shear Stress, τ_{max} (MPa)
PTN-1	tension	12036	34.7	34.7	1.71
PTN-2	tension	10353	36.4	36.4	1.75
PTN-3	tension	12079	35.5	35.5	1.87
PTN-4	tension	11363	36.9	36.9	1.91
PTG-1a	crushing and tension	10408	39.3	39.1	1.57
PTG-1b	crushing and tension	12302	46.9	46.6	1.85
PTG-2a	tension	14978	43.0	42.6	2.03
PTG-2b	tension	11642	51.0	50.5	2.48
PTG-10a	crushing	12180	42.3	40.2	2.10
PTG-10b	crushing and tension	12477	54.5	51.6	2.62
1TS-1	tension and shear	14787	58.6	52.1	2.85
1TS-2	tension and shear	12240	41.9	37.3	2.27
1TS-3	tension	12446	42.6	37.9	2.17
1TS-4	tension and shear	13077	48.0	42.5	2.46
1TS-5	tension and shear	12567	49.3	44.7	2.51
1TS-6	tension	13853	37.7	33.7	1.93
2TS-1	buckling and tension	13556	47.8	38.4	2.41
2TS-2	buckling and crushing	13422	51.9	41.1	2.84
4TS-1	buckling/crushing/shear	11700	48.4	29.9	2.78
4TS-2	buckling/crushing/shear	13219	50.5	33.8	2.80
8TS-1	shear	11295	46.7	19.9	2.84
8TS-2	crushing and shear	10126	47.6	20.7	2.43
2DR-1	tension and shear	11923	47.2	47.2	2.79
2DR-1	tension	10990	30.2	30.4	1.71
4DR-1	shear	12029	38.7	38.6	2.79
4DR-2	tension and shear	12344	44.6	44.4	3.47
8DR-1	shear	12016	31.5	31.1	2.63
8DR-2	shear	14276	33.1	33.5	3.22
1WT-1	tension and shear	10962	55.8	49.6	2.96
1WT-2	tension	13523	41.5	36.8	2.17
1WT-3	tension and shear	11677	56.0	49.9	3.10
1SAT-1	tension	11295	43.5	38.5	2.27
PT12-1	tension	12002	39.9	39.9	2.28
PT12-2	tension	12328	37.7	37.7	2.23
2T12-1	shear	11028	34.4	28.5	2.50
2T12-2	shear	8466	36.3	29.9	2.25
2D12-1	buckling and shear	10459	35.3	35.2	2.36
2D12-2	shear	8981	32.3	32.3	2.18

3.4.5 Determination of Mean Failure Stresses and Strains

Using the stress corresponding to the different failure modes, the average stress for each failure mode was determined. Using the strain data in Table 3.27 and the corresponding failure mode from Table 3.28, the average strain for each failure mode was also determined. Table 3.29 presents these average stress and strain values.

Table 3.29 Mean Failure Stress and Strain for Each Failure Mode

Failure Mode	Average Failure Stress (MPa)	Standard Deviation	Average Failure Strain ($\mu\varepsilon$)	Standard Deviation
unreinforced tensile failure	36.9	1.8	3162	242
reinforced tensile failure (σ_{trmax}avg)	42.3	6.2	3429	589
reinforced compressive failure (σ_{crmax}avg)	46.4	5.9	3883	414
reinforced shear failure (τ_{rmax}avg)	2.69	0.34	n/a	n/a

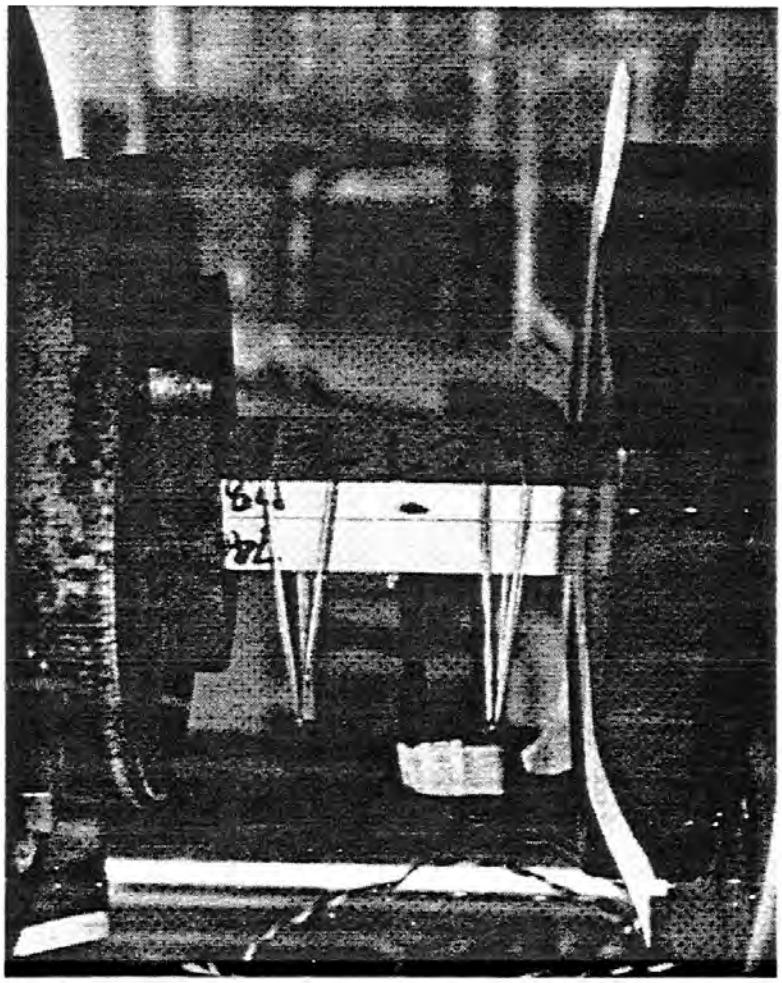

Figure 3.1
Photo of Wood Compression Test

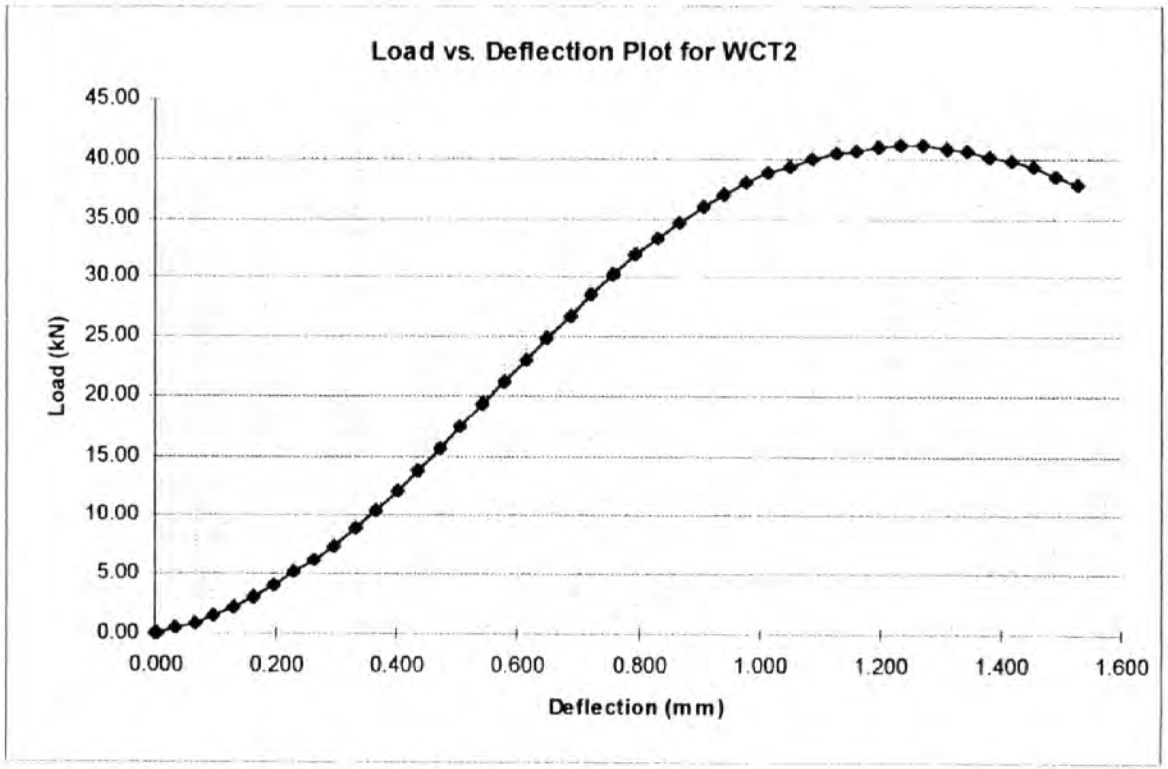

Figure 3.2
Typical Load-Deflection Plot for Wood Compression Material Test

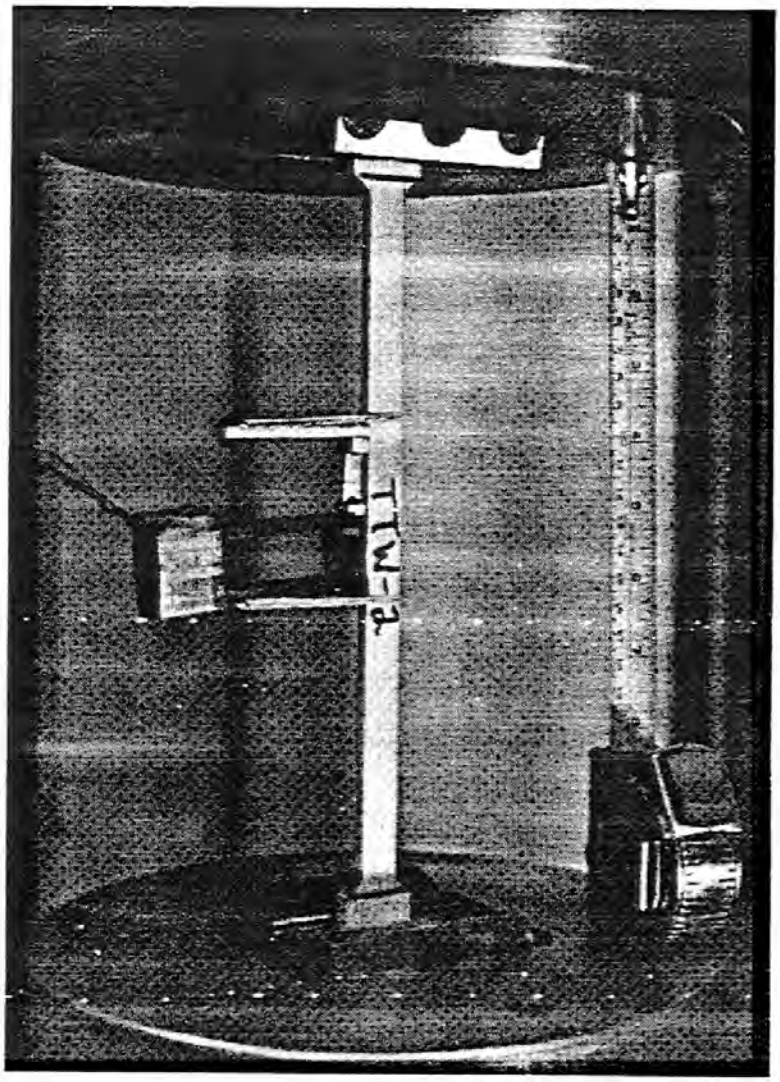

Figure 3.3
Photo of Wood Tension Test Specimen

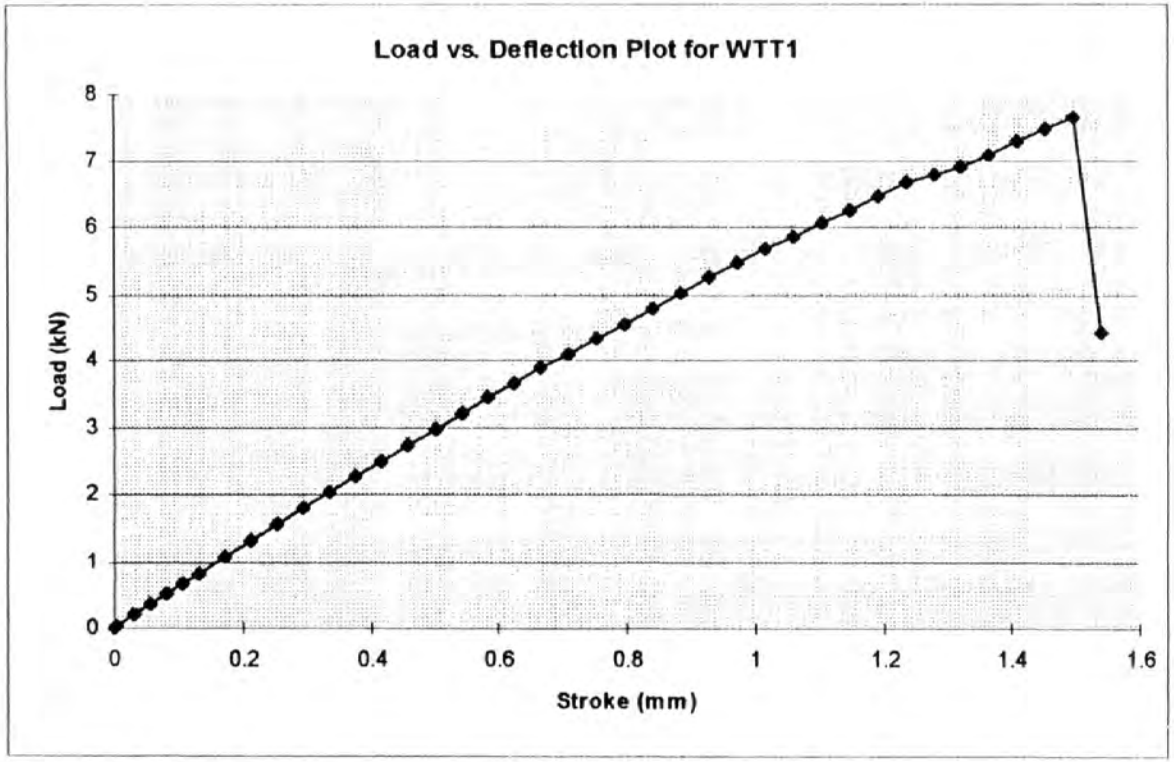

Figure 3.4
Typical Load-Deflection Plot for Wood Tension Material Test

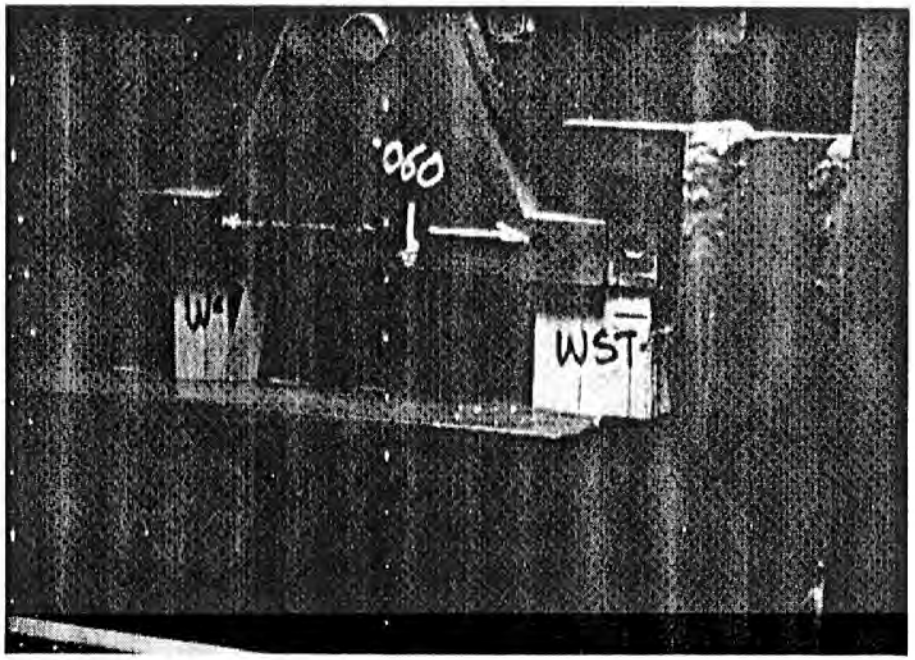

Figure 3.5
Photo of Wood Shear Test Specimen

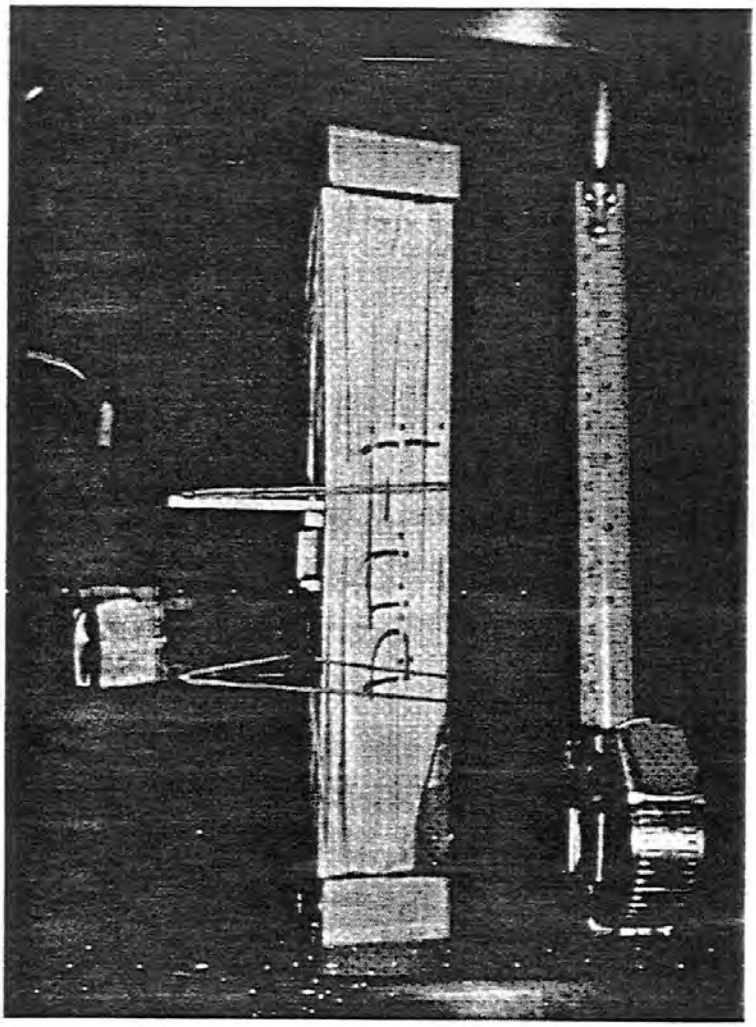

Figure 3.6
Photo of Pultruded Glass Strap Tension Test Specimen

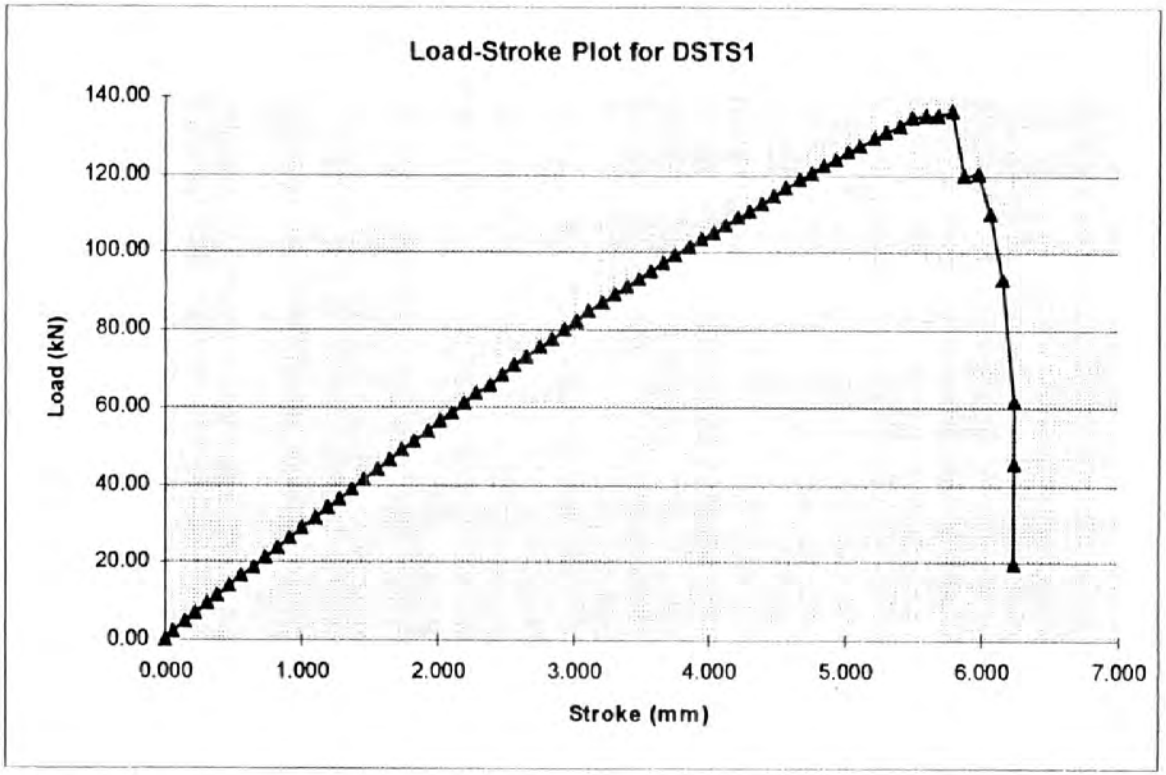

Figure 3.7
Typical Load-Deflection Plot for Pultruded Strap Tension Test

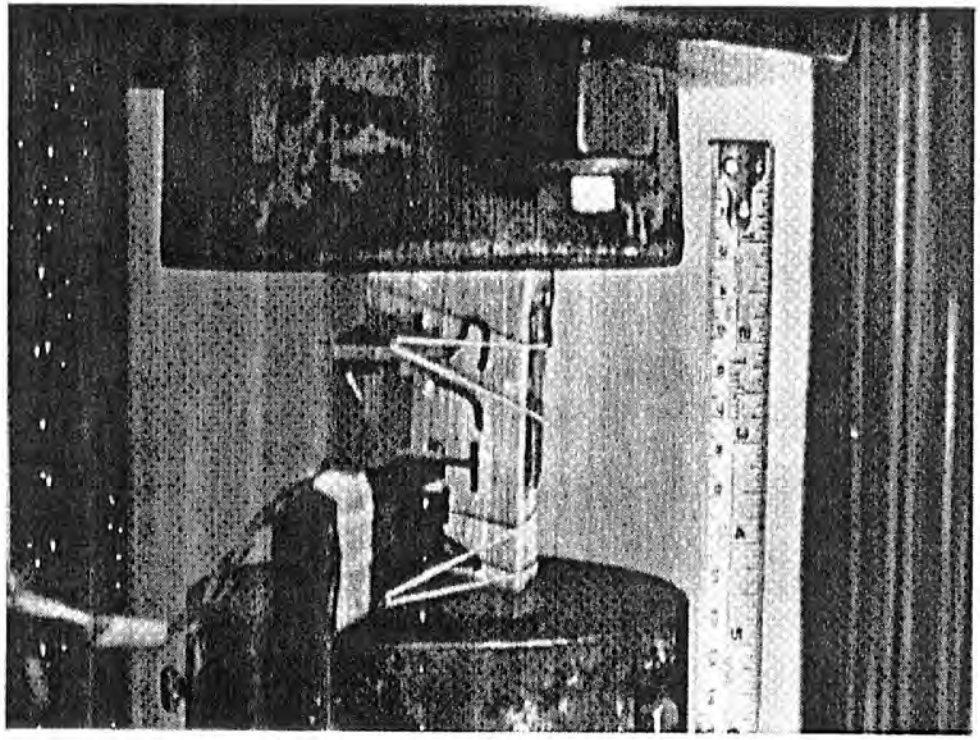

Figure 3.8
Photo of Pultruded Glass Strap Compression Test Specimen

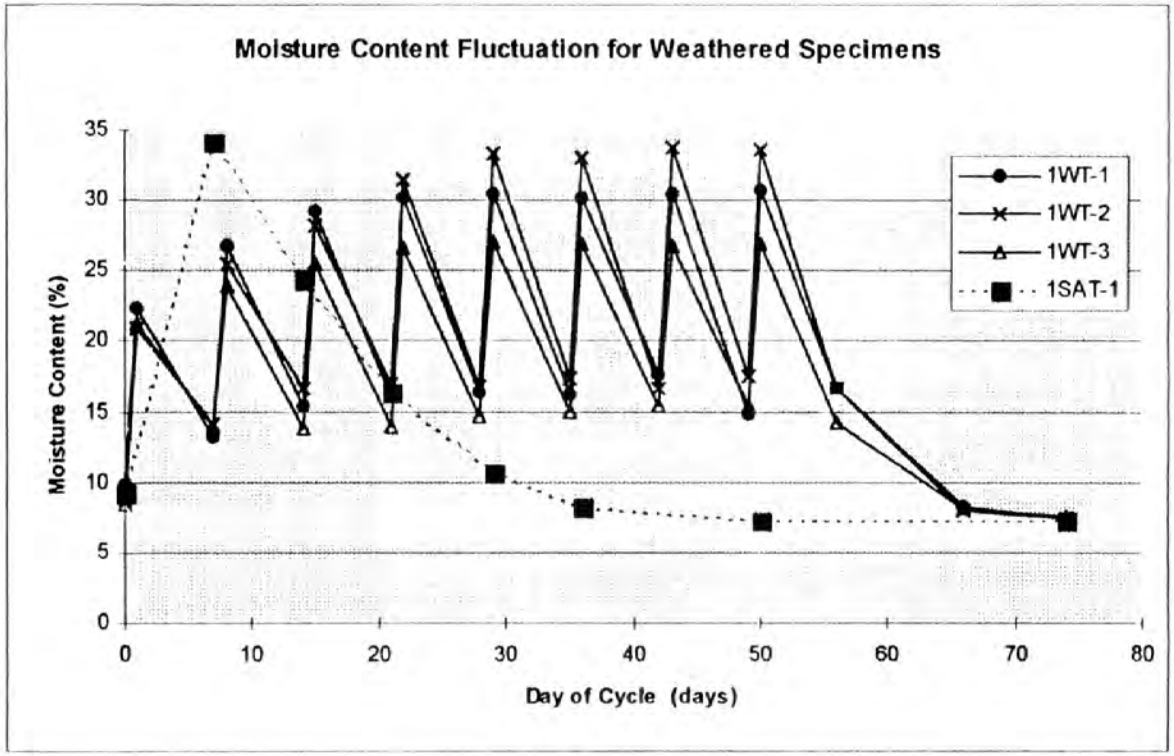

Figure 3.9
Plot of Moisture Content Fluctuation for Weathered Specimens

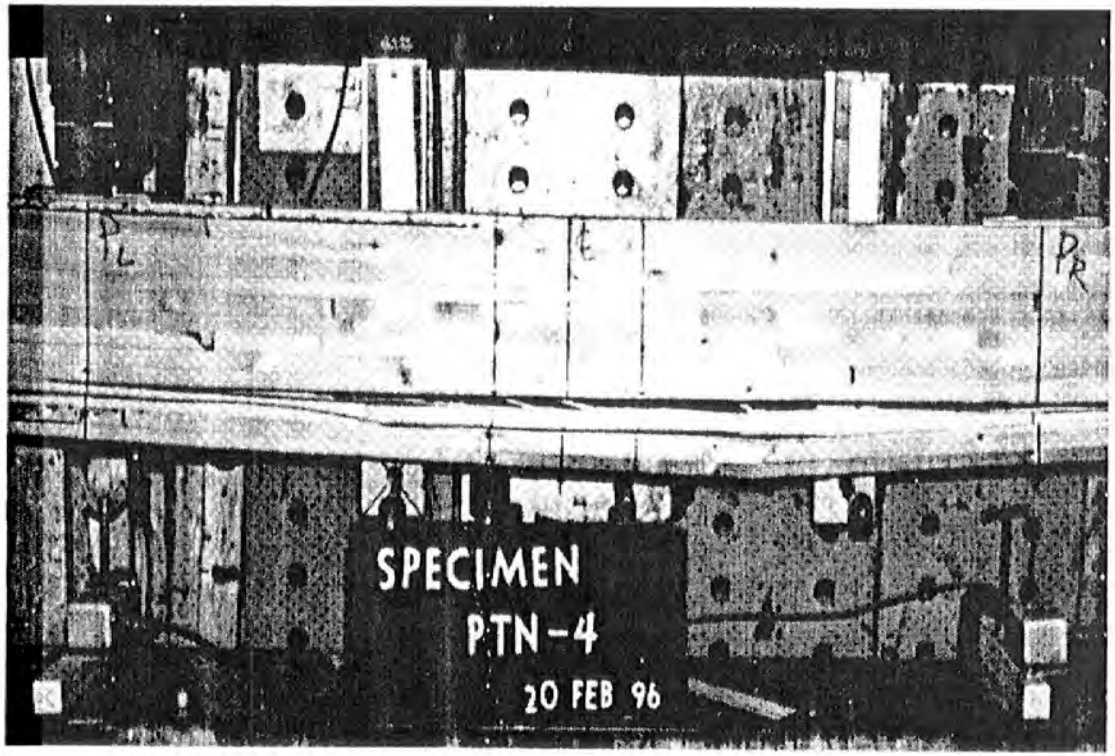

Figure 3.10
Photo of Typical Unreinforced Tensile Fracture

UNREINFORCED PLOTS FOR: **PTN-3**

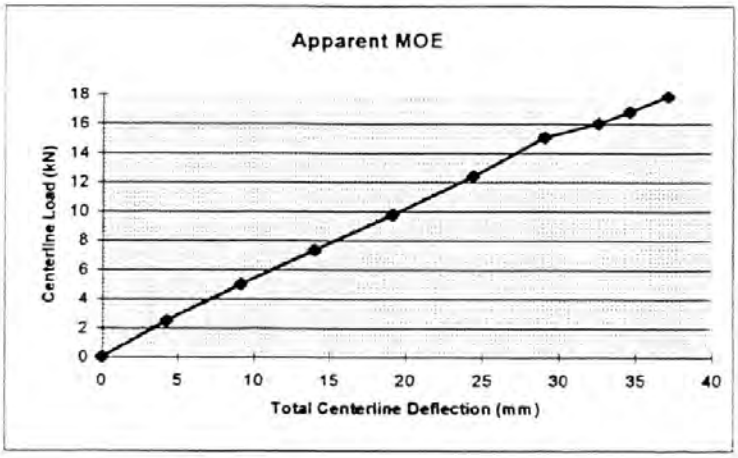

SUMMARY OUTPUT

Regression Statistics	
Multiple R	0.99801806
R Square	0.996040049
Adjusted R Square	0.884928938
Standard Error	0.399990655
Observations	10

	Coefficients
Intercept	0
X Variable 1	0.49709417

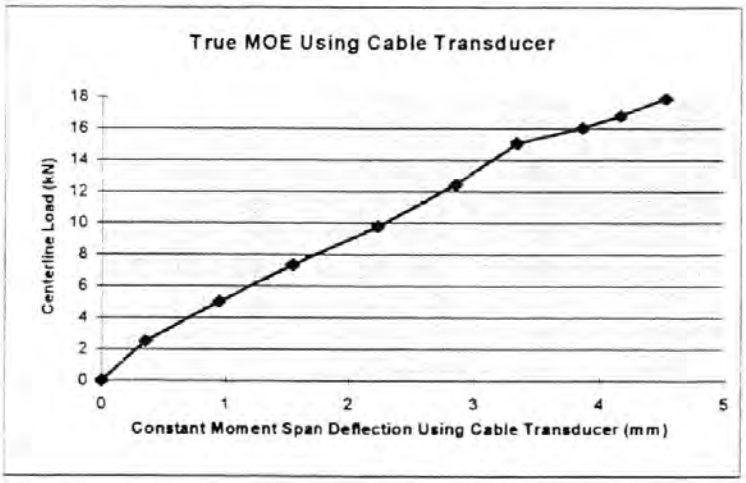

SUMMARY OUTPUT

Regression Statistics	
Multiple R	0.991831484
R Square	0.983729692
Adjusted R Square	0.872618581
Standard Error	0.810779588
Observations	10

	Coefficients
Intercept	0
X Variable 1	4.191555483

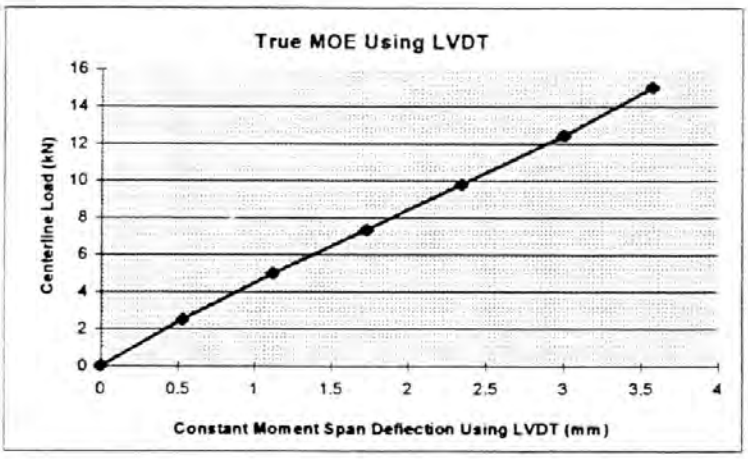

SUMMARY OUTPUT

Regression Statistics	
Multiple R	0.999463463
R Square	0.998927214
Adjusted R Square	0.832260547
Standard Error	0.176385755
Observations	7

	Coefficients
Intercept	0
X Variable 1	4.198676388

Figure 3.11
Typical Regression Analysis for an Unreinforced Specimen

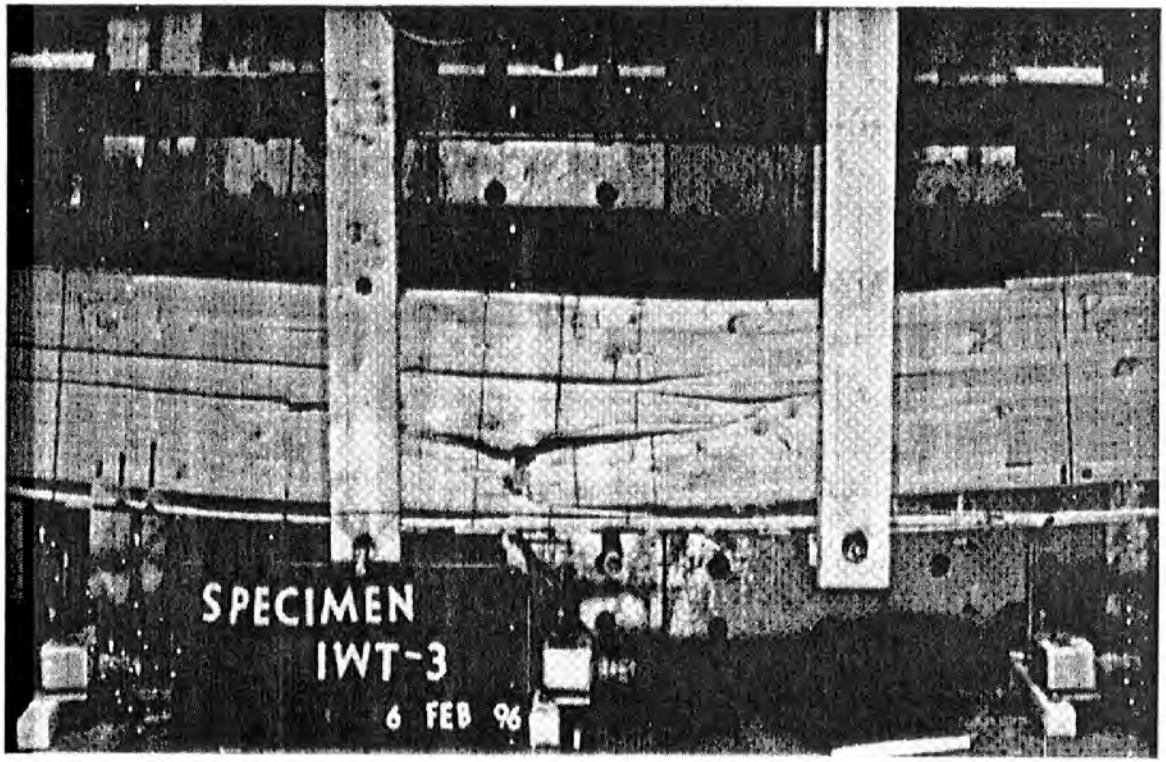

Figure 3.12
Photo of Typical Reinforced Tensile Fracture

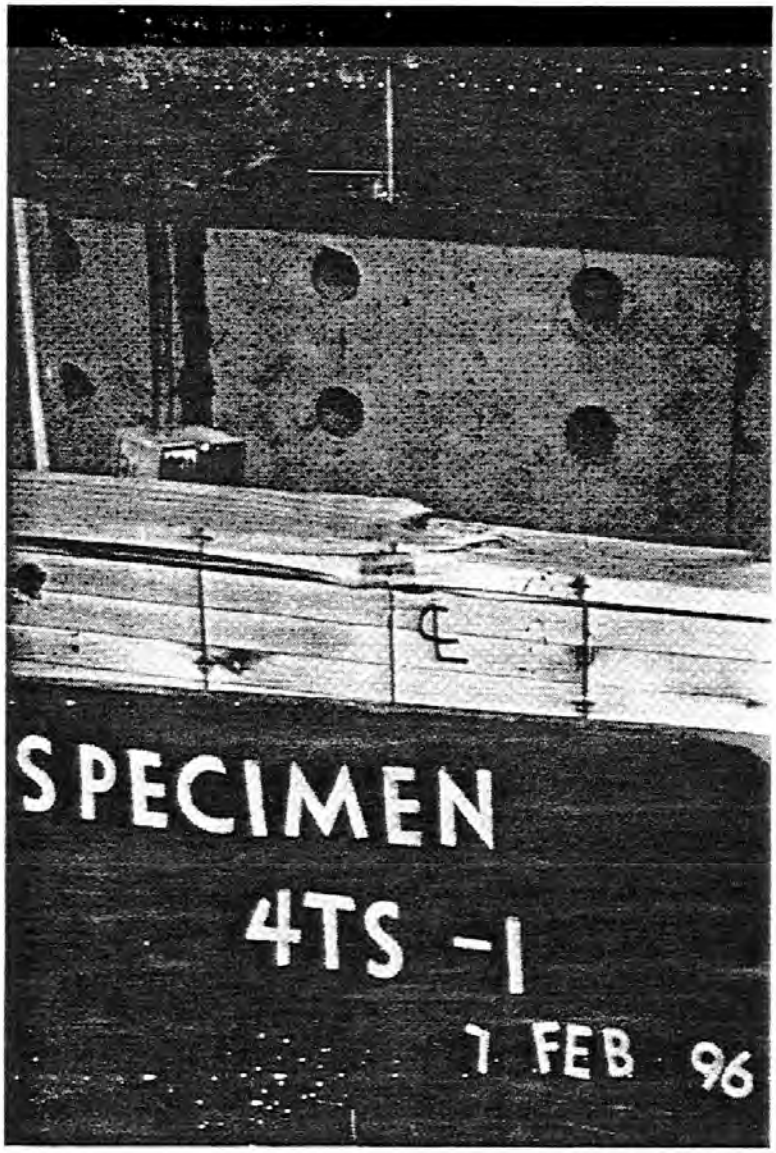

Figure 3.13
Photo of Typical Reinforced Compressive Crushing Failure

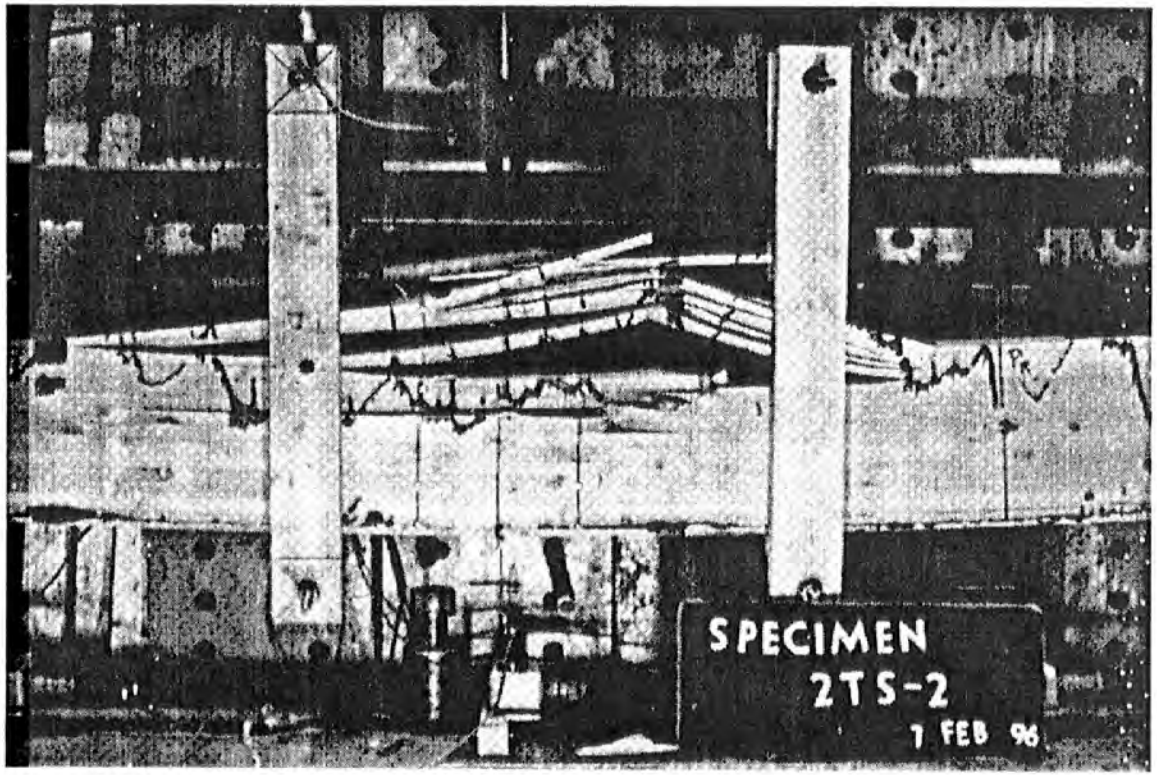

Figure 3.14
Photo of Typical Reinforced Buckling Failure

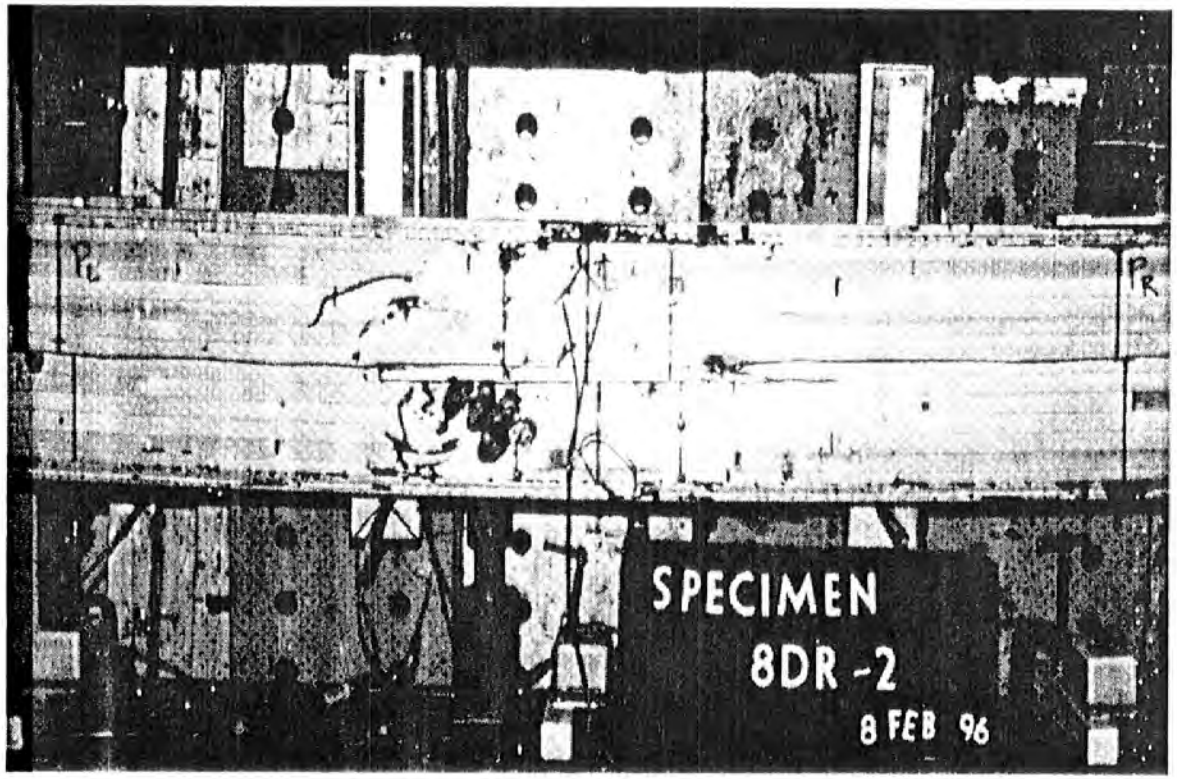

Figure 3.15
Photo of Typical Reinforced Shear Failure

REINFORCED PLOTS FOR: **4DR-2**

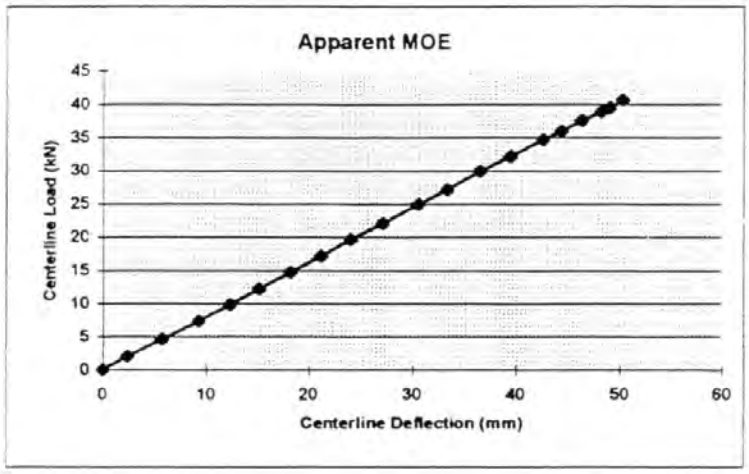

SUMMARY OUTPUT

Regression Statistics	
Multiple R	0.996590503
R Square	0.993192631
Adjusted R Square	0.94971437
Standard Error	1.213526387
Observations	24

	Coefficients
Intercept	0
X Variable 1	0.83091281

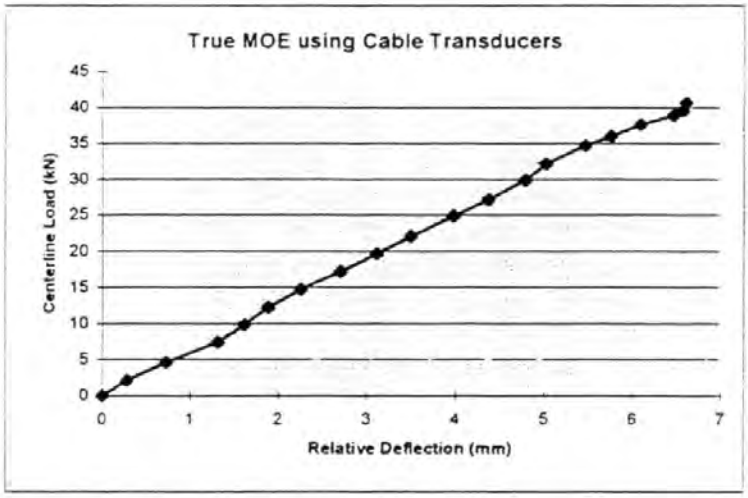

SUMMARY OUTPUT

Regression Statistics	
Multiple R	0.940385608
R Square	0.884325092
Adjusted R Square	0.840846831
Standard Error	5.002408483
Observations	24

	Coefficients
Intercept	0
X Variable 1	6.741865477

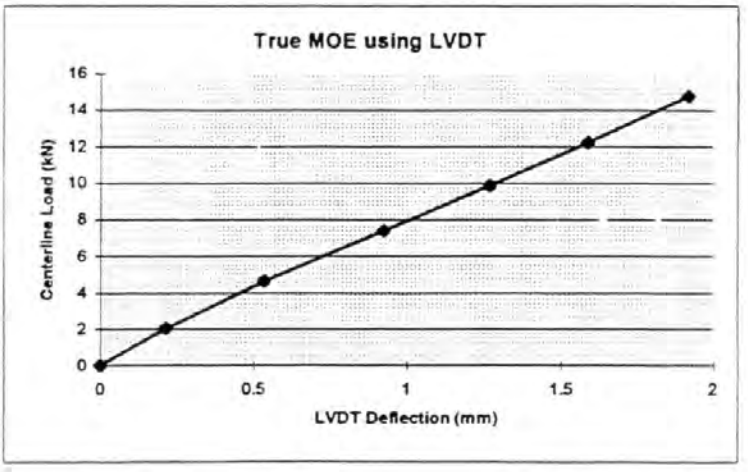

SUMMARY OUTPUT

Regression Statistics	
Multiple R	0.998748597
R Square	0.99749876
Adjusted R Square	0.830832093
Standard Error	0.269125241
Observations	7

	Coefficients
Intercept	0
X Variable 1	7.771663636

Figure 3.16
Typical Regression Analysis for a Reinforced Specimen

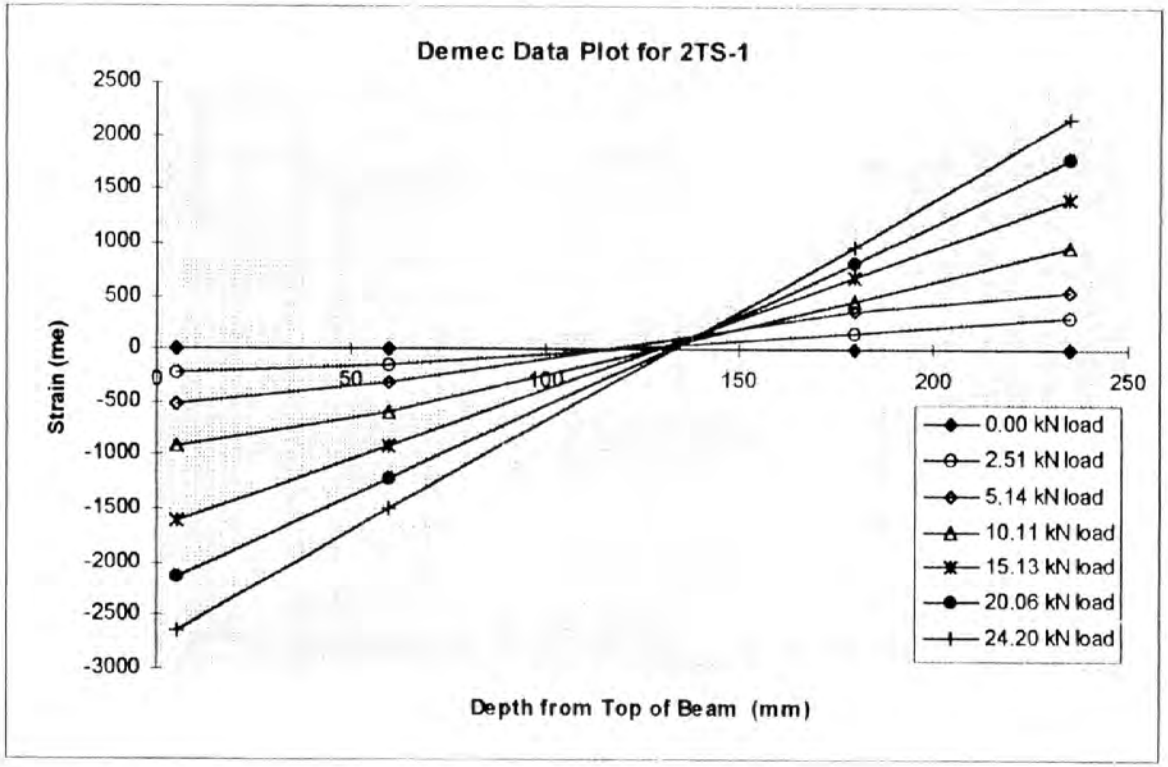

Figure 3.17
Typical Demec Data Plot

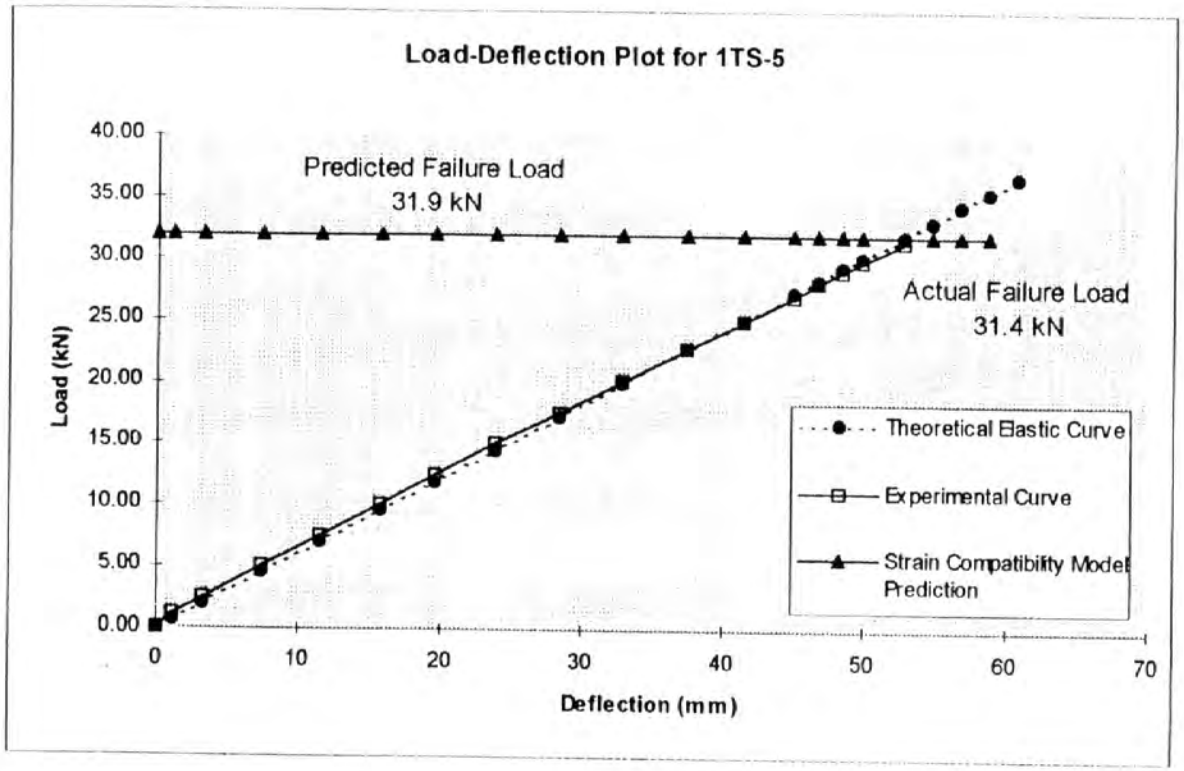

Figure 3.18
Typical Load-Deflection Plot

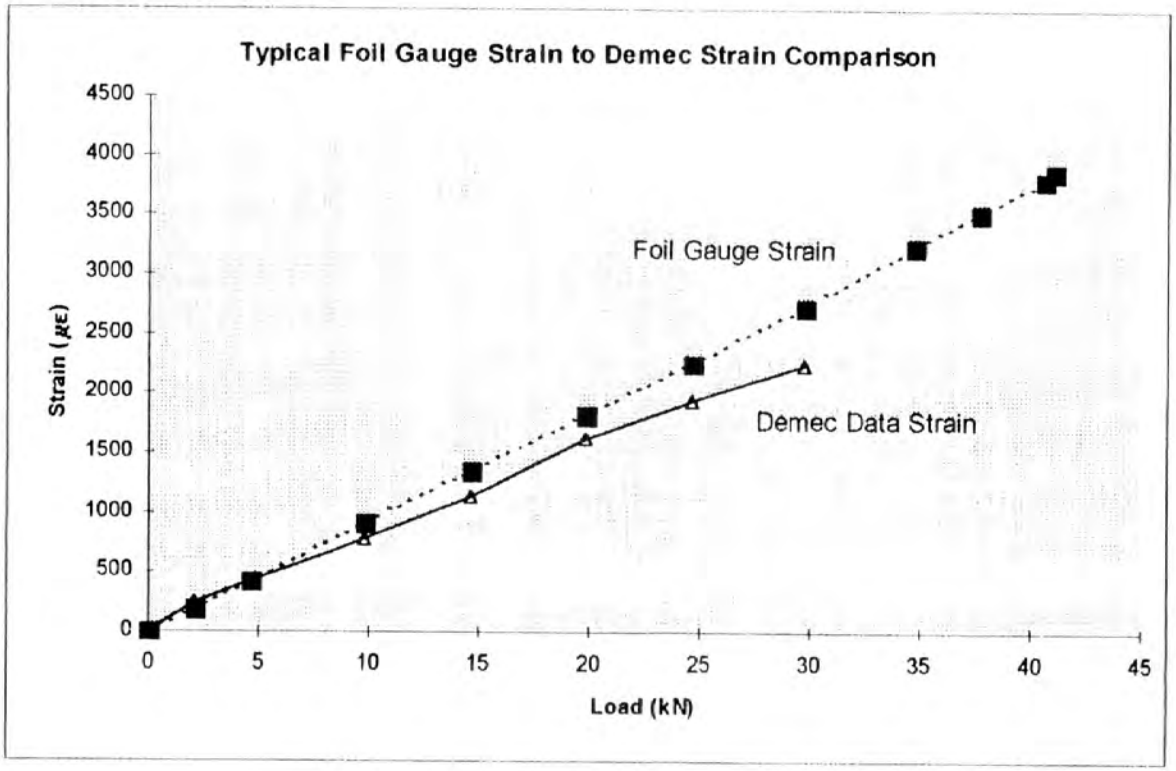

Figure 3.19
Foil Gauge Strain versus Demec Gauge Strain Plot

4.0 DISCUSSION

4.1 Material Test Results

4.1.1 Wood Material Test Results

Table 4.1 shows the mean material properties determined from the material tests for the S-P-F lumber used in the construction of the glulam beams. The specified values from CSA/CAN O86.1-94 (1994) for the particular member type used in the test program were also included in Table 4.1 for comparison.

Table 4.1 Mean Wood Material Properties

Material Property	Material Test Result (MPa)	CSA/CAN O86.1-94 (1994) Standard (MPa)
Mean Ultimate Compression Stress	56.7	25.2
Mean Ultimate Tensile Stress	75.6	17.0
Mean Ultimate Longitudinal Shear Stress	9.00	1.75
Mean Apparent MOE	11271	n/a
Mean Shear Free MOE	11378	10300

There appears to be a definite discrepancy between the material test results and the values reported in CSA/CAN O86.1-94 (1994). There are a number of reasons for these differences. First of all, the values in CSA/CAN O86.1-94 (1994) are design values based on the lowest fifth percentile for this type of specimen. Since the variations of wood can be quite significant, it is not surprising to find these values significantly lower that the material test results.

In addition to this, each respective ASTM Standard calls for clear specimens to be used in the material tests. In this experiment, close attention was paid to ensuring that the material test specimens were free of defects. This included the limitation on the test specimens that the fibers in the test specimens were parallel to the direction of loading. Since CSA/CAN O86.1-94 (1994) is a design criteria, it accepts the fact that the specimens may have defects in them and further compensates the design value for this. This results in an even more conservative design value.

One of the major differences between the two sets of data is in the relationship between the ultimate compressive stress and the ultimate tensile stress. CSA/CAN O86.1-94 (1994) indicates that the ultimate compressive stress of the wood is greater than that of the ultimate tensile stress, whereas the material test results indicate a reversal of this relationship. The reason for this is that the specimens used in the material tests were clear of defects. Clear wood is stronger in tension than it is in compression, as the

material tests indicate. However, defects cause a significant decrease in the ultimate stress capacity of timber. Therefore, since timber beams are rarely free of defects, CSA/CAN O86.1-94 (1994) takes this into consideration and further reduces the design ultimate tensile stress permitted in wood. This accounts for part of the observed reversal.

A second reason for the reversal of these two stresses is that there is a size effect that is not considered in the material test results. In wood, the size of the specimen plays a major role in the ultimate stresses that are allowed to be developed. From clause 5.5.7.4 of CSA/CAN O86.1-94 (1994), the size factor for compression parallel to grain (K_{zcp}) was found to be equal to 1.0 for cross-sectional crushing.

Examination of Table 5.4.5 in CSA/CAN O86.1-94 (1994) shows that, as the dimensions of a test specimen reduce, the size factor for shear (K_{zv}) and for tension parallel to grain (K_{zt}) increases. While Table 5.4.5 in CSA/CAN O86.1-94 (1994) is limited to a smallest dimension of 38 mm, by extrapolating the values of K_{zv} and K_{zt} given in the table, values of K_{zv} and K_{zt} were found to be approximately equal to 2.28 and 2.05, respectively, for the different material test specimen sizes. If these factors are taken into consideration and the individual ultimate stresses normalized relative to the ultimate shear stress, the results are shown in Table 4.2.

Table 4.2 Normalized Ultimate Stress Comparison

Material Property	Normalized Material Test Result Stresses	Normalized CSA/CAN O86.1-94 (1994) Stresses
Ultimate Compressive Stress	6.30	6.32
Ultimate Tensile Stress	8.40	8.73
Ultimate Shear Stress	1.00	1.00

Comparison of the two sets of normalized data shows excellent agreement between them. This provides confidence in the results obtained from the material tests and indicates that the difference between the values from the material test results and those in CSA/CAN O86.1-94 (1994) are probably a combination of size effect factors, variability and the use of clear specimens versus random defect specimens.

With respect to using the results of the material tests as a prediction for the stresses developed in beam specimens, it is obvious that the results of the material tests may not be used directly. Clearly, the results found in the material tests are merely a scaling factor different from the CSA/CAN O86.1-94 (1994) values, however, further investigation into the exact value for this scaling factor is required. In addition to this, a greater wood material test population is required in order to be able to obtain a realistic design value. This type of further investigative work would be an integral part of developing design criteria for design codes, however, it is not within the scope of the current research.

Considering that the MOE value reported in O86.1 is representative of the fifth lowest percentile, comparison of the material test results for the apparent MOE agrees very well with the value reported in CSA/CAN O86.1-94 (1994). Further to this, the original testing for the development of the beams used in this investigation was conducted at the University of Alberta (Cheng, 1994) and it is noted that the original testing program of the beams resulted in an apparent MOE of 10982 MPa and a shear free MOE of 11318 MPa. The results obtained in this test program show excellent agreement with respective differences of 2.6% and 0.53% when compared with this original test program.

4.1.2 Pultruded Glass Strap Material Test Results

The results for the pultruded strap material test presented in Table 3.4 do not provide a theoretical comparison. This is because the material properties of the configuration used were unknown. The supplier provided the material properties of the unbonded glass, however the composite plastic strap clearly does not have the same properties because of the effects on the composite action of the bonding adhesive used in the manufacturing of the straps.

The main test result required from the pultruded strap material tests was the fiber fraction of the straps. The remaining pultruded strap material properties, such as MOE, can be determined as a function of the fiber content of the strap. The supplier indicated that the fiber fraction of the straps used in this research was in the order of 55-65% fiber. The material test results indicate a fiber fraction of 49.6%, which is slightly less than the manufacturers estimate. The reasons for this may be numerous. Examination of the straps showed minor defects in the surface of the plastic composite. Under tension, this would mean that significant straining would be required in order to "straighten" these fibers out and have them contribute to the stiffness observed.

Secondly, the straps used in the material tests received the same surface preparation prior to testing as the ones used in the reinforcement schemes received prior to adhesion to the glulam specimens. It is possible that some of the fibers close to the surface of the strap were damaged in this preparation and were no longer continuous over the entire length of the material test specimen. Therefore, while the fiber is present, it does not fully contribute to the stiffness determined during testing.

Finally, it is possible that the estimate provided by the manufacturer is incorrect. Since the straps, in general, are made at a variety of fiber fractions and these particular straps were made many weeks prior to delivery for this project, it is possible that such an error was made.

For the purposes of this study, the fiber fraction based on actual material tests was used for all subsequent analysis. As a source of indirect confirmation for this value of 49.6%, it was observed that using this value resulted in excellent agreement of the predicted model with the actual failure loads. Manipulation of the strain compatibility model indicated that by varying the fiber fraction by as little as ten percent, the error between

the model and the actual failure loads increased dramatically. As a result, it was assumed that this calculated value of the fiber content was reasonably accurate.

These results also support the speculation that the results from the pultruded strap compression test, presented in Table 3.5, are not representative of the true compression behaviour for the strap. The close agreement of the test to predicted values further justifies the use of an equal stiffness for both compression and tension in the pultruded strap.

4.2 Discussion of Specimens With Only Tensile Reinforcing

From the results presented in Tables 3.24, 3.25, and 3.26, it is clear that substantial strength and stiffness enhancement are achieved with the application of glass fiber reinforcing to the tensile region of glulam timber beams.

Figure 4.1 shows the relationship between the strength enhancement achieved and the corresponding fiber fraction for the specimens with only tensile reinforcing. The figure shows that there is an initial dramatic increase in the strength capacity of the specimens with the application of even a very small fiber fraction of glass reinforcement. After this initial increase, the graph takes on a shape with a positive diminishing slope and appears to be approaching a plateau value. That is, it has an asymptotic shape.

Although it was initially postulated that this plot would show a linear relationship until a peak value was reached, the observed response was not unexpected. Even at the smallest of fiber fractions, a significant amount of strength enhancement could be achieved because of the confinement that the glass fiber would offer to the adjacent wood fibers. This confinement would significantly reduce the tendency of the wood fibers to fracture. With an increase in fiber fraction, the mechanical properties of the wood in the section begin to become prevalent and contribute to the overall observed behaviour until, ultimately, the material properties of the wood will overcome the initial changes due to the GFRP reinforcing and become the dominating factor that governs the behaviour of the reinforced section.

As seen in Table 3.12, the diminishing slope behaviour observed in Figure 4.1 may be attributed to the fact that, with the increased fiber fraction, the specimens are controlled by different failure mechanisms. Initially, the failure of the specimens are governed by a tensile fracture, originating in the lower lams of the specimen. Often this fracture resulted in an explosive delamination of the glass reinforcing. With the exception of the PTG-1 specimens and one of the PTG-2 specimens, the glass fiber did not fracture at failure of the beam specimen, rather it caused the shearing off of the bottom wood fibers from the rest of the specimen.

It is postulated that, as the levels of reinforcement increased, two phenomena occurred which propagated different failure mechanisms. First, the GFRP reinforcing provided sufficient confinement to allow an increase of approximately 10% in the tensile wood

fiber strain of the reinforced specimens over the unreinforced specimens. Secondly, as greater fiber fractions were applied to the tensile face of the specimens, the neutral axis of the section lowered. This had the effect of lowering the magnitude of the tensile strains, allowing the ultimate strength for other modes of failure to be reached prior to the ultimate tensile strength limit. From the observed failure patterns, it was observed that the next limiting ultimate strain to be reached was the compressive one. Additional increase in fiber fraction resulted in a further lowering of the neutral axis. This lowering resulted in the compressive region of the beam increasing to the point where sufficient compressive capacity was developed to promote the failure to move to the next mode of failure, which was shear failure at the neutral axis location.

The relationship shown in Figure 4.1 supports this theory. With the exception of the data for a fiber fraction of 0.99%, the remaining data fits the postulated relationship. The 0.99% fiber fraction point is only marginally off this expected relationship, however, given the variability of the mechanical properties of wood, the observed relationship is considered well within experimental limitations.

Since the trends for the apparent stiffness and the shear free stiffness are virtually identical, this use of the term 'stiffness' in this discussion will apply to both sets of stiffness data. Figure 4.2 gives a graphical representation of the apparent and shear free stiffness enhancement data from Tables 3.25 and 3.26, respectively.

The expected trend for the relationship between stiffness enhancement and fiber fraction would be an increasing slope relative to increasing fiber fraction. This is because the added stiffness from the GFRP reinforcing is a function of the square of the depth from the neutral axis to the line of action of the reinforcement. The shape was not expected to be parabolic because the plot includes the total stiffness of the reinforced cross section. The contribution from the wood portion of the section is not parabolic. It is also expected that the true stiffness should be slightly greater than the apparent stiffness.

More significantly, the depth from the neutral axis to the line of action of the reinforcement decreases with increasing fiber fraction. This causes the contribution of the area x depth^2 term of the moment of inertia to be a less significant factor in the overall stiffness and results in the pseudo-parabolic shape observed in Figure 4.2. In general, the figure shows an increasing slope with increasing fiber fraction, but the increase in slope lessens with increasing fiber fraction.

While the general trend for the stiffness enhancement relative to fiber fraction agrees quite well with the anticipated behaviour, the observed behaviour at the lower fiber fractions does not agree exactly with the postulated behaviour. In the case of the stiffness enhancement data, Figure 4.2 shows that there is a dramatic increase in the stiffness of the specimens in the lower fiber fraction region. This is contrary to the findings of the preliminary study where there was little or no stiffness enhancement observed with the application of low level fiber fractions of GFRP reinforcing. It was concluded that this was due to the variability of wood as an engineering material.

In the current study, the results indicate that there is a significant positive enhancement, even at the lowest fiber fraction studied. This is the expected behaviour of the stiffness enhancement and supports the theory proposed by Dorey and Cheng (1996) that the variability of the wood mechanical properties masked the actual stiffness enhancement achieved in the preliminary investigation. However, the rate of increase of the stiffness for these lower fiber fractions was substantially greater than expected and was not consistent with the overall model. Initially it was thought that this difference was due to the different construction techniques used, however, data from both construction techniques agree well with overall trends and it is only in the two lowest fiber fractions that there appears to be some disagreement.

Examination of Figure 4.2 shows that the data point (0,0) does not fit into the overall trend, while logically it must be there. With this in mind, it is presumed that there is a "transition" region in which the fiber fraction is so low that additional fiber reinforcing is significant enough to affect the overall section stiffness, but not significant to exhibit the changing slope theory. However, once the fiber fraction reaches a value around 0.4%, the amount of fiber reinforcing is substantial enough to have an impact on the overall member stiffness. The reason for this transition region may be due to the confinement provided by the glass fiber to the wood. The presence of defects in wood tends to "soften" the wood. The fiber essentially "bridges" over any of these defect areas in the wood, thereby increasing the stiffness of the wood in the composite section when compared to the stiffness of the wood in the unreinforced section. At greater fiber fractions, this stiffening of only the wood portion becomes less significant when compared with the glass fiber stiffness. Therefore, in a plot of stiffness enhancement versus fiber fraction, this stiffening of the wood section from this bridging would be more prominent at lower fiber fractions, but would get lost at greater fiber fractions due to domination by the glass fiber. This would account for the observed relationship in Figure 4.2.

One of the more critical relationships in new material development is the inter-dependence of the strength enhancement and the stiffness enhancement. When designing a timber structure, as with any structure, often the critical limit state is deflection. Therefore, it must be considered in any new material development. While strength enhancement is certainly a desired goal, strength enhancement relative to stiffness enhancement is also extremely important. This is because the stiffness is inversely proportional to deflection. Consequently, if a member is reinforced to carry an additional load, then it must also exhibit a corresponding increase in stiffness, otherwise the deflection limit state will prohibit full realization of the member's enhanced strength potential.

Figure 4.3 provides a graphical representation of the strength enhancement as it parallels it's corresponding shear free stiffness enhancement at a given fiber fraction for the specimens with only tensile reinforcement. Examination of the graph shows that 'convex' shape of the strength enhancement plot will ultimately intercept the 'concave' shape of the stiffness enhancement plot. However, the fiber fractions selected in this study were not large enough to allow these two curves to meet. The point of this

intersection would represent the optimum fiber fraction for the specimens with only tensile reinforcement because both the strength and stiffness enhancement would be equivalent. Extrapolation of the curves in Figure 4.3 suggests that this optimum fiber fraction is approximately 8.2%.

The graph in Figure 4.3 also represents the additional versatility glass fiber reinforcing introduces to member design. By varying the fiber fraction, a designer would be able to enhance the governing limit state so that two or more limit states would simultaneously govern the member's design, thereby making use of more of the member capacity. For example, if deflection governed the design of a member, a designer could select a fiber fraction greater than the estimated balanced fiber fraction of 8.2%. This would mean that the member would have a stiffness enhancement greater than strength enhancement and allow for a greater portion of the member's flexural capacity to be used. Similarly, if strength governed the design of a member, a designer could select a fiber fraction less than the estimated optimum 8.2%, thereby enhancing the strength capacity more than the stiffness capacity of the member and again utilizing more of the member's capacity.

4.3 Discussion of Doubly Reinforced Specimens

From the results presented in Tables 3.24, 3.25, and 3.26, it is obvious that there is significant strength and stiffness enhancement achieved with the application of glass fiber reinforcing to doubly reinforced glulam timber beams.

Figure 4.4 shows the relationship between the strength enhancement achieved for the doubly reinforced specimens and the corresponding fiber fraction. The plot shows a decreasing slope relationship with increasing fiber fraction. Further to this, it was again observed that the decrease in slope corresponded to changes in the failure modes. It should be noted that none of the doubly reinforced specimens failed in compression. This was due to the fact that the glass fiber reinforcement provided adequate confinement and additional compressive capacity and that the wood section failure modes went directly from a combined tension-shear failure to a pure shear failure mode.

This plot has the same basic shape and exhibits the same basic relationship as was observed for the specimens with only tensile reinforcement. The main difference between them is that there is no data below 2% fiber fraction for the doubly reinforced specimens. This is due to the fact that the all of the doubly reinforced specimens were constructed using the pultruded glass fiber straps. This predetermined the minimum fiber fraction to be approximately 2%. As a result, the behaviour of the doubly reinforced specimens with glass fiber reinforcement below a fiber fraction of 2% is unclear. However, given the similarities of the behaviour of the doubly reinforced specimens above 2% fiber fraction to the behaviour of the specimens with only tensile reinforcement above 2% fiber fraction, it is postulated that the behaviour of the doubly reinforced specimens below 2% fiber fraction is similar to the behaviour of the specimens with only tensile reinforcement below 2% fiber fraction.

Examination of Table 3.15 revealed an interesting phenomena. At the lower doubly reinforced fiber fractions, the failure mode was a combined tension-shear mode. However, as the fiber fraction increased, the failure mode was exclusively shear failure. It is therefore presumed that the slope of the graph in Figure 4.4 should be nearly linear because all of the failure modes include some sort of shear failure and, in fact, this is what was observed in the graph. This suggests that the ultimate limit state for the optimum design of the doubly reinforced specimens is the shear limit state.

Figure 4.5 presents the relationship between the apparent and shear free stiffness enhancement and the corresponding fiber fraction for the doubly reinforced specimens. It is again noted that there is a similar trend between the shear free stiffness and the apparent stiffness results, with the shear free stiffness being slightly greater than the apparent stiffness, as expected.

As with the strength enhancement plot, there was no data available for a fiber fraction less than 2%. Because of this, the relationships presented in Figure 4.5 appear to be representative of a parabolic shape. This is the expected shape for the doubly reinforced specimens because there is no lowering of the neutral axis as more glass fiber is added due to symmetry. Because there is no lowering of the neutral axis with increased fiber fractions, the area x depth^2 term of the moment of inertia plays a more significant role in the determination of the member's stiffness. As a result of this increased role, the shape is more parabolic for the doubly reinforced specimens than observed for the specimens with only tensile reinforcement.

Figure 4.2 showed that at the lower fiber fractions (< 2%) there was some unique behaviour being exhibited by the reinforced specimens. From Figure 4.5, it is unclear whether the doubly reinforced specimens exhibit the same unique behaviour. If the explicit behaviour of the doubly reinforced specimens at these low fiber fractions is required, then it is recommended that further studies be conducted.

Figure 4.6 gives a graphical representation of the strength enhancement as it parallels it's corresponding shear free stiffness enhancement at a given fiber fraction for the doubly reinforced specimens. Examination of the graph shows that the 'convex' shape of the strength enhancement plot intercepts the 'concave' shape of the stiffness enhancement plot. This point of interception indicates that the optimum fiber fraction is 4.3%, which corresponds to a 115% strength and stiffness enhancement.

As was discussed for the specimens with only tensile reinforcing, Figure 4.6 also shows the versatility of glass fiber reinforced beams. By varying the fiber fraction from this optimum value, a designer may improve the governing limit state so that two limit states will simultaneously govern the design of a particular member. This results in a more efficient section.

4.4 Discussion of Weathered Specimens

As with most structural engineering components, the effects of the environment greatly influence the performance of the component. As high alkalinity affects the performance of concrete and the presence of water is an integral part in the rusting of steel, moisture affects the behaviour of timber. Saturation of timber generally leads to a decrease in strength and stiffness. Timber becomes weaker and more flexible when wet. In addition to this, when timber is cycled in and out of water, large cyclic stress are placed on the wood through drying and wetting, which leads to the wood exhibiting symptoms similar to fatigue. Considering this behavior, it was postulated that the weathering conditions imposed on the test specimens would result in a lower stiffness enhancement and a lower reinforced stiffness for the weather specimens, and that the cyclic weather specimens should suffer greater reductions than the saturated beam because of the greater impact of the cycling.

Figure 4.1 includes the strength enhancement results of the specimens that received the weather treatment. A comparison of the weather specimens with the unweathered tests results shows that the cyclic weathered specimens numerically performed better than the unweathered beams, while the saturated specimen performed worse. While the saturated specimen's behaviour is as expected, the cyclic weathered beam performed significantly better than anticipated. It may be due to the "bridging" effect offered by the glass fiber to the adjacent wood fibers. Specimen weathering usually causes cracking of the specimen and loss of tensile strength, however, with the presence of the glass fiber, this cracking is not allowed to take place and the specimen does not lose its tensile capacity. That is, the fiber confines the wood against moisture cracks. However, this is only speculation and it could also be suggested that the observed behaviour is due to the variability of wood.

Coincidentally, the weathered specimens were made up at the same fiber fraction as the only specimens in the tensile reinforcement series that did not fit exactly into the general behavioral trend. Because this data point is a little low, it appears as if the cyclic weathered specimens performed even better than anticipated. Close examination of Figure 4.1 shows that the data point for the cyclic weather specimens lies nearly exactly on the smooth curve for the non-weathered data series, indicating that there is little adverse effects on the strength enhancement from the cyclic weathering.

From a similar comparison made between the smooth curve result and the saturated result, it could be interpolated that there is an approximate 50% reduction in strength enhancement when a specimen is fully saturated. However, it is important to note that the strength test results for the saturated specimen have to be considered non-conclusive because only one specimen was tested.

The stiffness results agreed more closely with the expected behaviour. As seen in Figure 4.2, both the reinforced cyclic weathered specimens and the reinforced saturated specimen exhibited a reduction in stiffness when compared with the reinforced

unweathered specimens. This was expected. The exact magnitude of this stiffness reduction is indeterminable from the available test data.

One of the main purposes of the weathering tests was to observe the behaviour of the bond between the glulam beam and the glass fiber reinforcement. Consequently, the tests were designed to induce a worse case scenario on the specimens and the beams were fully submerged in a water bath and the moisture content maximized. During this program, it was observed that the bond in the weather specimens performed no differently than the bond in the unweathered beams, and it could be concluded that adverse environmental conditions do not affect the adhesion capabilities of the phenolic resorcinol formaldehyde in this application.

Notwithstanding, it is recognized that this does not represent actual real life weathering. In reality, after a glulam member is constructed, it will only be exposed to the conditions induced in this investigation in special situations, such as swimming pools. The most likely environmental condition that such a beam might be exposed to would be minor moisture content fluctuations over the life cycles of a structure.

In the fatigue of steel, it is a well known fact that large number of cyclic loads at a lower stress gradient can be much more damaging that a small number of cycles at a higher stress gradient. It is therefore recommended that these reinforced specimens be subjected to an extensive number of lower level moisture fluctuations to represent a more realistic usage and that the reinforcement bond be carefully examined.

4.5 Discussion of Size Effects

The results from the size effects are plotted on the respective graphs in Figures 4.1 through 4.6. Examination of Figures 4.1 and 4.3 shows that none of the size effect results met the expected strength enhancement behaviour. Neither the 300 mm deep specimens with only tensile reinforcement nor the doubly reinforced specimens achieved the strength enhancement for the corresponding fiber fraction that the 240 mm deep specimens did. In fact, they were approximately an order of magnitude less than the 240 mm deep specimens. This can be readily explained by considering the mode of failure.

In all of the reinforced 300 mm deep beams, the primary mode of failure was shear. Examination of the results in Table 3.10 shows that the unreinforced 300 mm deep specimens failed in tension, however the shear stresses developed in these specimens was very close to the ultimate limit state shear. This indicates that there is very little shear capacity left in the unreinforced specimens and that shear failure was imminent prior to reinforcing.

Based on this information, it can be interpreted that the fiber reinforcing provided adequate confinement to any defects in the tension zone that the small reserve shear capacity of the specimen was now exceeded and the mode of failure moved from tensile

fracture to shear failure. The unreinforced 300 mm deep beams had an average shear stress at failure of 2.26 MPa, which is within 16% of the ultimate limit state for shear. When the glass fiber was applied, it provided the specimens with the initial confinement to the tension zone defects that was observed in the 240 mm specimens. Once these defects were "bridged", additional shear stress was allowed to develop before the tension zone failed. However, this reserve shear stress capacity was so small (16%) that the beams failed in shear without developing the full benefit of the glass fiber reinforcement.

Examination of the compressive and tensile stresses of the 300 mm deep specimens at failure offers further support to this explanation. Table 3.21 shows that the compressive stresses developed in the specimens were well below the average compressive failure stress of 46.4 MPa shown in Table 3.29. Table 3.21 also shows that the tensile stresses developed were well below the 42.3 MPa average from Table 3.29. From this, it is clear that neither the tensile capacity nor the compressive capacity of the 300 mm deep specimens were fully developed, and again the full benefit of the glass fiber reinforcement was not invoked.

Figure 4.2 and Figure 4.5 provide the stiffness enhancement results of the 300 mm deep beams. Theoretical calculations indicate that the apparent stiffness and the true stiffness for the deeper specimens should be slightly less than the respective stiffness for the more shallow beams. Figure 4.2 and Figure 4.5 show that the apparent stiffness enhancement of the 300 mm deep beams appears to be slightly greater than the stiffness enhancement of the 240 mm, and that the true stiffness enhancement of the 300 mm deep beams appears to be slightly less than the stiffness enhancement of the 240 mm beams. Since the magnitudes of these differences are within the experimental variations which are often observed in testing wood and wood products, it is assumed that, as the size of the test specimen changes, there is no effect on the stiffness enhancement achieved with the application of glass fiber reinforcing.

It is therefore concluded that, due to the limited size of this portion of the test program, the results are insufficient to draw any size effect conclusions, and it is recommended that specimens with a lower height to width ratio be examined with glass fiber reinforcing to test the adequacy of applying the relationship developed for the 240 mm deep specimens to specimens of other dimensions.

4.6 Model Development

A model was developed to predict the failure load of the reinforced specimens. This model was based on the compatibility of strain between the glass fiber reinforcing and the adjacent wood fiber and the assumption that there was a plane strain distribution through the depth of the entire member. The measured dimensions and properties for each specific specimen were used in the model.

Figure 4.7 shows a schematic of the model used to predict the ultimate failure load of the specimens and the relevant equations used. For specimens with no compressive reinforcement, the term that represent the contribution from the compression zone fiber in Figure 4.7 is neglected. It should be noted that, since a linear strain assumption is used in the model, the centroidal axis of the transformed section is coincidental with the neutral axis in Figure 4.7.

There were three criteria used to determine the failure load: flexural failure in tension, flexural failure in compression and shear failure. For the two predicted flexural failure loads, the average extreme fiber strain for the different failure modes was taken from Table 3.29, 3429 με and 3883 με for tension and compression respectively. Since the strain compatibility model requires the input of the strain at each extreme bending fiber, the non-governing extreme fiber strain on the face opposite to the limiting strain being used had to be determined. The simple linear strain relationship, based on similar triangles, presented in equation 4-1 was used to determine the non-governing strains.

$$\varepsilon_{NG} = \varepsilon_G \, c_{NG} / c_G \qquad \text{[eq. 4-1]}$$

where:

ε_{NG} = non-governing strain (mm/mm)
ε_G = governing strain (mm/mm)
c_{NG} = distance between neutral axis and the line of action of the non-governing strain (mm)
c_G = distance between neutral axis and the line of action of the governing strain (mm)

The failure load using shear as the governing failure mode was determined using equation 4.2, the average shear stress at failure from Table 3.29, 2.69 MPa, and the sectional properties for the individual specimens.

$$P = 2 \, \tau_{max} \frac{It}{Q} \qquad \text{[eq. 4-2]}$$

where:

P = total failure load due to shear (N)
τ_{max} = 2.69 (MPa) (from Table 5.29)
I = transformed moment of inertia (mm^4)
t = thickness of specimen at τ_{max} (mm)
Q = first moment of area (mm^3)

Table 4.3 presents the results of failure load predictions. The shaded loads indicate the governing failure mechanism.

Table 4.3 Predicted Failure Loads

Specimen ID	Strain Compatibility Model Predicted Failure Mechanisms			
	Tensile Failure Load (kN)	Compressive Failure Load (kN)	Shear Failure Load (kN)	Governing Failure Mode
PTN-1	22.4	-	34.4	tension
PTN-2	19.4	-	34.8	tension
PTN-3	22.3	-	34.4	tension
PTN-4	21.2	-	34.7	tension
PTG-1a	21.5	24.2	35.1	tension
PTG-1b	24.8	27.9	34.6	tension
PTG-2a	30.6	34.3	34.7	tension
PTG-2b	23.7	26.6	34.7	tension
PTG-10a	26.7	28.2	35.7	tension
PTG-10b	26.6	28.6	35.4	tension
1TS-1	35.0	35.3	35.4	tension
1TS-2	30.5	30.7	36.3	tension
1TS-3	31.1	31.3	36.4	tension
1TS-4	31.9	31.9	35.6	tens./comp.
1TS-5	30.7	31.6	35.8	tension
1TS-6	33.2	33.6	35.3	tension
2TS-1	40.2	36.6	37.6	compress.
2TS-2	40.1	36.0	36.9	compress.
4TS-1	53.9	37.8	39.9	compress.
4TS-2	55.8	42.2	40.3	shear
8TS-1	92.4	44.6	42.1	shear
8TS-2	85.7	42.2	42.9	compress.
2DR-1	33.0	37.4	37.3	tension
2DR-2	30.4	34.5	37.5	tension
4DR-1	43.3	48.9	41.6	shear
4DR-2	43.0	48.4	40.8	shear
8DR-1	66.9	74.7	46.6	shear
8DR-2	69.8	79.9	51.8	shear
1WT-1	28.0	28.2	36.6	tension
1WT-2	33.0	33.1	35.9	tension
1WT-3	28.9	29.1	35.9	tension
1SAT-1	27.9	27.9	35.5	tens./comp
PT12-1	34.9	-	43.2	tension
PT12-2	36.3	-	43.5	tension
2T12-1	51.7	48.6	47.9	shear
2T12-2	40.6	37.8	45.3	compress.
2D12-1	44.2	50.0	44.7	tension
2D12-2	38.8	44.0	41.4	tension

From the results in Table 4.3, an average predicted failure load and failure mechanism were determined and compared with the actual failure loads and mechanisms. Table 4.4 presents this comparison.

Table 4.4 Comparison of Test to Predicted Failure Loads and Mechanisms

Specimen ID	Actual Specimen Behaviour		Predicted Specimen Behaviour		Test to Predicted Ratio (%)
	Test Failure Load (kN)	Test Failure Mechanism	Predicted Failure Load (kN)	Predicted Failure Mechanism	
PTN	21.6	tension	21.3	tension	1.014
PTG-1	26.3	comp. & tens.	23.2	tension	1.134
PTG-2	28.7	tension	27.2	tension	1.055
PTG-10	30.6	comp. & tens.	26.4	tension	1.159
1TS	31.6	tens. & shear	32.1	comp. & tens	0.984
2TS	35.9	comp. & tens.	36.3	compression	0.989
4TS	42.2	comp. & shear	39.1	comp. & shear	1.079
8TS	49.1	comp. & shear	42.2	comp. & shear	1.164
2DR	38.7	tens. & shear	33.0	tension	1.173
4DR	45.2	tens. & shear	41.2	shear	1.097
8DR	53.7	shear	49.2	shear	1.091
1WT	33.9	tens. & shear	30.0	tension	1.130
1SAT	28.4	tension	27.9	tension	1.018
PT12	36.8	tension	35.6	tension	1.034
2T12	39.4	comp. & shear	42.9	comp. & shear	0.918
2D12	39.5	shear	41.5	shear	0.952

From the results in Table 4.4, the average test to predicted ratio for the failure loads was found to be 1.062 with a standard deviation 0.079. Considering that the failure strains from the tested specimens had a range of nearly 100% (2430 $\mu\varepsilon$ to 4526 $\mu\varepsilon$ for tensile strain in Table 3.27 and 2686 $\mu\varepsilon$ to 4697 $\mu\varepsilon$ for compressive strain in Table 3.27) and that the average of this range was used in the strain compatibility model to predict the failure loads, these results show excellent agreement. It is important to note that a difference of 6.2% could be considered well within the experimental variations of timber.

In addition to this, the predicted failure mechanism is the same as the actual failure mechanism in nearly every case, as shown in Table 4.4. This further indicates the suitability of the strain compatibility model.

A second observation is that the range of the errors may also be considered excellent. The range, from -8% to +17%, is considered very good, considering the variations that exist in timber. This suggests that the application of the glass fiber reinforcement not only increases the strength of the specimens, but it may also reduce the variability in mechanical properties of the timber beams. Timber is notorious for having huge variations, even within a given specimen. This results in the extremely conservative design limit state in CSA/CAN O86.1-94 (1994) for timber stresses. If the application of the glass fiber reinforcing can help control the variability of the mechanical properties then the lowest fifth percentile of the specified design strengths may be increased. By allowing greater design stresses, more efficient sections may be used.

Finally, the results and the accuracy of the predictions from this model further supports the belief that using the bending strain theory is the best method for predicting the strains that develop in the specimens. This, in turn, suggests that the demec gauge strain data and the foil strain gauge data are both slight over-estimates or the real strain. Input of either of these two sets of strain data into the strain compatibility model leads to an decrease in the test to predicted ratios. This implies that there may be some inelastic behaviour occurring as the specimens approach their failure load, which results in the decrease in test to predicted ratios from the demec gauges. However, the small decrease caused by using the demec data suggests that this inelastic behaviour is minimal.

Using the strains recorded by the foil strain gauges shows that the test to predicted ratios are further reduced. This suggests that these foil gauge strains are over estimated. It also supports the postulate that the strain gauges are being significantly affected by the normal compressive stresses developed between the wood core and the glass fiber reinforcement.

4.6.1 Design Recommendations

From the close agreement obtained, it is obvious that the strain compatibility model is an excellent method for predicting the behaviour and failure mechanism of glass fiber reinforced glulam beams. From the test to predicted ratios determined in this study, it was found that using the average strains calculated from the test data using the bending strain theory provide a more than suitable prediction. The average reinforced shear free MOE for the specimens modeled was 12011 MPa. Average design stresses were calculated by multiplying this average MOE by the average strains used in the model. Table 4.5 presents the design values to be used in the strain compatibility model to predict the failure load and behaviour of glass fiber reinforced glulam beams.

Table 4.5 Design Strains and Stresses for Glass Fiber Reinforced Glulam Beams

Governing Criteria	Unfactored Design Strain ($\mu\varepsilon$)	Unfactored Design Stress (MPa)
Tensile Failure	3429	41.2
Compressive Failure	3883	46.6
Shear Failure	-	2.69

By using the flexural design limits in the strain compatibility model or the shear stress limit, a governing design load and mechanism may be determined. It is important to recognize that these design limits are mean values based on limited test data and do not take into account any statistical analysis or confidence intervals. Further studies with additional specimens would be required in order to establish design value suitable for a design code.

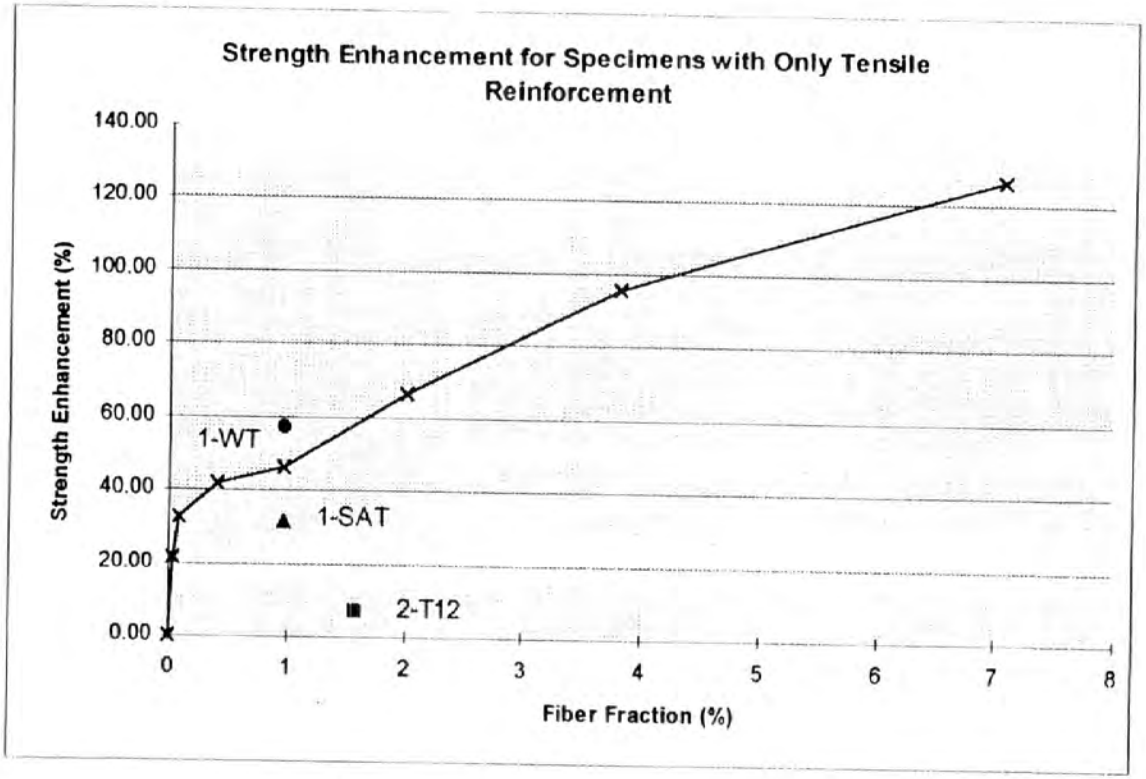

Figure 4.1
Strength Enhancement Plot for Tensile Reinforced Specimens

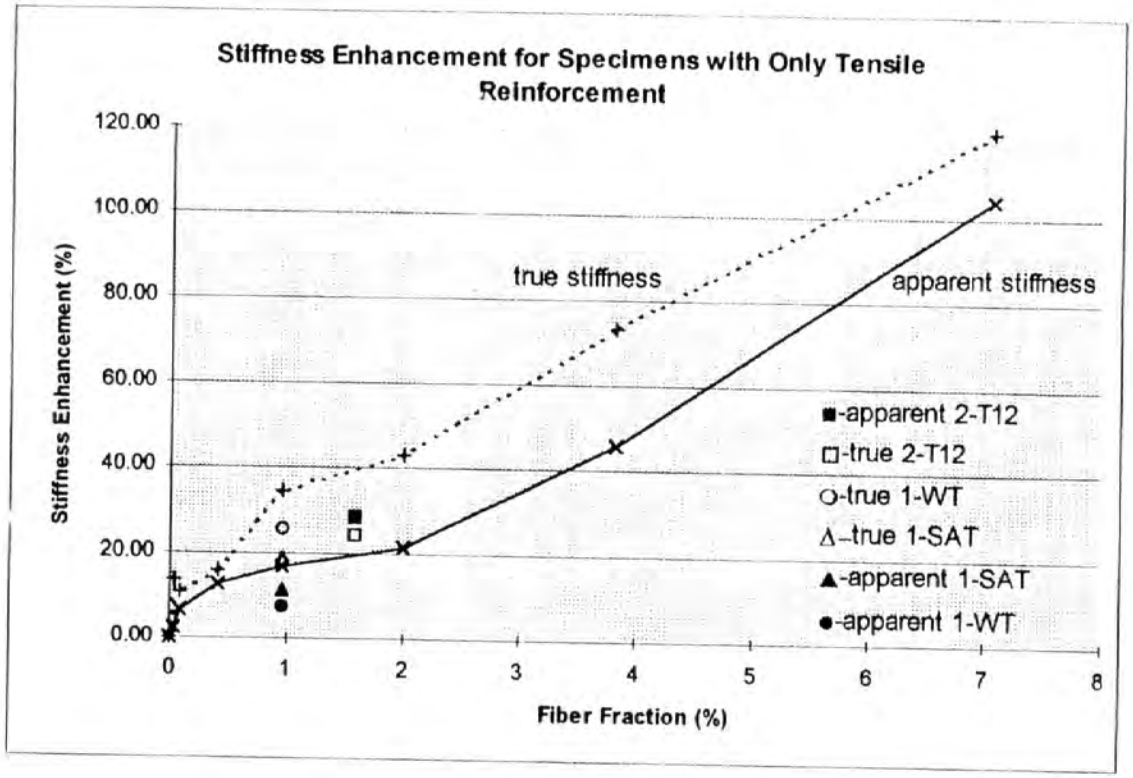

Figure 4.2
Stiffness Enhancement Plot for Tensile Reinforced Specimens

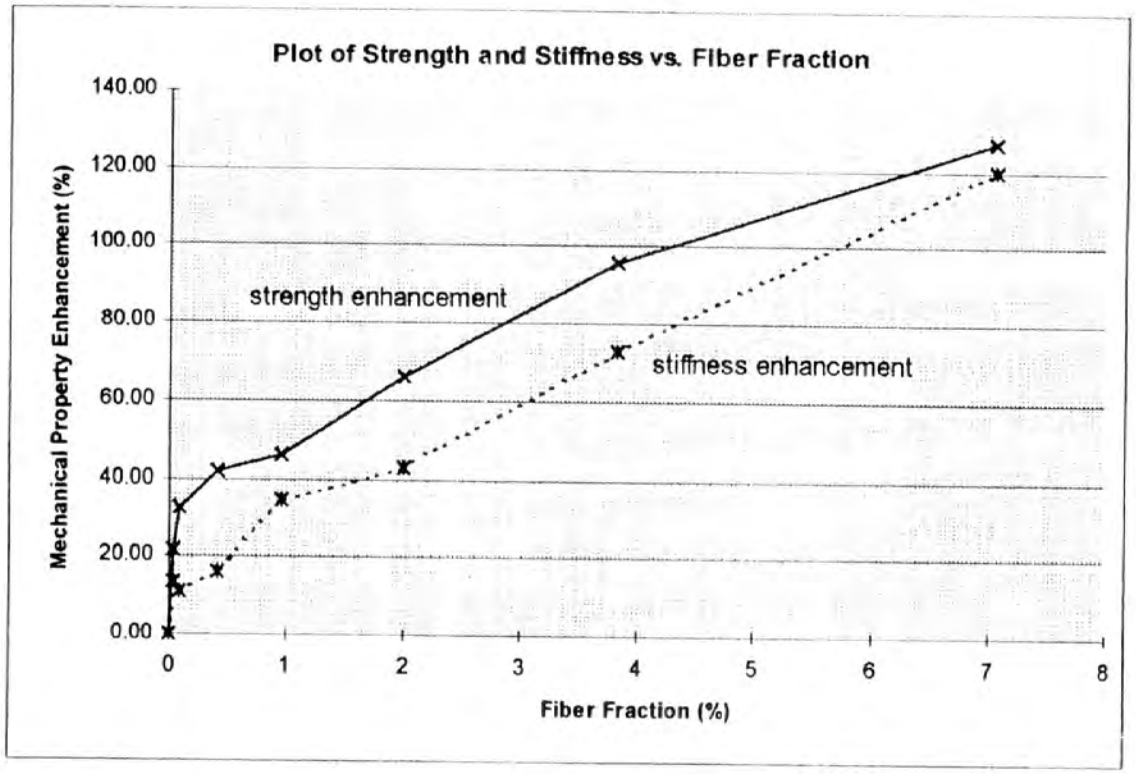

Figure 4.3
Strength versus Stiffness Relationship for Tensile Reinforced Specimens

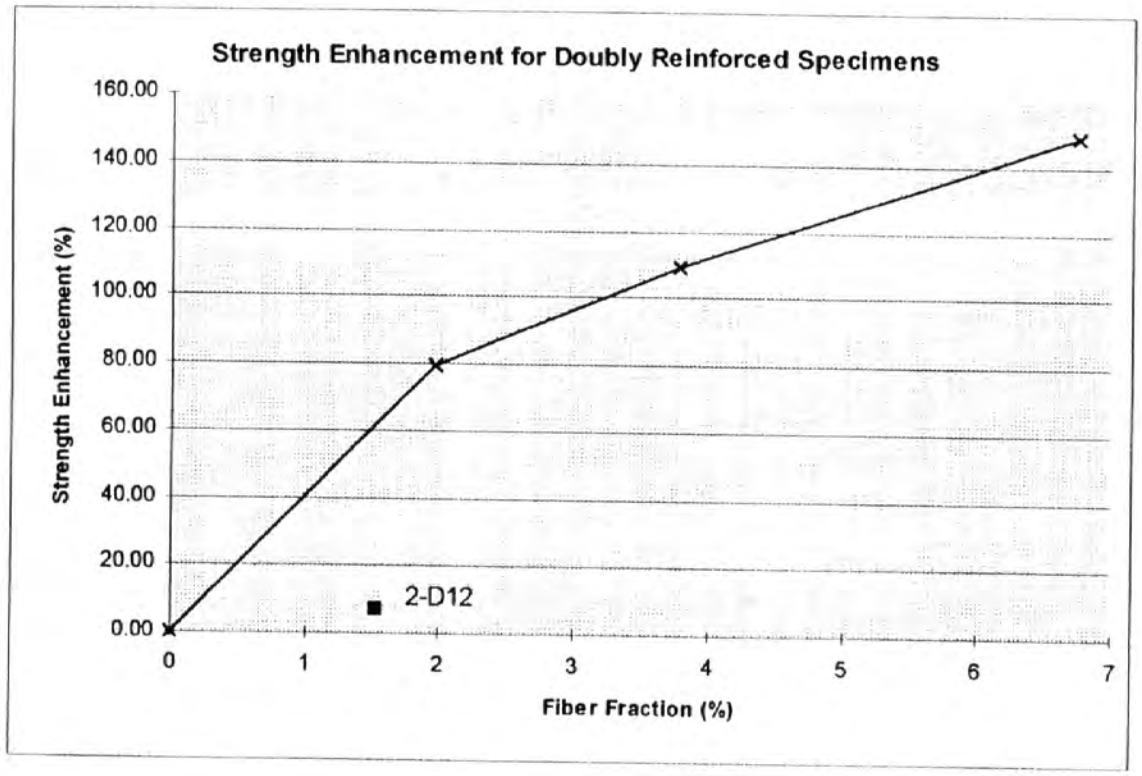

Figure 4.4
Strength Enhancement Plot for Doubly Reinforced Specimens

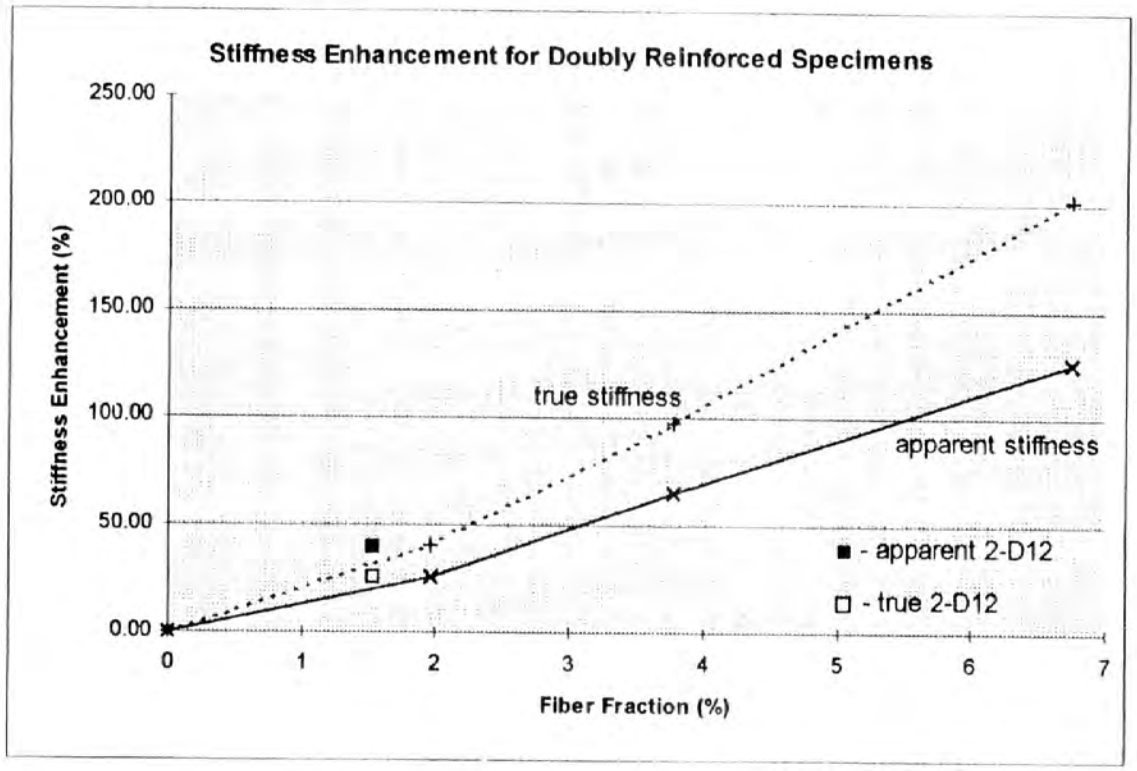

Figure 4.5
Stiffness Enhancement Plot for Doubly Reinforced Specimens

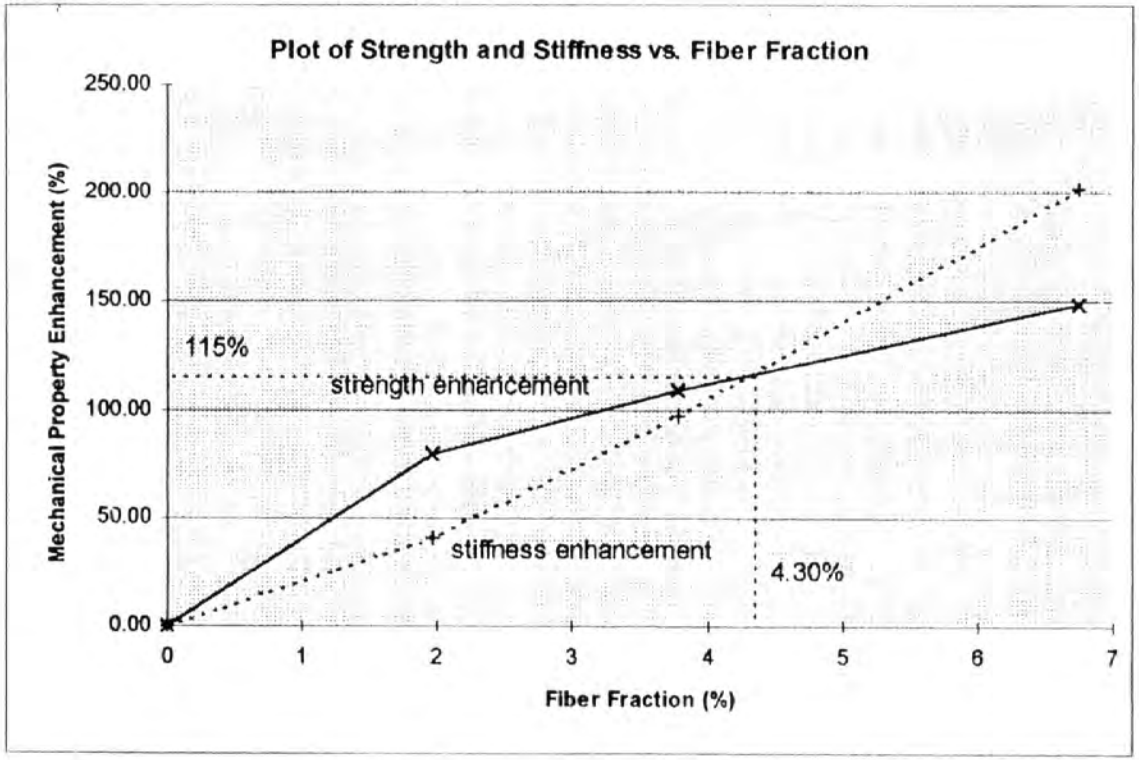

Figure 4.6
Strength versus Stiffness Relationship for Doubly Reinforced Specimens

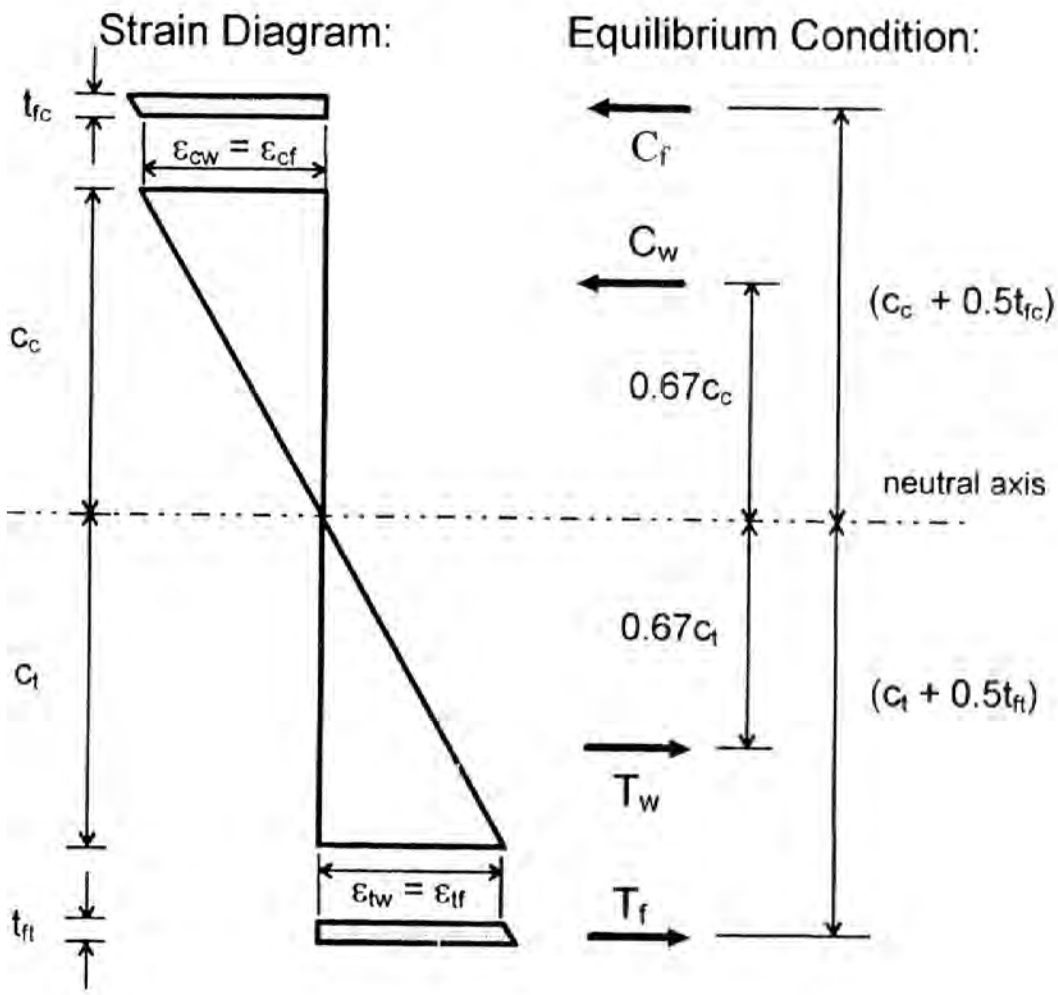

Equations:

$C_f = \varepsilon_{cf(avg)} E_f t_{fc} b_{fc}$

$C_w = 0.5 \varepsilon_{cw} E_w b_w c_c$

$T_w = 0.5 \varepsilon_{tw} E_w b_w c_t$

$T_f = \varepsilon_{tf(avg)} E_f t_{ft} b_{ft}$

$M = C_f (c_c + 0.5t_{fc}) + C_w (0.67c_c) + T_w (0.67c_t) + T_f (c_t + 0.5t_{ft})$

$P = 6 M / L$

where:

L = total length of specimen

Figure 4.7
Schematic and Calculations for Strain Compatibility Analysis

5.0 SUMMARY AND RECOMMENDATIONS

5.1 Summary

1. A total of 6 unreinforced and 32 glass fiber reinforced specimens were tested using different reinforcing schemes and different test conditions. From the results of the test program, it is clear that, in all cases, the application of glass fiber reinforcement to S-P-F glualm timber beams results in the enhancement of the overall mechanical behaviour of the specimens. Specifically, the most prominent benefits were seen by an increase in both the bending strength capacity and the composite stiffness of the reinforced member.

2. From the results of the preliminary investigation, it was concluded that the fiber type of choice for use in the application to fiber reinforced glulam timbers was glass fiber. While carbon fiber did behave in a technically superior manner to the glass fiber, when economics were considered, the mechanical advantage achieved by using carbon fiber were lost to commercial viability and glass fiber became the reinforcing material of choice.

3. Two different fiber orientations were investigated. One orientation had glass fiber reinforcement applied to only the tension side of the beam and the other had glass fiber reinforcement applied to both the tensile and compressive regions. For the specimens with only tensile glass fiber reinforcement, the maximum strength enhancement of 127% was achieved using a fiber fraction of 7.06% of the total cross sectional area. This fiber fraction also resulted in the maximum apparent stiffness enhancement of 104 % and the maximum shear free stiffness enhancement of 120%.

   For the specimens doubly reinforced, the maximum strength enhancement of 149% was achieved using a fiber fraction of 6.74%. This fiber fraction also resulted in the maximum apparent stiffness enhancement of 126% and the maximum shear free stiffness enhancement of 202%.

4. As expected, it was evident that the doubly reinforced specimens performed better than their tensile reinforcement counterpart of equal fiber fraction. However, often timber structural members support floor or roof membranes and are required to accept fasteners for the connection of these membranes. Further investigation is required to determine if standard connection techniques can be used to fasten such membranes to the glass fiber reinforcement. Acceptance of standard connection techniques will greatly influence which is truly the preferred reinforcement orientation.

5. A strain compatibility model, using the maximum strains recorded from the individual test specimens, yielded excellent predictions for the failure load. The test to predicted ratios for the test specimens ranged from 0.92 to 1.17, with a mean of 1.062 and standard deviation of 0.079.

6. Despite insufficient data, extrapolation of the data from the specimens with only tensile reinforcement indicated that equal strength and stiffness enhancements were achieved at fiber fraction of approximately 8% for this fiber orientation. It is obvious that this equal enhancement fiber fraction lies beyond the upper limit selected for this research, therefore the objective of determining this unique fiber fraction can only be estimated for the specimens with only tensile reinforcement and further research will be required to determine the exact value.

   For the doubly reinforced specimens, the strength and stiffness data indicated that the balanced fiber fraction for this reinforcing scheme was 4.3%. This resulted in equal strength and stiffness enhancements of 115%.

7. Results of the weathering tests indicate that the stresses induced through extreme environmental conditions have no appreciable effect on the bond between the glass fiber reinforcing and the adjacent wood section. The results also indicated that there was a reduction in the stiffness of the saturated specimen and the cyclic weathered specimens. This variation in stiffness of the weathered specimens is consistent with current beliefs in the behaviour of weathered timber. However, the results indicated that there was little or no effect on the strength of the reinforced specimen with exposure to high moisture environments or exposure to environments where there is a fluctuation moisture content. These strength results are contrary to the accepted understanding of the behaviour of timber exposed to adverse environmental conditions and may be due to the "bridging" effect offered the wood fibers adjacent to the glass fiber reinforcing.

8. Due to a poor height to width ratio selection for the specimens used, inconclusive data resulted from the size effects comparison tests. For the specimens selected for the size comparison, the height to width ratio was such that the specimens fell into the "deep beam" category and shear was a factor in the failure mode for all of the reinforced specimens. Since the glass fiber reinforcing was applied in a fashion such that it enhanced either the tensile capacity or both the tensile and the compressive capacities, and shear was the governing failure mode, the results obtained from the size effect specimens were significantly below expected. At a comparable fiber fraction, the test data projects the 240 mm deep beams, with either reinforcement scheme, to have a strength enhancement of approximately 55 to 60%. However, the 300 mm deep beams each failed slightly above 7% strength enhancement. This is attributed to the fact that the specimens selected fell into the deep beam category and the shear mode of failure governed the capacity of the specimen.

   Theoretically, the stiffness of the 300 mm deep beams should be slightly less than the stiffness of the 240 mm deep beams. The test data showed that for the 300 mm deep beams there was a small increase in the apparent stiffness values and a small decrease in the true stiffness values when compared with the 240 mm deep beams. It also showed that these differences were well within experimental variations that are observed in timber specimens and it was therefore concluded that there appears to

be no effect on the stiffness enhancement achieved with the application of glass fiber reinforcing as the size of the test specimen changes.

9. From the test results of both the preliminary study and the main testing program, it was observed that the fiber reinforcing did not fracture in any of the specimens with a fiber fraction greater than 0.09%. It is therefore concluded that a fiber fraction of 0.09% acts as a minimum level of reinforcement for specimens of this size. However, it is unclear whether this limit is valid for specimens of different size.

5.2 Significance

From the test results of this project, it is clear that the application of glass fiber reinforcing has a potential to play a significant role in glulam structures. The observed increases in flexural strength and composite stiffness could play a major role in lessening the depletion of one of our most valuable natural resources. Since it is evident that the capacity of glulam beams can be substantially increased using glass fiber reinforcing, use of this composite construction will reduce the demands placed on our ever decreasing prime lumber stocks. Furthermore, it presents the opportunity to use low grade lumbers in situations that used to demand high grade stock.

Another significance of these test results is the seeming decrease in the variability between similar constructions. As discussed, this may allow higher design limit states through greater design stresses or an increase in the resistance factors. This would further reduce the amount of lumber required in the construction of the glulam beam.

In terms of cost savings, such an analysis was not part of this current research. However, a cost savings analysis conducted on the glulam beams constructed by Tingley (1993), which used a pultruded aramid fiber strap, indicated that the savings were approximately 25%. Given that the only significant difference between the two constructions is the fiber type and that glass fiber is substantially less expensive than aramid fiber, it is presumed that the cost savings of the glass fiber reinforced glulam beams is at least 25% and quite possibly greater.

In summary, the use of glass fiber reinforcing in a composite glulam construction not only has the potential to put significantly less pressure on our natural resources, but it appears to make timber products technically more competitive with other materials and will most likely do it economically.

5.3 Recommendations for Future Research

With any new product development, there are a large number of behavioral aspects that need to be investigated prior to its acceptance as an engineering product. This research

was designed as a starting point for the development of glass fiber reinforced glulam beams. There is substantial work yet to be done.

The following list of recommendations are considered to be the main factors that required thorough investigation prior to the development of a complete set of design criteria for glass fiber reinforced glulam beams.

1. A more complete set of fiber fractions should be studied using both application profiles because not all fiber ranges were covered. This would allow the determination of the equal enhancement fiber fraction for the specimens with only tensile reinforcement. It would also allow for the determination of the behaviour of the doubly reinforced specimens at fiber fractions less than the 2% minimum studied. In addition to this, it would provide researchers with a greater data set on which to base design specifications.

2. A program should be developed to further investigate the effects of adverse environmental conditions. The main focus investigated in this research was to investigate the adequacy of the phenolic resorcinol formaldehyde bond between the glass fiber and the adjacent wood section under extreme environmental conditions. As discussed, this is not a true representation of the conditions that a fiber reinforced member may be subjected to. Therefore, it is recommended that a program be established in which the specimens are subjected to a long term fluctuating moisture content as well as other environmental effects.

3. A complete investigation into size effects should be conducted. It is recommended that specimens with identical height to width ratios be used for comparison purposes. If different height to width ratios are used, then the results will not be directly comparable, as was seen in this investigation, and there may be other factors other than the difference in size that are affecting the test results. Included in this size effect study should be an investigation into the minimum fiber fraction required so that the fiber reinforcement does not fracture when the wood core of the specimen fails.

4. Additional material tests should be conducted on the pultruded glass strap to confirm that the strap exhibits the same material behaviour in compression as it does in tension. Specifically, the protocol called for in ASTM D3410 should be adhered to exactly to confirm or refute the assumption that the strap exhibits the same behaviour in tension and compression.

5. It is imperative that an investigation into the serviceability of the reinforced specimens be conducted. Next to load carrying capacity, serviceability is probably the most important design criteria. Factors that should be investigated include the fatigue of the specimen, the creep behaviour of the reinforced specimens under long term sustained loading, and an evaluation of the specimens under the current deflection limit state criteria.

6. As previously mentioned, one of the big advantages of using timber as the main elements in a structure is the ease of connection to the adjacent building components. Therefore, in order to maintain the attractiveness of a timber superstructure, the effects of bearing directly on the straps and the ease of connecting to the straps should be investigated.

7. Finally, member to member connections should also be investigated. With the increase load carrying capacity of the members, greater loads will be placed on the inter-member connections. Therefore, it is recommended that a detailed investigation be conducted to determine the suitability of the current design clauses of CAN/CSA O86.1-94 (1994).

6.0 REFERENCES

American Society for Testing Materials, 1994, **"Standard Terminology Relating to Wood"**, Designation D9-87, Annual Book of ASTM Standards, Vol. 04.10.

American Society for Testing Materials, 1994, **"Standard Methods of Testing Small Clear Specimens of Timber"**, Designation D143-94, Annual Book of ASTM Standards, Vol. 04.10.

American Society for Testing Materials, 1994, **"Standard Methods of Static Tests of Timbers in Structural Sizes"**, Designation D198-84, Annual Book of ASTM Standards, Vol. 04.10.

American Society for Testing Materials, 1994, **"Standard Test Method for Tensile Strength and Young's Modulus for High-Modulus Single-Filament Materials"** Designation D3379 - 75, Annual Book of ASTM Standards, Vol. 15.03.

American Society for Testing Materials, 1994, **"Standard Test Method for Compressive Properties of Polymer Matrix Composite Materials with Unsupported Gage Section by Shear Loading"** Designation D3410/D3410M-94, Annual Book of ASTM Standards, Vol. 15.03.

American Society for Testing Materials, 1994, **"Standard Practice for Establishing Stresses for Structural Glued Laminated Timber (Glulam)"**, Designation D3737-93c, Annual Book of ASTM Standards, Vol. 04.10.

American Society for Testing Materials, 1994, **"Standard Methods for Direct Moisture Content Measurement of Wood and Wood-Base Materials"**, Designation D 4442-92, Annual Book of ASTM Standards, Vol. 04.10.

Canadian Wood Council, 1990, **"Wood Design Manual",** Canadian Wood Council, Ottawa, Canada.

Cheng, J.J.R., 1994, **"Testing of Spruce and Pine Glued-Laminated Joists"**, A Report prepared for Western Archrib Limited of Edmonton.

Dorey, A.B., and Cheng, J.J.R., 1996, **"Development of Composite Glued Laminated Beams"**, Canadian Forest Service Report No. A5030.

FORCA Tow Sheet Technical Notes, Revision 3.0, Toten Corporation, Japan, January 1995.

National Standard of Canada, 1989, **"Structural Glued-Laminated Timber"**, CAN/CSA-0122-M89 : Clause 6, Canadian Standards Association, Rexdale, Canada.

Tingley, D.A., and Leichti, R.J., 1993, **"Reinforced Glulam: Improved Wood Utilization and Product Performance"**, Technical Forum, Forest Products Society.

Tingley, D.A., 1994, **"Wood and Wood Composite Design Using High-Strength Fiber Reinforced Plastic (FiRP Panel) With Special Emphasis on Glued Laminated Beam Bridges"**, Oregon State University.